

**Density of States
and
Delocalization
in Low-dimensional
Disordered Electron Systems**

Inaugural-Dissertation
zur
Erlangung des Doktorgrades
der Mathematisch-Naturwissenschaftlichen Fakultät
der Universität zu Köln

vorgelegt von

Rainer Merkt

aus Wesseling

Köln 2000

Berichterstatter: Prof. Dr. J. Hajdu
Prof. Dr. M.R. Zirnbauer

Tag der mündlichen Prüfung: 4. August 2000

Für meine Eltern

Contents

1	Introduction	9
2	Mesoscopics and Symmetries	15
2.1	Characteristic Length and Energy Scales	15
2.2	Approaches and Methods	17
2.3	Symmetries of Mesoscopic Systems	18
I	Density of States in quasi-1D Systems of AIII Symmetry	23
3	Systems of AIII Symmetry	25
3.1	Peculiarities of Chiral Symmetry	25
3.2	Physics of the Random Flux Model	28
4	Non-linear σ-Model for Systems of AIII Symmetry	33
4.1	Supersymmetric Generating Functional	34
4.2	Color-Flavor Transformation	36
4.3	Saddle Point Approximation	38
4.4	Non-linear σ -Model for a Wire of AIII symmetry	40
4.4.1	Natural Formulation	40
4.4.2	Coordinates and Invariant Measure on $GL(1 1)$	42
4.4.3	Formulation in Terms of EFETOV'S Q -Matrices	43
4.5	From the $NL\sigma M$ to the DoS	44

5	Derivation of the Heat Equation	47
5.1	Transfer Matrix Method	47
5.2	Calculation of the Contributions	49
5.2.1	Laplacian corresponding to F_{fl}	49
5.2.2	Laplacian corresponding to $F_{\text{fl}} + F_{\epsilon}$	51
5.2.3	Laplacian corresponding to $F_{\text{fl}} + F_{\text{top}}$	51
5.2.4	Laplacian corresponding to $F_{\text{fl}} + F_{\text{Gade}}$	52
5.3	Discussion of the Generalized Heat Equation	53
6	Calculation of the DoS and Discussions	57
6.1	Ergodic Regime	57
6.1.1	Exact Calculation	58
6.1.2	Large Energy Asymptotics	60
6.2	Diffusive Regime	61
6.2.1	General Formulae	61
6.2.2	Zero-Mode Approximation	65
6.2.3	Large System Approximation	65
6.2.4	Exact Momentum Summation	66
6.2.5	Perturbation Theory with the Replica σ -model	69
6.2.6	Discussion	71
6.3	Quantum Regime	71
6.3.1	Calculation without Gade Term	71
6.3.2	Influence of the Gade Term	75
II	Localization-Delocalization Transition in 2D Systems of AII symmetry	77
7	Systems of AII Symmetry	79
7.1	Introduction and Motivation	79
7.2	Localization-Delocalization Transition	81

<i>CONTENTS</i>	7
8 Network Model	85
8.1 Topology	85
8.2 Potential Scatterers	86
8.3 Spin Scatterers	89
8.4 Parameter space	90
9 Finite-Size Scaling	93
9.1 Transfer Matrix Method	94
9.2 Transfer Matrices of the AII Network Model	96
9.3 LD Transition in the AII-NWM	98
9.4 Methods of evaluation	100
9.4.1 Fit Procedure for the Scaling Function	100
9.4.2 Testing the Fit of the Scaling Function	102
9.4.3 Fit for the Critical Exponent ν	102
9.4.4 Determination of Λ^*	104
10 Results and Discussions	107
10.1 Localization Lengths and Phase Diagram	107
10.2 Scaling Function	112
10.3 Critical Exponent ν and Critical RLL Λ^*	114
11 Real-Space RG for the Manhattan Model	117
11.1 Introduction	117
11.2 Manhattan Model	119
11.3 Real-Space RG Algorithm and Results	122
12 Summary and Outlook	125
A Power Series of the Adjoint Action	129
B Similarity Transformation of the Laplacian	131
C Zero-Mode Regime	133
D Efetov's Q-Matrices	137

E	Contraction Rules	141
E.1	Pair Correlations for $GL(1 1)$	141
E.2	Wick's Theorem for Correlations in $GL(n n)$	142
E.3	Contraction Rules for Gaussian Integrals over Hermitean Matrices	144
E.4	Perturbative Corrections to the DoS	145
F	Solution of the Heat Equation in the Quantum Regime	147

Chapter 1

Introduction

In the last two decades mesoscopic physics ("mesoscopics") has evolved to one of the leading and most attended fields of research in modern theoretical and experimental condensed matter physics. Exhibiting a rich phenomenology and accommodating a lot of new physical effects it is last but not least of large interest for present and future technologies. Essentially governed by the mechanisms of ordinary quantum mechanics some of its features were theoretically found and predicted more than 50 years ago. However, the experimental and technological requirements necessary to prepare suitable samples and to measure the predicted effects could not be provided until about 20 years ago. Since then a lot of effort has been invested in theoretical as well as experimental research transferring mesoscopic physics into a major subfield of condensed matter physics. Recently, considerable overlaps with other fields of physics, such as superconductivity, quantum chaos, microwave physics and optics, QCD, and spin physics were discovered.

Roughly speaking mesoscopic physics deals with phenomena which result from the interference of non-interacting multiply scattered electron waves in disordered media (metals or semi conductors). The existence of such quantum interference effects is intimately related to the phase coherence of the waves in a given sample. The linear extent of the maximal region within which the electron waves are still phase coherent is called *phase coherence length* L_ϕ . While by disorder (impurities, defects, dislocations etc.) the electron waves are scattered elastically, which conserves phase coherence, it is destroyed by inelastic scattering (e.g. electron-phonon interaction). Therefore, electrons are phase coherent within the sample if its (linear) size L is sufficiently small and if the temperature is low enough. This is realized in samples of size less than about 100 nm if the temperature is about 1 K or less. Thus, although being of *macroscopic* size such samples are governed by *microscopic* wave mechanical effects. This intermediate state motivates the notion *mesoscopics*. Although in the last years one has realized that electron-

electron interaction can play a crucial role in mesoscopic systems, we imply by the term "mesoscopics" in the following that electrons are non-interacting. For a review about mesoscopics we refer the reader to Refs. [1,2] and the references therein.

Some of the most famous phenomena characteristic for mesoscopic systems are the electronic Aharonov-Bohm effect [3], persistent currents [4,5], and the universal conductance fluctuations (UCF) [6]. The latter effect manifests in (e.g.) magnetic field dependent and reproducible fluctuations of the conductance, which are of the order of e^2/h . While the pattern of the fluctuations is sample specific ("magneto fingerprint"), their amplitude is *universal*. This means that it depends only on the dimensionality and the symmetries of the Hamiltonian and not on the geometry and microscopic details of the sample. *Universality* is one of the most remarkable features of weakly disordered mesoscopic systems, which is intimately related to quantum interference.

Another example of universality is the phenomenon of *weak localization*, which results in the decrease of the conductance of a mesoscopic sample compared to its classical value. This can be explained by an enhanced backscattering probability caused by destructive quantum interference. The corrections to the classical conductance due to this effect have been calculated by means of diagrammatic perturbation theory, cf. e.g. Ref. [7]. It turns out that the perturbative contributions depend only on the dimensionality and symmetries, e.g. time-reversal symmetry, which is broken by a magnetic field. The weak localization effect is interpreted as a precursor of *strong localization*. Mapping the quantum disorder problem to a lattice model ANDERSON predicted in 1958 that in a system with strong disorder the electronic wave function can be exponentially localized due to quantum interference effects [8]. As a consequence the dimensionless conductance $g = Gh/e^2$ (G conductance) decreases exponentially with the system length L , $g \propto e^{-2L/\xi}$, where a new characteristic length scale occurs, the *localization length* ξ . While for $L \gg \xi$ the electron wave function is localized and the system behaves like an insulator, states are extended in the opposite case, resulting in metallic behaviour of the sample. Under the assumption of one-parameter scaling it has been shown by ABRAHAMS ET AL. in 1979 that due to the effect of weak localization all disordered systems of dimension $d \leq 2$ flow into strong localization under renormalization of the system size [9]. In other words, there are good reasons to expect extended states only in dimension larger than two.

Nevertheless, 1D and 2D systems which can exhibit delocalized states are known for many years. Contradicting the scaling theory of the "gang of four" such systems are of special interest and have attracted the attention of a lot of researchers. In the two parts of this work we address two examples of systems with $d \leq 2$, in which delocalization occurs by completely different mechanisms. The first subject is the disorder averaged density of states (DoS) in a quasi-1D random flux system. In the second part we investigate the localization-delocalization transition in 2D disordered systems with additional scattering in spin space.

Since the 50's investigations of 1D systems had shown, that there can exist delocalized states or related phenomena. The DoS, e.g., which is usually a smooth function, can exhibit a singularity in the middle of the tight-binding band corresponding to a lattice model with purely *off-diagonal* disorder [10–12]. Later, in the 90's GADE and WEGNER [13–15] found an analogous behaviour within a non-linear σ -model (NL σ M) approach to a 2D model with *sublattice* or *chiral* symmetry. They further argued (see also [16,17]), that the chiral symmetry results in three new universality classes, extending the three-fold classification scheme elaborated earlier by DYSON [18]. Since then a lot of related problems have been investigated and the existence of delocalization as well as the underlying mechanisms have been discussed controversially. In the last years, new insight has been gained considering systems with chiral symmetry (cf. e.g. [19,20] and references therein). In particular, for the random magnetic flux and the random hopping problem, which correspond to chiral systems with broken and conserved time-reversal symmetry, respectively, a lot of analytical (see e.g. [21–27] and references therein) and numerical (see e.g. [28,29]) work has been done.

Due to the rigorous analytical methods available in one dimension the localization behaviour in 1D systems is meanwhile well understood. But in 2D this is not the case. It is much harder to obtain analytical and numerical results and we are far from having any exhausting picture. Therefore, it is recommendable to consider the quasi-1D case. On the one hand it allows for both, diffusive transport and strong localization, as in 2D, on the other hand it can be treated by controllable analytic methods, similar as in 1D. As mentioned above, the DoS of systems with chiral symmetry shows non-trivial behaviour. Although being one of the simplest quantities (a one-point Green function), there exists no comprehensive picture of this quantity in dimensions higher than strictly 1D. Moreover, in order to make further progress, in particular in order to investigate the non-perturbative quantum regime, one needs a suitable tool.

Recently, a supersymmetric NL σ M for the random magnetic flux problem has been derived by ALTLAND and SIMONS [22]. This is an effective long-range —or low-energy— field theory, which allows for the calculation of arbitrary n -point Green functions for chiral systems with broken time-reversal symmetry, i.e. systems of so-called AIII symmetry. The random flux problem is of interest in and applicable to various fields of condensed matter physics, e.g. in the Quantum Hall Effect at half filling, in high- T_c superconductivity, in non-Hermitian quantum mechanics. Further, it is related to the low energy sector of a single anti-ferromagnetic spin- $N/2$ chain or to the low energy sector of N coupled anti-ferromagnetic spin-1/2 chains. Beyond condensed matter physics the random flux model plays an important role in lattice QCD and for Dirac fermions subject to a random gauge field (see e.g. Ref. [22,24] for references).

In the first part of this work we calculate the DoS for a quasi-1D random flux system in the ergodic, diffusive and quantum regimes by means of this NL σ M.

Evaluating the action of the field theory in the zero-dimensional limit we find that the DoS vanishes at $\epsilon = 0$, where ϵ measures the distance from the middle of the tight-binding band. Furthermore, it turns out that in the ergodic regime one rediscovers results known from chiral random matrix theory [16,17]. We further calculate perturbative corrections to the DoS by a diagrammatic perturbation scheme. We find that all corrections up to three loop order vanish. The non-perturbative quantum regime is the most difficult and most interesting regime. We map the problem of the functional integration, involved in the corresponding expression for the DoS, to the solution of a diffusion type partial differential equation (heat equation). The occurring second order differential operator plays the role of a generalized Laplacian on the underlying supergroup and contains a contribution for each of the terms in the NL σ M action. These contributions are calculated by means of the transfer matrix method. After the solution of the heat equation the DoS in the localized regime is calculated in the limit of small energies $\omega = \epsilon/\Delta_\xi$, where Δ_ξ is the level spacing corresponding to the localization volume. The interesting result is that the DoS depends drastically on the parity of the channel number N_c . While for even N_c the DoS vanishes in the middle of the band as $\langle \rho(\omega) \rangle \propto |\omega| \ln|\omega|$, it diverges for an odd number of channels as $\langle \rho(\omega) \rangle - \rho_0 \propto 1/|\omega \ln^3|\omega||$. The existence of this even-odd effect, which is intimately related to the chiral symmetry, was first noticed by MILLER and WANG Ref. [21].

We now turn to the second subject. In recent years a lot of experiments have shown that there exists a localization-delocalization (LD) transition in 2D systems, which are non-chiral but time-reversal invariant [30–36]. This led to discussions about the underlying mechanism. In particular, the influence of spin-orbit and electron-electron interaction has been discussed controversially [37–42]. In the second part of this work we will focus on the former aspect and elaborate the universal features of the LD transition in time-reversal invariant systems with spin-orbit interaction.

From general arguments [43] breaking of spin-rotational symmetry has an impact on the quantum interference effects occurring in disordered systems. Due to the 4π -periodicity of the spin, backscattering can be suppressed by interference mechanisms. More precisely, it turns out that the corrections to the conductance of weakly disordered systems are *positive* in the case of broken spin-rotational invariance [44,45], i.e. the weak localization effect changes its sign and is therefore called *weak anti-localization*. Within the scaling theory of ABRAHAMS ET AL. [9] it can be argued, that due to the weak anti-localization effect there exist delocalized states. This, in particular, implies the existence of a LD transition which is triggered by the strength of the spin scattering.

We investigate this transition numerically within a scattering theoretical network model (NWM). In a recent paper [46] it was shown that such models are well suited to describe disordered electron systems. NWMs are generic in the sense

that the disorder of the physical system is directly represented by a network of unitary scattering matrices, which are merely subject to the symmetry constraints of the system. The triggering of disorder and spin scattering strength is in our case provided by three independent parameters, two for disorder and one for spin. Having constructed the scattering matrices we determine the transfer matrices corresponding to a quasi-1D strip geometry of width M . By means of the transfer matrix method we calculate the renormalized localization length $\Lambda = \xi/M$ for various values of the system parameters and the system width. Since Λ is well-suited as a scaling variable (cf. [2]), we are able to investigate the localization behaviour of the extended (2D) system using the finite-size scaling method. It turns out that the system exhibits a LD transition, and we determine the corresponding phase diagram in the three-dimensional parameter space.

In order to investigate the universal features of the transition we make the crucial assumption of one-parameter scaling. This assumption is usually justified by the determination of a scaling function. But often not much effort is invested in the construction of this function. Transparencies containing data sets are shifted and the quality of the fit is judged subjectively by eye. We use a more sophisticated and objective method adopted from [47]. Essentially, this method is based on a numerical procedure which fits a set of Chebyshev polynomials to the data points. Furthermore, the credibility of the fit is tested by a χ^2 -test. Under these conditions we find one-parameter scaling to be fulfilled with a high likelihood. Consequently, we proceed by calculating the critical value of Λ and the critical exponent ν of the correlation length. Again we use a numerical fit procedure and a corresponding test in order to get a reliable result. We obtain the critical exponent to be $\nu = 2.51 \pm 0.18$ which coincides with most of the values published in the last years. Using a conformal mapping [48] we obtain the scaling exponent of the typical local density of states to be given by $\alpha_0 = 2.174 \pm 0.003$.

The transfer matrix method requires a lot of computational effort. At the end of the second part we shortly introduce the numerical real-space renormalization method for hierarchical NWM [49–52], which allows us to qualitatively determine the localization behaviour of a system with very little computational effort. The basic idea is to put elementary scatterers together in such a way that the resulting composite scatterer allows to be interpreted as new elementary scatterer for the iteration step. Thus, the number of incoming and outgoing channels must be equal before and after such an RG step. Repeating this procedure several times one very quickly gets very large system sizes. The price which has to be paid is that the extended system possibly has a fractal dimension smaller than the spatial dimension, meaning that the extended network does not contain the full information. But often it still possesses the generic features of the underlying model. We apply the real-space RG method to the so-called Manhattan model in order to test whether it can exhibit the quantum Hall critical point.

This dissertation is organized as follows. After an introduction to mesoscopics and novel symmetry classes we introduce systems of AIII symmetry and their physics. In the fourth chapter the derivation of the corresponding non-linear σ -model in Ref. [22] is sketched and general formulas for the calculation of the DoS are derived. After that we turn to the derivation of the generalized Laplacian corresponding to the σ -model action, and discuss the heat equation. In Ch. 6 the DoS is calculated and discussed in the ergodic, diffusive, and quantum regimes. The second part starts with an introduction to general scattering theoretical network models and the phenomenology of the localization-delocalization transition. The construction of the scattering matrices is presented in Ch. 8. It follows an introduction to the finite-size scaling method, where the fit procedure employed is explained in detail. The results of the calculations are presented and discussed in Ch. 10. The subsequent chapter presents the real-space renormalization method applied to the Manhattan model. To conclude, all of the results are summarized.

Chapter 2

Mesoscopics and Symmetries

2.1 Characteristic Length and Energy Scales

In order to facilitate a systematical classification of mesoscopic systems let us first look at the length and energy scales relevant for electronic transport. Consider an electron in a d -dimensional system of linear size L as sketched in Fig. 2.1. The *Fermi energy* ϵ_F is the largest relevant energy scale, since transport is governed by electrons at the Fermi edge, where they propagate with Fermi velocity v_F . Correspondingly, we have the *Fermi wave length*, $\lambda_F \propto 1/v_F$, as a microscopic, i.e. quantum mechanical length scale. As long as no scattering takes place an electron propagates freely. This characterizes the so-called *ballistic* regime, where the electron's motion is determined solely by kinematics. If we wait long enough the electron will meet an impurity. The typical distance between two (elastic) scattering events characterizes the strength of the disorder. More precisely, we define the *elastic mean free path* as $l_e = v_F \tau$, where τ is the momentum relaxation time, i.e. the typical time after which information over the direction of the momentum is lost.

The mean free path allows for the definition of what is called a *quasi-one-dimensional* (quasi-1D) system. While a (strictly) 1D system of length L (a "wire") allows for exactly one transport mode (energy channel) a quasi-1D system has a small but finite width M (a "thick wire"). Due to quantization in the transverse direction a certain amount of transverse modes exists, each of them serving as a transport channel. To be more specific, on one hand M should be much larger than the Fermi wave length but should not exceed the mean free path on the other hand it, $\lambda_F \ll M \lesssim l_e$, in order to miss the characteristics of a 2D system. Furthermore, by means of the two length scales λ_F and l_e we are able to characterize the strength of the disorder. For $l_e \gg \lambda_F$ we speak of *weak disorder* (or weak scattering) otherwise of strong disorder. In the former case the wavy nature of the electron is substantially irrelevant and it can be regarded as a prop-

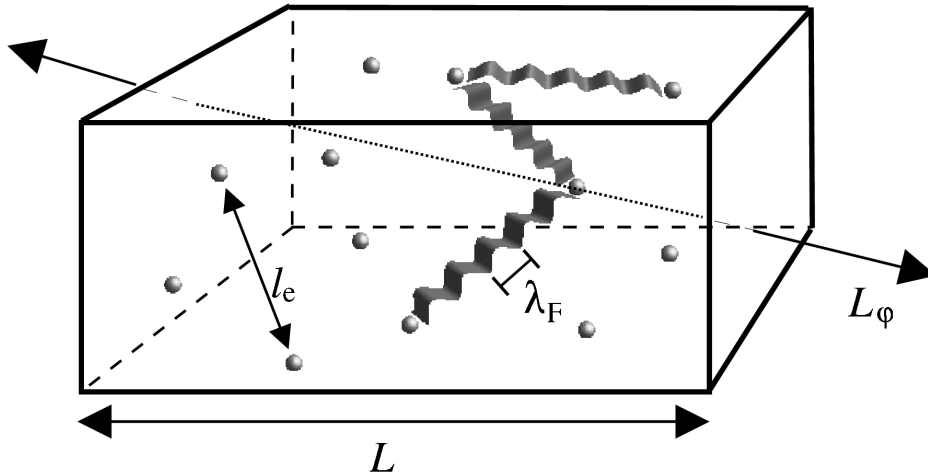


Figure 2.1: Characteristic length scales in mesoscopic physics.

agating particle. Hence, the weak disorder condition allows for a semi-classical approximation. In the following we focus only on weakly disordered systems.

For times larger than τ , the type of the electrons' motion is changed. Instead of ballistic propagation, the direction of motion is constantly modified due to scattering processes. Thus, we enter the regime of *diffusive* dynamics, where (in the case of weak disorder) the electrons behave as classical diffusing particles. The diffusive motion is therefore characterized by the classical diffusion constant $D = v_F^2 \tau / d = v_F l_e / d$. Within this regime the dynamics depends sensitively on individual properties of the system, such as disorder configuration, geometry, and dimensionality. Although we are dealing with the semi-classical approximation, the quantum mechanical nature of the electrons gives rise to a characteristic behaviour of spectral properties and small quantum corrections to classical transport quantities as e.g. the diffusion constant and the conductance. An example for the latter are the weak localization and anti-localization corrections mentioned above. We stay as long in the diffusive regime as the electrons propagate at most once across the system within the time of observation. This motivates the introduction of the classical diffusion time $t_D = L^2 / D$ which is the typical time needed to cross the whole system. The related energy scale $E_c = h / t_D$ is called *Thouless energy*.

Exceeding the diffusion time, $t > t_D$, or equivalently falling below the Thouless energy, $\epsilon < E_c$, we leave the diffusive regime. In particular, if $\epsilon \ll E_c$ the system is crossed many times, provided that $L \ll \xi$. In a corresponding classical system the whole phase space would be explored. This motivates us to call this regime *ergodic*. The only impact on the dynamics is now given by the symmetries of the underlying Hamiltonian. In this sense a system behaves *universal* in the ergodic

regime. All information about individual scattering events gets lost. Even the geometry (the boundaries) and the dimensionality do not play a role. Therefore, this regime is also called *zero-dimensional* (0D) limit. This denotation is further motivated by the fact that due to the system length dependence of the Thouless energy, the condition $\epsilon \ll E_c$ can be realized by going to sufficiently small system sizes. If the energy is further decreased we will meet the *mean level spacing* Δ which sets the smallest characteristic energy scale. For energies $\epsilon < \Delta$ or equivalently times exceeding the *Heisenberg time* $t_H = \hbar/\Delta$ we finally enter the *quantum* regime, where the structure of the energy spectrum is resolved.

It has been realized by THOULESS that the ratio of the Thouless energy and the mean level spacing defines a dimensionless conductance, $g = E_c/\Delta$, (g is the conductance measured in units of e^2/h), which can serve as the single parameter for the classification of the localization behaviour of a system. In the diffusive regime, where quantum interference effects merely attach small corrections to the classical diffusion constant, we have $\xi \gg L$. In particular, for quasi-1D systems it turns out that $g = \xi/L \gg 1$. Hence, diffusive dynamics implies a large conductance. We also speak of "metallic" behaviour in this case. For $E_c \simeq \Delta$ the dimensionless conductance is of the order of unity, which means that the localization length is of the order of the system size. For even larger values of L , the multiply scattered electron waves interfere destructively, leading to strong localization, $\xi \ll L$. The conductance decays exponentially on the localization length in this localized regime.

2.2 Approaches and Methods

Let us mention at this stage, that for the various energy regimes of mesoscopic physics different methods of evaluation have been established. Within the diffusive regime, i.e. $\epsilon > E_c$ and $\lambda_F \ll l_e$ which implies $g = E_c/\Delta \gg 1$ (weak scattering), the impurity diagram technique ("diagrammatics") is widely used (cf. e.g. [53,54]). This perturbative method is based on the systematical expansion in contributions which are related to coherently coupled scattering paths. Thereby, Δ/ϵ occurs as small expansion parameter. Hence, the range of validity of perturbation theory is restricted to energies being much larger than the mean level spacing and to the conditions mentioned above. If one is interested in an energy resolution comparable to Δ perturbation theory breaks down. Consequently, the low energy ergodic regime and the quantum regime are not accessible by diagrammatics. Instead, one has to use non-perturbative methods, e.g. the method of orthogonal polynomials introduced by МЕЙТА (cf. e.g. [55]). For quasi-1D system all regimes can be explored by the so-called DMPK equation [56,57] which is a kind of diffusion equation. Then, the problem is reduced to the solution of a

differential equation. In two dimensions a lot of results can be obtained by using the renormalization group. With regard to the more or less restricted techniques the field theoretical approach introduced by WEGNER in 1979 [15,58] is a milestone in the history of modern condensed matter physics. Deriving an effective long-range field theory, a so-called *non-linear σ -model* (NL σ M), he invented a tool, which in principle allows for the investigation of mesoscopic (and other) systems in all relevant energy regimes and arbitrary dimensions. Subsequently, this method has been improved by EFETOV [59], who invented a supersymmetric formulation of the NL σ M as an alternative to the replica trick used by WEGNER. Both version are still in use, but there are some formal reasons to prefer the supersymmetric formulation (cf. [60]).

2.3 Symmetries of Mesoscopic Systems

After the introduction to mesoscopic phenomena and a discussion of central quantities, we will give a survey of the fundamental symmetries in the following. We therefore focus on the ergodic regime, where the behaviour of a system is solely characterized by symmetries. As a consequence, the zero-dimensional limit of a disordered system can be described by *random matrix theory* (RMT). Originally, RMT was developed by WIGNER [61] and DYSON [18] in order to investigate the energy spectrum of complex atomic nuclei. The basic idea is to model a complex (e.g. disordered) system by a Gaussian ensemble of Hermitean random matrices, hence only taking the fundamental symmetries of the system into account and neglecting any individual structure. Each random matrix representing a Hamiltonian H is considered to have a large dimension $N \gg 1$ corresponding to a large number of eigenenergies. Now the question arises, which symmetries occur in typical mesoscopic systems and how can they be classified within RMT. For a long time three symmetry classes have been known, which we refer to as standard or Wigner-Dyson classes. Disordered systems with broken time-reversal symmetry are realized by an ensemble of general Hermitean random matrices. Since they can be diagonalized by unitary matrices the ensemble is called *Gaussian unitary ensemble* (GUE). In the presence of time-reversal invariance, $\mathcal{T}H\mathcal{T}^\dagger = H$, where \mathcal{T} denotes the time-reversal operator, we have to distinguish two cases. If the system allows for spin scattering we have $\mathcal{T} = -i\sigma_2^{\text{sp}}K$, where the Pauli matrix σ_2^{sp} acts in spin space and K is the operator of complex conjugation. Consequently, we get $H = \sigma_2^{\text{sp}}H\sigma_2^{\text{sp}}$, i.e. the Hamiltonian is real quaternion, $H = \begin{pmatrix} A & B \\ -B^* & A^* \end{pmatrix}$ (A Hermitean, B anti-symmetric), and thus can be diagonalized by symplectic matrices. Therefore, the corresponding random matrix ensemble is called *Gaussian symplectic ensemble* (GSE). The highest symmetry is realized if the system is additionally invariant under spin-rotation, $[H, \sigma_i^{\text{sp}}] = 0$ for two and therefore

all of the indices $i = 1, 2, 3$. Then, the grading in spin space is redundant and it turns out that H is symmetric. Hence, it can be diagonalized by orthogonal matrices yielding the *Gaussian orthogonal ensemble* (GOE). By means of RMT a lot of insight could be gained about disordered systems in the ergodic regime. See Ref. [62] for a comprehensive review. But an open question remained: Is the Wigner-Dyson classification scheme really exhaustive or do other symmetry classes possibly exist?

This question could not be answered using the scheme based on diagonalizing matrices. A first hint on a way out was given by DYSON itself [63] when he noticed, that the three Gaussian random matrix ensembles are related to three families of Riemannian symmetric spaces of compact type. These spaces have been known (in mathematics) for a long time¹ and have been classified by CARTAN, who has proved that there exist exactly *ten* of them². Before addressing the question whether the other seven symmetric spaces are also realized within RMT let us reconsider the three Wigner-Dyson ensembles in order to see how the new classification scheme works.

The basic idea [65] is to regard the random Hamiltonians H (multiplied by i) as the *generators* of symmetric spaces. By "generator" we mean that for each element S of the symmetric space there exists an H such that $S = \exp(iH)$. Anticipating the result, we start from the symmetric spaces $U(N)$, $U(N)/O(N)$ and $U(2N)/Sp(N)$ and consider elements iH of the corresponding tangent spaces (at the origin). Hamiltonians H with $iH \in \mathfrak{u}(N)$ are just arbitrary Hermitean random matrices and belong to the GUE, whereas Hamiltonians with $iH \in \mathfrak{u}(N) \setminus \mathfrak{o}(N)$ are real symmetric and therefore elements of the GOE. Finally, if $iH \in \mathfrak{u}(2N) \setminus \mathfrak{sp}(N)$, H is a real quaternion and, hence, belongs to the GSE. Here, the capital and small letters denote the standard Lie groups and corresponding Lie algebras, respectively. Thus, it turns out that random Hamiltonians belonging to one of the standard ensembles are just tangent vectors of the three symmetric spaces mentioned above³. In order to explore the physical significance of the other seven spaces we identify the symmetry of the corresponding tangent space elements and look for physical systems whose Hamiltonian is just subjected to such a symmetry. All ten symmetric spaces are listed in Tab. 2.1. The first column shows the denotations introduced by CARTAN and the second the structure of the symmetric space. The next four columns specify the realized symmetries. In the seventh column the corresponding random matrix ensembles are listed. The meaning of the last two columns is explained later. From now on we will use

¹For a definition and mathematical background on symmetric spaces cf. e.g. Ref. [64].

²For completeness we mention that there is one more if the dimension of the random matrix ensembles is odd.

³Note that so far there exists an obvious relation between both classification schemes. The symmetric spaces corresponding to the three Wigner-Dyson ensembles are just obtained by dividing off the diagonalizing groups from the unitary group. But it is not clear how to make further progress using the Wigner-Dyson scheme.

class	symmetric space (compact)	\mathcal{T}	sp	ch	p-h	RMT	M_B	M_F
A	$U(N)$	-	\pm	-	-	GUE	AIII	AIII
AI	$U(N)/O(N)$	+	+	-	-	GOE	BDI	CII
AII	$U(2N)/Sp(N)$	+	-	-	-	GSE	CII	BDI
$AIII$	$U(N+M)/U(N) \times U(M)$	-	\pm	+	-	chGUE	A	A
BDI	$SO(N+M)/SO(N) \times SO(M)$	+	+	+	-	chGOE	AI	AII
CII	$Sp(N+M)/Sp(N) \times Sp(M)$	+	-	+	-	chGSE	AII	AI
C	$Sp(N)$	-	+	-	+	N.N.	$DIII$	CI
CI	$Sp(N)/U(N)$	+	+	-	+	LOE	D	C
D	$SO(N)$	-	-	-	+	N.N.	CI	$DIII$
$DIII$	$SO(2N)/U(N)$	+	-	-	+	LSE	C	D

Table 2.1: The ten large families of Riemannian symmetric spaces (of compact type) and the corresponding symmetries (\mathcal{T} : time-reversal, sp: spin-rotational, ch: chiral, p-h: particle-hole) of their tangent spaces. The seventh column refers to the corresponding random matrix ensembles. The last two columns specify the structure of the bosonic and fermionic sector of the integration manifold of a corresponding non-linear σ -model. (adopted from Ref. [66])

CARTAN'S names for the symmetric spaces, also for the Wigner-Dyson symmetry classes.

Let us, as an example, consider the non-standard space $AIII$. Its tangent space is given by $u(2)/u(1) \times u(1)$. Using that the Lie algebra elements of the $U(2)$ are anti-Hermitian 2×2 matrices, $i \begin{pmatrix} a & c \\ c^* & b \end{pmatrix} \in u(2)$ (a, b real, c complex), we obtain the generators of the symmetric space to have the form $i \begin{pmatrix} 0 & c \\ c^* & 0 \end{pmatrix} \in u(2)/u(1) \times u(1)$. The generalization to an arbitrary $2N$ -dimensional matrix reads

$$iH = i \begin{pmatrix} 0 & h \\ h^\dagger & 0 \end{pmatrix} \in u(2N)/u(N) \times u(N), \quad (2.1)$$

where h is Hermitean. The block off-diagonal structure of H is equivalent to

$$[H, \sigma_3^{AB}]_+ = 0, \quad (2.2)$$

where σ_3^{AB} denotes the Pauli matrix w.r.t. the (so far not further specified) block structure of H . The symmetry Eq. (2.2) is well-known in QCD⁴ and denoted as *chiral symmetry*. Indeed, it also plays a role in the framework of mesoscopic systems, e.g. in the so-called *random flux model*, where time-reversal and spin rotational invariance is broken. Thus, it belongs to the class $AIII$. In a disordered system subjected to a imaginary vector potential the system is time-reversal and

⁴It turns out that in the eigenbasis of γ_5 the Dirac operator describing a Dirac fermion subjected to a random gauge field exhibits this symmetry in the massless limit.

spin-rotational invariant, additionally to the chiral symmetry. Hence such a system is a physical realization of the class $BD1$. Altogether, we get, as for the standard universality classes three classes with additional chiral symmetry. The corresponding random matrix ensembles are called *chiral GUE* (chGUE), *chiral GOE* (chGOE), and *chiral GSE* (chGSE) and have been discovered and investigated in the context of QCD [67,16]. The four remaining symmetry classes have been found to be relevant in the framework of normal conductor-superconductor systems (so-called NS-junctions) [68,69]. Instead of the chiral symmetry, Eq. (2.2), here a particle-hole symmetry occurs, $H = -\sigma_2^{\text{ph}} H^T \sigma_2^{\text{ph}}$, where H is the Gor'kov Hamiltonian and the Pauli matrix σ_2^{ph} acts in the particle-hole space. Considering the zero-dimensional limit one obtains four more related random matrix ensembles. Two of them have the specific denotation, LOE and LSE, where the "L" stands for Laguerre and the remaining two are nameless. The class C is realized in SN-junctions in the presence of a magnetic field, whereas the class of highest symmetry (among these four), CI , plays a role in dirty d -wave superconductors.

To summarize, we have seen that according to a new classification scheme the standard Wigner-Dyson random matrix ensembles have to be supplemented by seven non-standard classes. The new scheme is based on interpreting the ensembles over the tangent spaces of the large families of Riemannian symmetric spaces. As proven by CARTAN there are exactly ten (eleven, cf. footnote above) of these spaces. Comparing the symmetry of the corresponding random matrices to the symmetry of Hamiltonians of certain disordered systems realized in mesoscopic physics one finds that all ten universality classes are realized in the zero-dimensional limit. Furthermore, no other symmetry classes are known until now. Thus, if we believe the physics to conform to mathematics we should assume that all physical universality classes are discovered. This believe is far from being a proof and actually is not motivated very well. The reason is that the symmetric spaces on which the classification is based are mathematical objects which have no direct physical significance. Fortunately, this lack of motivation could be eliminated. In 1996 ZIRNBAUER proved that there exists a mapping from the ten random matrix ensembles (corresponding to the ten symmetric spaces) onto the ten families of Riemannian symmetric *superspaces* [66,68]. The latter ones turn out to be the integration manifolds of the low-energy sectors of supersymmetric effective field theories for disordered systems. These are just the supersymmetric NL σ Ms mentioned above, which EFETOV has derived for the standard symmetry classes A , AI , and AII . By the mapping onto the symmetric superspaces the relation between the original symmetric spaces and the physical universality classes becomes much closer, since the geometry of the integration manifolds is manifestly governed by the symmetry of the underlying Hamiltonians. It turns out that the manifolds consist of a non-compact *bosonic* sector M_B and a compact *fermionic* sector, M_F . These sectors have the same dimension

for all symmetry classes. In Tab. 2.1 the domains of integration are listed. In conclusion, we have given an overview about the symmetries of random matrix ensembles, which are able to describe the ergodic limit of disordered phase coherent electronic quantum systems. By mapping these systems onto a NL σ M their symmetry can be shown to be closely related to the ten Riemannian symmetric spaces, the random matrix ensembles are related to. It is believed that a complete classification of possible *physical* universality classes is given by the symmetric spaces. As already mentioned, once a non-linear σ -model is derived, it is possible to explore the behaviour of mesoscopic systems in arbitrary dimensions and all interesting regimes, at least in principle. Therefore, it is desirable to have also the NL σ Ms for the non-standard symmetry classes at hand. The motivation for the investigation of the corresponding physical systems is the existence of unusual and new physical behaviour as compared to the classes A, AI, and AII.

Part I

Density of States in quasi-1D Systems of AIII Symmetry

Chapter 3

Systems of AIII Symmetry

In Ch. 2 we have got to know the symmetry class AIII as one of seven novel, non-standard symmetry classes [66,69] realized in mesoscopic systems. Non-standard means that the symmetry classes differ from the three Wigner-Dyson universality classes of RMT, A (GUE), AI (GOE), and AII (GSE). This part of the thesis is dedicated to the investigation of the DoS for systems of AIII symmetry. In the present chapter we point out why it is worth while to do this. Therefore, we show how off-diagonal disorder is related to chiral symmetry and why this symmetry implies a special role of the energy in the middle of the tight-binding band. We further introduce the generalized random flux model as an important example of systems with AIII symmetry. In the second section we present some qualitative arguments for the non-trivial behaviour of the DoS in terms of Green functions.

3.1 Peculiarities of Chiral Symmetry

The early theory of localization in disordered electron system was substantially influenced by the introduction of the Anderson tight-binding model [8]. This model allows for nearest neighbour hopping, characterized by a fixed parameter t , and interaction with some random on-site potential, described by random energies ε_i . In the language of second quantization the Anderson tight-binding Hamiltonian writes

$$H^{\text{And}} = \sum_{\langle i,j \rangle} t c_i^\dagger c_j + \sum_i \varepsilon_i c_i^\dagger c_i, \quad (3.1)$$

where c_i is an electron field operator at site i and the notation $\langle i,j \rangle$ restricts the summation to all nearest neighbour sites. In a suited real-space basis the Anderson Hamiltonian can be represented by a tri-diagonal matrix, the fixed hopping matrix elements sitting on the left and right secondary diagonal and the

random energies being placed on the diagonal. This Hamiltonian as it stands models disordered systems of symmetry A . Demanding H^{And} to be symmetric we get a model for the class AI corresponding to time-reversal invariant disordered systems. If additionally scattering in the spin degrees of freedom is allowed one gets the Ando Hamiltonian [70], a tight-binding Hamiltonian which governs systems of AII symmetry. Thus, within the Anderson tight binding model mesoscopic systems corresponding to the three Wigner-Dyson universality classes can be investigated. According to the scaling theory of ABRAHAMS ET AL., in one or two dimensions, systems of A and AI symmetry show always localized behaviour, whereas for the class AII a localization-delocalization transition occurs. The latter is the subject of the second part of this thesis.

Later, the Anderson model was generalized to the case of *off-diagonal* disorder, thus providing additionally or exclusively the hopping matrix elements with some site dependent randomness keeping the on-site potential fixed in the second case. But no new behaviour was recovered, until one considered the random hopping without any on-site potential (cf. e.g. [11,12,71,72]). In this case one found in 1D in the middle of the tight-binding band singular behaviour of the DoS and anomalous behaviour of the conductance distribution. GADE and WEGNER [13–15] found analogous results in a 2D sublattice model. New insight was gained, when one realized that systems with purely off-diagonal disorder are intimately related to sublattices (or bipartite lattices) with a special symmetry [73–76]. Denoting the two species of a two-sublattice decomposition by "A" and "B", an off-diagonal Hamiltonian contains elements corresponding either to an A-B or to a B-A coupling. Consequently, in the sublattice, or AB representation the Hamiltonian turns out to be block-off-diagonal,

$$H = \begin{pmatrix} 0 & H_{AB} \\ H_{BA} & 0 \end{pmatrix}, \quad (3.2)$$

where $H_{BA} = H_{AB}^\dagger$. In Ch. 2 we had already seen that the off-diagonal form of the Hamiltonian is equivalent to *chiral* symmetry,

$$[H, \sigma_3^{\text{AB}}]_+ = 0. \quad (3.3)$$

Therefore, systems with purely off-diagonal disorder are typical systems of chiral symmetry. If no other symmetries as time-reversal or spin-rotational symmetry are present, the Hamiltonian falls into the symmetry class $AIII$. A famous example for such a Hamiltonian is given by the so-called *random flux model*,

$$H^{\text{RF}} = - \sum_{\langle i,j \rangle} c_i^\dagger e^{i\phi_{ij}} c_j, \quad (3.4)$$

describing electrons on a lattice subject to a strong perpendicular random magnetic flux. Here, the hopping matrix elements have an amplitude of unity. The

disorder is governed by the random phases, $\phi \in [0, 2\pi[$. Note, that the denotation "random flux model" actually is not correct. One should rather speak of a "random vector potential model". Indeed, there is a subtle difference, since a short range correlated magnetic field can imply long range correlations in the vector potential [77,78]. Nevertheless, we will use the more common term random flux model for the Hamiltonian Eq. (3.4). A related model is the so-called random hopping model, where randomness is implemented via *real* hopping matrix elements. This model, conserving time-reversal invariance, falls into the symmetry class *BDI*. Both, the random flux and the random hopping model have revealed renewed interest recently [21–29].

There exists a natural generalization of the random flux model. Note that due to the unity amplitude the hopping matrix elements can be considered to stem from the one-dimensional unitary group, $U(1)$. Grading the quantum mechanical states w.r.t. some inner degrees of freedom of dimension N , $c_i \rightarrow c_i^\alpha$, $\alpha = 1, \dots, N$, the generalization of Eq. (3.4) reads

$$H = - \sum_{\langle i,j \rangle} c_i^\dagger U_{ij} c_j, \quad (3.5)$$

where the matrices $U \in U(N)$ are homogeneously taken from the unitary group in N dimensions. This corresponds to a maximum of randomness and therefore to strong disorder. We will perform the analysis of the DoS for systems of AIII symmetry within the generalized random flux model Eq. (3.5). Recently, for this model a non-linear σ -model has been derived [22]. The derivation is outlined in Ch. 4. The investigations of the DoS will be based on this NL σ M.

Let us have a first look at the consequences of the chiral symmetry Eq. (3.3). Consider the Schrödinger equation corresponding to the chiral Hamiltonian Eq.(3.5), $H\psi_\epsilon = \epsilon\psi_\epsilon$, where ψ_ϵ is an eigenstate corresponding to the eigenenergy ϵ . Multiplying the equation by σ_3^{AB} we obtain from Eq. (3.3)

$$(\sigma_3^{\text{AB}} H \sigma_3^{\text{AB}})(\sigma_3^{\text{AB}} \psi_\epsilon) = \epsilon \sigma_3^{\text{AB}} \psi_\epsilon \quad (3.6)$$

$$\implies H \psi_{-\epsilon}^{\text{AB}} = -\epsilon \psi_{-\epsilon}^{\text{AB}}, \quad (3.7)$$

where $\psi_{-\epsilon}^{\text{AB}}$ denotes the "chiral transform" of ψ_ϵ , which is an eigenstate corresponding to the eigenenergy $-\epsilon$. In the sublattice representation the transformed state is given by

$$\psi_{-\epsilon}^{\text{AB}} = \sigma_3^{\text{AB}} \psi_\epsilon = \begin{pmatrix} \psi_{-\epsilon, \text{A}} \\ -\psi_{-\epsilon, \text{B}} \end{pmatrix}. \quad (3.8)$$

Thus, the eigenvalues of chiral Hamiltonians appear in pairs of opposite sign and therefore the spectrum is symmetric. This singles out the band center $\epsilon = 0$, and the question arises, whether this has an impact on the behaviour of physical quantities. The question is further motivated by the observation that in the standard symmetry classes the (averaged) spectrum is uniform. This uniformity is broken in the vicinity of $\epsilon = 0$.

3.2 Physics of the Random Flux Model

In this section we will argue that the DoS, having few structure in systems of standard symmetry, has the complexity of coupled Green functions in systems of chiral symmetry. We therefore give a short introduction to the role of Green function in mesoscopic physics.

The spectral and transport quantities relevant in mesoscopic systems can be expressed in terms of disorder averaged n -point Green functions. By this notion we mean expressions of the structure

$$\left\langle \prod_{m=1}^n G^\pm(\epsilon_m) \right\rangle,$$

where $G^\pm(\epsilon) = (\epsilon^\pm - H)^{-1}$ is the resolvent operator of the Hamiltonian H w.r.t. complex energy $\epsilon^\pm = \epsilon \pm i\gamma$ ($\gamma \in \mathbb{R}^+$). The brackets denote the average over all possible configurations of the disorder. Note that $G^-(\epsilon) = [G^+(\epsilon)]^\dagger$.

Let us introduce the real space representation of the Green function,

$$G^\pm(x_1, x_2; \epsilon) \equiv \langle x_1 | G^\pm(\epsilon) | x_2 \rangle,$$

and its Fourier transform $G^\pm(x_1, x_2; t)$. The relevance of Green functions for transport (or other) quantities in mesoscopic physics can be seen by recalling that $G^+(x_1, x_2; t)$ is nothing else than the *propagator* describing the motion from point x_2 to point x_1 within time t . This quantity contains a quantum mechanical phase factor, which depends very sensitively on the disorder configuration if $|x_2 - x_1| \gg l_e$. As a consequence, after averaging over the disorder the propagator decays exponentially on the length scale l_e ¹,

$$\langle G^\pm(x_1, x_2; t) \rangle \propto e^{-|x_2 - x_1|/2l_e}.$$

Using similar arguments we conclude that all n -point Green functions containing either $G^+(\epsilon)$ or $G^-(\epsilon)$ only drop down on the same length scale. Thus, we should not be surprised, that transport quantities or expressions they can be extracted from, consist of combinations of $G^+(\epsilon)$ and $G^-(\epsilon)$ that survive the disorder average on macroscopic length scales.

¹This result can be obtained by re-transforming the averaged momentum depending Green function $\langle G^\pm(k; \epsilon) \rangle = [\epsilon - \epsilon_k + i/(2\tau)]^{-1}$ into real space ($\epsilon_k = k^2/2m$). For the sake of completeness we mention here that this result is obtained by the approximation $(\epsilon\tau)^{-1} \ll 1$ and therefore valid only for weak disordered systems.

Let us consider the following examples:

- *diffusion modes* In the following expression the phase factors of the Green functions cancel each other by construction:

$$G^+(x_1, x_2; t)G^-(x_1, x_2; t) = |G^+(x_1, x_2; t)|^2.$$

Hence, this quantity survives the disorder average and corresponds to long-range modes, whose first perturbative contribution is called a *diffuson*.

- *density of states*

In terms of Green functions the DoS, $\nu(\epsilon) = \delta(\epsilon - H)$, can equivalently be expressed by

$$\begin{aligned} \rho(\epsilon) &= \frac{1}{2\pi i} \text{tr} (G^-(\epsilon) - G^+(\epsilon)) = -\frac{1}{\pi} \text{Im tr } G^+(\epsilon) \\ &= \frac{1}{\pi} \text{Im tr } G^-(\epsilon) = \frac{1}{\pi} \text{Im} \int d^d x \sum_k \frac{|\phi_k(x)|^2}{\epsilon - i\gamma - \epsilon_k}. \end{aligned} \quad (3.9)$$

In the last line we have performed an expansion in energy eigenfunctions $\phi_k(x)$ with corresponding eigenvalues $\epsilon_k = k^2/2m$. Due to the combination $\bar{\phi}_k(x)\phi_k(x)$ there is again no phase dependence by construction. The only effect caused by disorder is a broadening of the δ -peaks in the energy spectrum. After the disorder average we end up with the bulk DoS

$$\langle \rho(\epsilon) \rangle = \int d^d x \sum_k \frac{|\phi_k(x)|^2}{\epsilon - i/(2\tau) - \epsilon_k} = \rho_0.$$

- *two-level correlation function* The two-level correlation function is defined by

$$R_2(\omega) \equiv \Delta^2 \langle \rho(E + \frac{\omega\Delta}{2}) \rho(E - \frac{\omega\Delta}{2}) \rangle,$$

where ω is an energy shift in units of the mean level spacing $\Delta = 1/\rho_0$. This quantity measures the probability to find two levels with distance ω . Since levels become uncorrelated for large energy differences, $R_2(\omega)$ should approach unity for $\omega \rightarrow \infty$. In the diffusive regime, it turns out that the two-level correlation function for system of the symmetry class A is given by (cf. Ref. [79])

$$R_2(\omega) = 1 + \frac{1}{2\pi^2} \text{Re} \sum_{\mathbf{p}} \frac{1}{(\frac{D}{\Delta} \mathbf{p}^2 - i\omega)^2}, \quad (3.10)$$

whereas in the ergodic regime one obtains (cf. e.g. Refs. [55,62])

$$R_2(\omega) = 1 - \frac{\sin^2(\pi\omega)}{(\pi\omega)^2}. \quad (3.11)$$

Fig. 3.1 shows a plot of this function. Note that both expressions match together, which can be seen by calculating the zero-mode approximation of Eq. (3.10), i.e. considering only $\mathbf{p} = 0$, and the high energy asymptotics of Eq. (3.11), i.e. substituting the $\sin^2(\pi\omega)$ term by its period average $1/2$. In both cases we obtain

$$R_2^{0d, \omega \gg 1}(\omega) \simeq 1 - \frac{1}{2\pi^2} \omega^{-2}$$

Turning back to the DoS, we have seen that the lack of sensitivity to disorder as compared to the propagator, and the lack of energy level coupling as compared to the level-level correlation function makes the DoS of A , AI and AII system a less interesting quantity. It has no remarkable structure on energy scales below the Fermi energy. But as we have seen in the foregoing section a lot of hints have been given, that the DoS of systems with $AIII$ symmetry shows non-trivial behaviour at least in the middle of the tight-binding band. Therefore, the question arises, where the difference in the qualitative behaviour of the DoS stems from. It seems that there *are* quantum interference mechanisms involved in the expression for the $AIII$ DoS. Let us search for evidence for such a mechanism in terms of Green functions. We write the Green function in the sublattice representation according

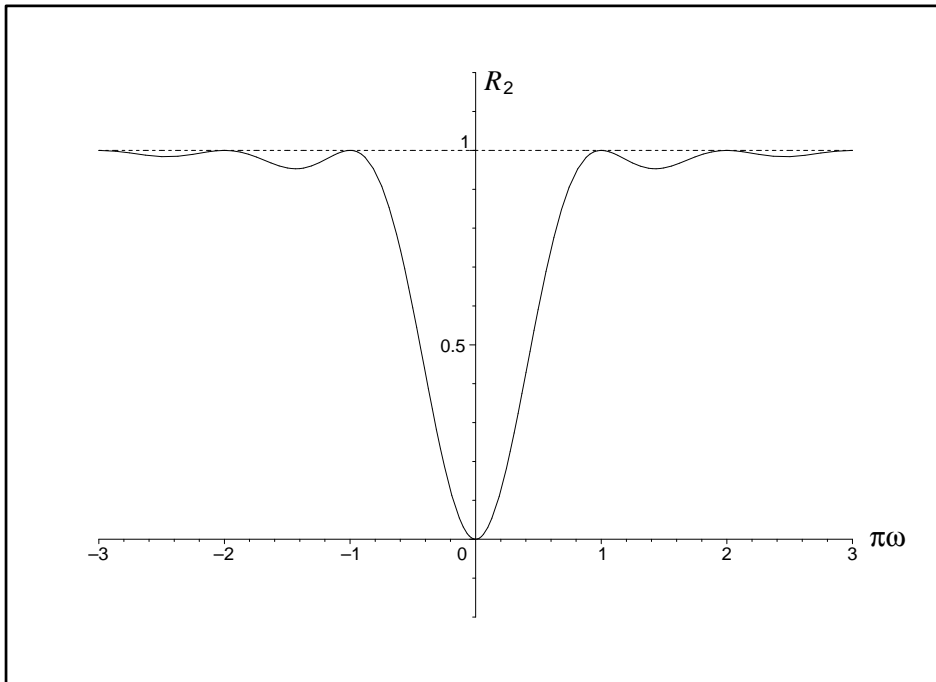


Figure 3.1: Two-level correlation function in the ergodic regime for the symmetry class A (GUE).

to Eq. (3.2). Then the chiral symmetry of the Hamiltonian Eq. translates to the relation

$$G^\pm(\epsilon) = -\sigma_3^{\text{AB}} G^\mp(-\epsilon) \sigma_3^{\text{AB}}.$$

Obviously, this symmetry is broken by a finite ϵ , which singles out the middle of the band. Particularly, we now have an argument for possible unusual behaviour of physical quantities at $\epsilon = 0$. Furthermore, by decomposing the sublattice Hamiltonians in Eq. (3.2), $H_{\text{AB}} = H_1 - iH_2$ and $H_{\text{BA}} = H_{\text{AB}}^\dagger$, with Hermitean operators H_1 and H_2 , we get

$$G^+(\epsilon) = U^\dagger \begin{pmatrix} g^+(\epsilon) & iH_2 \\ -iH_2 & -g^-(-\epsilon) \end{pmatrix}^{-1} U,$$

where $U = (1 + i\sigma_2)/\sqrt{2}$ and we have introduced the stochastic Green functions $g^+(\epsilon) \equiv (\epsilon^+ - H_1)^{-1}$ and $g^-(-\epsilon) \equiv (-\epsilon^- - H_1)^{-1}$. In order to calculate the DoS we invert the center matrix. The result is given by

$$\begin{aligned} 2\pi i\nu(\epsilon) &= \text{tr} (G^-(\epsilon) - G^+(\epsilon)) \\ &= \text{tr} g^-(\epsilon) + \text{tr} [(H_2 g^-(\epsilon))^2 (-g^+(-\epsilon)^{-1} - H_2 g^-(\epsilon) H_2)^{-1}] \\ &\quad + \text{tr} [-g^+(-\epsilon)^{-1} - H_2 g^-(\epsilon) H_2]^{-1} \\ &\quad - [g^+ \leftrightarrow g^-], \end{aligned} \tag{3.12}$$

where the notation $[g^+ \leftrightarrow g^-]$ means the exchange of g^+ and g^- in the terms in the second and third line. It turns out that the expression for the DoS of systems with AIII symmetry is much more complicated than that for the symmetry classes A, AI and AII. In order to become more concrete, we perform a geometric expansion for the term in the third line of Eq. (3.12) yielding

$$\text{tr} [-g^+(-\epsilon)^{-1} - H_2 g^-(\epsilon) H_2]^{-1} = -\text{tr} \left[g^+(-\epsilon) \sum_k (-1)^k (g^+(-\epsilon) H_2 g^-(\epsilon) H_2)^k \right].$$

Thus, we realize that in addition to the usual $\text{tr} g^\pm$ expressions we get terms that describe the *coupling* between the two auxiliary Green functions $g^+(-\epsilon)$ and $g^-(\epsilon)$ (and $[g^+ \leftrightarrow g^-]$) by means of H_2 . We therefore have an indication that the DoS of systems with AIII symmetry has much higher complexity than that of systems belonging to the standard symmetry classes. Finally, we notice that the energy arguments of the coupled Green functions differ in sign resulting in expressions similar to the two-level correlation function.

In conclusion, we have given some qualitative arguments for the non-trivial behaviour of the AIII DoS. Due to the chiral symmetry and the resulting sublattice structure the expression for this quantity contains *coupled* Green functions with different energy arguments. In the next chapter we prepare the investigation of the AIII DoS by the presentation of a corresponding non-linear σ -model.

Chapter 4

Non-linear σ -Model for Systems of AIII Symmetry

In the last chapter we have seen that n -point Green functions play a central role in the calculation of quantities relevant in condensed matter physics. Now, we will address the question how to obtain Green functions. One of the most powerful ways to do that is the use of field theoretical methods, namely the non-linear σ -model (NL σ M). Invented in the context of high energy physics its application to disordered systems has been fundamentally developed by SCHÄFER and WEGNER in 1980 [58] and later by EFETOV [59,80,81]. The former authors used the so-called replica trick whereas the latter one invented the supersymmetric version of the NL σ M. Both alternatives are able to describe the long-range physics of disordered systems with symmetry A , AI or AII . The originator is a Hamiltonian, whose matrix elements are drawn from a Gaussian random distribution (A , AI and AII just correspond to the Gaussian ensembles GUE, GOE and GSE, cf. Ch. 2). The derivation of a corresponding NL σ M involves a Hubbard-Stratonovich transformation, which can be applied only to systems with *Hermitean* disorder. But as we have pointed out in Ch. 3.1, in the random flux problem we have to deal with *unitary* disorder. It took more than ten years from the first formulation of the NL σ M until a Hubbard-Stratonovich decoupling scheme was found by ZIRNBAUER [65] in order to handle unitary disorder. This transformation applied to a related NL σ M in QCD effectively couples flavor degrees of freedom in favor of the decoupling of color degrees of freedom. Therefore, it has been christened the *color-flavor transformation*.

In the present chapter we outline the derivation of the supersymmetric NL σ M of the random flux problem given by ALTLAND and SIMONS in Ref. [22]. Originator is a supersymmetric generating functional for the n -point Green functions. Then, the average over the *unitary* disorder is performed by means of a color-flavor transformation. This transformation introduces an integral over supermatrices, which are coupled such a way that the theory remains sensitive to long-range

correlations. We calculate the saddle point and identify the saddle point manifold. Performing a gradient expansion and the continuum limit we finally end up with an effective long-range field theory, which will be our starting point for the calculation of the DoS.

4.1 Supersymmetric Generating Functional

The general idea of calculating n -point Green functions by means of field theory can be sketched in a few lines. Let us start with the real space representation of a Hamiltonian $H = \{H_{ij}\}$ on a d -dimensional lattice consisting of K sites. Let further $\hat{\epsilon}^+ = \text{diag}(\epsilon_1^+, \dots, \epsilon_n^+)$ be a diagonal matrix consisting of n independent complex energies ($\epsilon^+ \equiv \epsilon + i\gamma$), and $\{\psi_{i,m}\}, \{\bar{\psi}_{i,m}\}$ ($i = 1, \dots, K, m = 1, \dots, n$) arbitrary fields. For reasons we will point out later, we refer to the index m as *flavor degree of freedom*. Consider now the following Gaussian integral

$$\mathcal{Z}[J] = \int d[\psi, \bar{\psi}] e^{i\bar{\psi}(\hat{\epsilon}^+ \otimes \mathbb{1}_K + J - \mathbb{1}_n \otimes H)\psi}, \quad (4.1)$$

where $J = \text{diag}(J_1, \dots, J_n)$, and each J_m , ($m = 1, \dots, n$), is a arbitrary matrix on the lattice. The measure is given by $d[\psi, \bar{\psi}] = \prod_{i=1}^K \prod_{m=1}^n d\psi_{i,m} d\bar{\psi}_{i,m}$. Evaluating the integral yields the normalization factor

$$\mathcal{N} = \mathcal{Z}[0] = \begin{cases} \prod_{m=1}^n \det^{-1}(\epsilon_m^+ \mathbb{1}_K - H) & \text{for bosonic fields,} \\ \prod_{m=1}^n \det(\epsilon_m^+ \mathbb{1}_K - H) & \text{for fermionic fields.} \end{cases} \quad (4.2)$$

Bosonic fields take values in the complex numbers, whereas fermionic fields take values in the (anti-commuting) Grassmann variables (cf. [81,82]). Taking the derivative w.r.t. the source element $J_{m,ij}$ we get

$$\begin{aligned} \left. \frac{\delta \mathcal{Z}[J]}{\delta J_{m,ij}} \right|_{J=0} &= i \int d[\psi, \bar{\psi}] \psi_{i,m} \bar{\psi}_{j,m} e^{i\bar{\psi}(\hat{\epsilon}^+ \otimes \mathbb{1}_K - \mathbb{1}_n \otimes H)\psi} \\ &= \left(\frac{\mathcal{N}}{\epsilon_m^+ \otimes \mathbb{1}_K - H} \right)_{ji} = \mathcal{N} G_{ji}^+(\epsilon_m), \end{aligned} \quad (4.3)$$

or in general

$$\left. \frac{\delta^n \mathcal{Z}[J]}{\delta J_{1,i_1 j_1} \cdots \delta J_{n,i_n j_n}} \right|_{J=0} = \mathcal{N} \prod_{m=1}^n G_{j_m i_m}^+(\epsilon_m).$$

The determinants occurring in Eq. (4.3) make the outlined procedure quite useless, because they prohibit the applicability of the usual approximation schemes. Therefore we have to think about how to get rid of them. There are two ways to proceed. The first one is the so-called *replica trick* which will be explained

in Sec. 6.2.5. The second one is to use *supersymmetry*, which we will do in the following. The idea is quite simple. We combine bosonic and fermionic fields to *superfields*, $\psi \rightarrow \psi_a$ with $a \in \{\text{b}, \text{f}\}$, and also grade the matrices w.r.t. the boson-fermion space, $A \rightarrow A \otimes \mathbb{1}^{\text{bf}}$, where $\mathbb{1}^{\text{bf}}$ is the unity matrix in this superspace. Consequently, the normalization factors Eq. (4.2) that we get by Gaussian integration over the bosonic and fermionic sector cancel each other. Thus, each Gaussian superintegral with matrices which are block diagonal in superspace is automatically normalized to one (apart from a numerical constant in the integration measure).

We now turn to the non-Abelian generalization of the random flux problem. Since we are going to calculate the density of states we only need a one-point Green function. Thus, we consider from now on the special case $n = 1$ and suppress the flavor index. On the other hand, we have to grade the fields w.r.t. the dimension N of the general non-Abelian unitary disorder matrix, $U(N)$. We therefore introduce an upper index $\alpha \in \{1, \dots, N\}$, which we refer to as *color degree of freedom*, so that $\psi_i \rightarrow \psi_i^\alpha$ (and similar for $\bar{\psi}$). Furthermore, we grade the vectors in superspace. Hence the fields at any lattice site i are given by a supervector

$$\{\psi_{i,a}^\alpha\}_{\substack{a=\text{b},\text{f} \\ \alpha=1,\dots,N}} = \begin{pmatrix} \{S_i^\alpha\}_{\alpha=1,\dots,N} \\ \{\chi_i^\alpha\}_{\alpha=1,\dots,N} \end{pmatrix} \quad \text{and} \quad \{\bar{\psi}_{i,a}^\alpha\}_{\substack{a=\text{b},\text{f} \\ \alpha=1,\dots,N}} = \begin{pmatrix} \{\bar{S}_i^\alpha\}_{\alpha=1,\dots,N} \\ \{\bar{\chi}_i^\alpha\}_{\alpha=1,\dots,N} \end{pmatrix}, \quad (4.4)$$

respectively, where $\{S_i^\alpha\}_\alpha \in \mathbb{C}^N$, $\{\bar{S}_i^\alpha\}_\alpha$ is its complex conjugate and $\{\chi_i^\alpha\}_\alpha$ and $\{\bar{\chi}_i^\alpha\}_\alpha$ are independent N -dimensional vectors of Grassmann variables. With the Hamiltonian given by Eq. (3.5) we can now formulate the disorder averaged supersymmetric generating functional,

$$\langle \mathcal{Z}[J] \rangle = \left\langle \int d[\psi, \bar{\psi}] e^{-S[\psi, \bar{\psi}]} \right\rangle, \quad (4.5)$$

where the action is given by

$$\begin{aligned} S[\psi, \bar{\psi}] = & -i \sum_{\langle i \in A, j \in B \rangle} (\bar{\psi}_i U_{ij} \otimes \mathbb{1}^{\text{bf}} \psi_j + \bar{\psi}_j U_{ji}^\dagger \otimes \mathbb{1}^{\text{bf}} \psi_i) \\ & - i \sum_{k,l} \bar{\psi}_k (\epsilon^+ \delta_{kl} \mathbb{1}_N \otimes \mathbb{1}^{\text{bf}} + J_{kl} \mathbb{1}_N \otimes \sigma_3^{\text{bf}}) \psi_l, \end{aligned} \quad (4.6)$$

and the measure by

$$d[\psi, \bar{\psi}] = \prod_i \prod_{\alpha=1}^N dS_i^\alpha d\bar{S}_i^\alpha d\chi_i^\alpha d\bar{\chi}_i^\alpha.$$

The outer brackets in Eq. (4.5) denote the average over the unitary disorder,

$$\langle \dots \rangle \equiv \prod_{\langle i,j \rangle_{U(N)}} \int dU_{ij}(\dots), \quad (4.7)$$

where dU_{ij} denotes the Haar measure on $U(N)$. Note that for any pair of next neighbour lattice sites (i, j) , $i \in A$, $j \in B$ the disorder terms in Eq. (4.6) imply the following summations

$$\bar{\psi}_i U_{ij} \psi_j = \sum_{\alpha, \beta} \sum_{a=b, f} \bar{\psi}_{i,a}^{\alpha} U_{ij}^{\alpha\beta} \psi_{j,a}^{\beta}.$$

Finally, from

$$\begin{aligned} \left. \frac{\delta \mathcal{Z}}{\delta J} \right|_{J=0} &= i \int d[\bar{\psi}, \psi] \bar{\psi} \psi e^{-i\bar{\psi}[(H - \epsilon^+ \mathbb{1}_N) \otimes \mathbb{1}^{bf}] \psi} \\ &= i \text{sdet} [(H - \epsilon^+ \mathbb{1}_N) \otimes \mathbb{1}^{bf}]^{-1} \frac{2}{i(H - \epsilon^+ \mathbb{1}_N)} = -2(\epsilon^+ \mathbb{1}_N - H)^{-1} \\ &= -2G^+(\epsilon) \end{aligned}$$

we obtain the supersymmetric version of Eq. (4.3),

$$\langle G_{ji}^+(\epsilon) \rangle = -\frac{1}{2} \left. \frac{\langle \delta \mathcal{Z}[J] \rangle}{\delta J_{ij}} \right|_{J=0}. \quad (4.8)$$

4.2 Color-Flavor Transformation

The next step is to perform the average over the unitary disorder. This task can be handled by an identity which is called color-flavor transformation. It was introduced and proved by M.R. Zirnbauer [65]. Applied to a link (ij) this identity reads

$$\begin{aligned} \int_{U(N)} dU \exp \sum_{\alpha, \beta=1}^N \left(\sum_{a=b, f} \bar{\psi}_{i,a}^{\alpha} U_{ij}^{\alpha\beta} \psi_{j,a}^{\beta} + \sum_{b=b, f} \bar{\psi}_{j,b}^{\alpha} \bar{U}_{ji}^{\beta\alpha} \psi_{i,b}^{\beta} \right) \\ = \int d\mu_N(Z_{ij}, \tilde{Z}_{ij}) \exp \sum_{a, b=b, f} \left(\sum_{\alpha=1}^N \bar{\psi}_{i,a}^{\alpha} Z_{ij, ab} \psi_{i,b}^{\alpha} + \sum_{\beta=1}^N \bar{\psi}_{j,b}^{\beta} \tilde{Z}_{ij, ba} \psi_{j,a}^{\beta} \right), \end{aligned} \quad (4.9)$$

where $Z_{ij}, \tilde{Z}_{ij} \in \text{GL}(1|1)$ are 2×2 supermatrices which in boson-fermion decomposition can be written as

$$Z_{ij} = \begin{pmatrix} Z_{ij, bb} & Z_{ij, bf} \\ Z_{ij, fb} & Z_{ij, ff} \end{pmatrix} \quad \text{and} \quad \tilde{Z}_{ij} = \begin{pmatrix} \tilde{Z}_{ij, bb} & \tilde{Z}_{ij, bf} \\ \tilde{Z}_{ij, fb} & \tilde{Z}_{ij, ff} \end{pmatrix}.$$

The measure of integration is given by

$$d\mu_N(Z_{ij}, \tilde{Z}_{ij}) = \text{sdet}(1 - Z_{ij} \tilde{Z}_{ij})^N d[Z_{ij}, \tilde{Z}_{ij}],$$

where $D(Z_{ij}, \tilde{Z}_{ij})$ is the flat Berezin measure (cf. [81,82])

$$d[Z_{ij}, \tilde{Z}_{ij}] = \prod_{a,b=b,f} dZ_{ij,ab} d\tilde{Z}_{ij,ab}.$$

It turns out that the domain of integration on the right hand side of Eq. (4.9) is not the full supergroup $GL(1|1)$. It is rather restricted by some constraints. First of all, the eigenvalues of the Hermitean product matrix $Z_{bb}^\dagger Z_{bb}$ must be smaller than unity. Further, the bb-blocks of Z_{ij} and \tilde{Z}_{ij} are related by

$$\tilde{Z}_{ij,bb} = Z_{ij,bb}^\ddagger, \quad (4.10)$$

where the non-standard \ddagger -adjunction is for $Z_{ij,bb} \in GL(1)$ defined by¹

$$(e^{iy} e^x)^\ddagger \equiv (e^{-x} e^{iy}).$$

For the ff-blocks we have the more common anti-Hermitecity relation

$$\tilde{Z}_{ij,ff} = -Z_{ij,ff}^\dagger. \quad (4.11)$$

The bf and fb components consist of independent Grassmann variables. For more details the reader is referred to the original references [65,22]. Applying now the color-flavor transformation to the generating functional Eq. (4.5) we obtain

$$\begin{aligned} \langle \mathcal{Z}[J] \rangle = & \int d[Z, \tilde{Z}] \int d[\bar{\psi}, \psi] e^{N \sum_{\langle i \in A, j \in B \rangle} \text{str} \ln(1 - Z_{ij} \tilde{Z}_{ij})} e^{i \sum_{k,l} \bar{\psi}_k J_{kl} \mathbb{1}_N \otimes \sigma_3^{\text{bf}} \psi_l} \\ & \times e^{i \sum_{i \in A} \bar{\psi}_i (\epsilon^+ \mathbb{1}_N \otimes \mathbb{1}^{\text{bf}} + \sum_{j \in N_i} \mathbb{1}_N \otimes Z_{ij}) \psi_i} \\ & \times e^{i \sum_{j \in B} \bar{\psi}_j (\epsilon^+ \mathbb{1}_N \otimes \mathbb{1}^{\text{bf}} + \sum_{i \in N_j} \mathbb{1}_N \otimes \tilde{Z}_{ij}) \psi_j}, \quad (4.12) \end{aligned}$$

where we have already re-exponentiated the integration density². The set N_i (N_j) contains all nearest neighbour lattice sites of the site i (j). We should mention that the convergency of the Gaussian integral is not obvious, because the expression $\sum_{i \in A} \bar{\psi}_i (\epsilon^+ \mathbb{1}_N \otimes \mathbb{1}^{\text{bf}} + \sum_{j \in N_i} \mathbb{1}_N \otimes Z_{ij}) \psi_i$ and its analogue may have negative imaginary parts. But as is shown in Ref. [22] this problem can be solved by providing the complex energy with a finite instead of an infinitesimal imaginary part, i.e. we shift the energy deeply into the complex plane. Having integrated over the fields this shift can be redone. Keeping this subtle point in mind we now perform the integration and get

$$\begin{aligned} \langle \mathcal{Z}[J] \rangle = & \int d[Z, \tilde{Z}] X[J] e^{N \sum_{\langle i \in A, j \in B \rangle} \text{str} \ln(1 - Z_{ij} \tilde{Z}_{ij})} \\ & \times e^{-N \sum_{i \in A} \text{str} \ln(\epsilon^+ \mathbb{1}^{\text{bf}} + \sum_{j \in N_i} Z_{ij}) - N \sum_{j \in B} (\epsilon^+ \mathbb{1}^{\text{bf}} + \sum_{i \in N_j} \tilde{Z}_{ij})}, \quad (4.13) \end{aligned}$$

¹Note that $GL(1) = U(1) \times [GL(1)/U(1)] \cong U(1) \times \mathbb{R}^+$. Hence, the bb component of the supermatrices can be decomposed, $Z_{ij,bb} = e^{iy} e^x$ with $x \in \mathbb{R}^+$ and $y \in [0, 2\pi]$.

²Recall that for each supermatrix A we have $\text{sdet} A = \exp(\ln \text{sdet} A) = \exp(\text{str} \ln A)$.

where we have already re-exponentiated the occurring superdeterminants. The factor $X[J]$ results from an expansion of the source term in Eq. (4.12) up to some order in J .

At the end of this quite formal section let us extract the physical meaning of the color-flavor transformation. As can be seen from Eq. (4.9) this transformation does not only reduce the coupling between N^2 'color' degrees of freedom to the coupling of two 'flavor' degrees of freedom, which is convenient if $N \gg 1$. Rather, to each link (ij) a pair of matrices (Z_{ij}, \tilde{Z}_{ij}) is assigned, where the former one couples the flavor degrees of freedom at site i and the latter one those at site j . Thus, there is no coupling of fields at different sites. Since pairs of the type $\bar{\psi}_i \psi_i$ are not affected by mechanisms of quantum interference, the theory becomes able to describe long-range correlations, i.e. diffusion modes.

Until now we have performed exact calculations and transformations. But with regard to the str ln expressions in the action we now have to think about approximations.

4.3 Saddle Point Approximation

The standard method being applied at this stage is a saddle point approximation, i.e. the functional integral is subjected to the following manipulations. First, we determine the minimum of the action, the *saddle point*, which provides the main contribution to the functional integral, and identify the saddle point manifold. The knowledge of the latter enables us to divide the domain of integration into Goldstone (massless) modes and massive modes. Having performed a gradient expansion, i.e. expansion of the action around the saddle point up to quadratic order, and having integrated over the massive modes we perform a continuum limit. We end up with an effective long-range field theory describing the low-energy sector of the system. In the following we present only the main results of the program outlined above. For details cf. Ref. [22].

We start by determining the saddle point (Z_0, \tilde{Z}_0) , which can be found as solution of the saddle point equations

$$\left. \frac{\delta S[Z, \tilde{Z}]}{\delta Z_{ij}} \right|_{Z=Z_0, \tilde{Z}=\tilde{Z}_0} = 0 \quad \text{and} \quad \left. \frac{\delta S[Z, \tilde{Z}]}{\delta \tilde{Z}_{ij}} \right|_{Z=Z_0, \tilde{Z}=\tilde{Z}_0} = 0. \quad (4.14)$$

It turns out that the (spatially constant) saddle point is given by

$$Z_0 = \tilde{Z}_0 \simeq i\zeta \mathbb{1}^{\text{bf}},$$

where $\zeta \equiv (2d-1)^{-1/2}$. Since the symmetry of the action is spontaneously broken by the saddle point, there is a whole manifold of configurations, which solve the

Eqs. (4.14). For $z = 0$ the chiral symmetry implies the invariance of the functional integrals Eqs. (4.5) and (4.12) under the action of corresponding transformation groups on the fields $(\psi, \bar{\psi})$ and (Z, \tilde{Z}) , respectively. The saddle point manifold is now obtained as the action of these transformation groups on the saddle point (Z_0, \tilde{Z}_0) . A detailed analysis of the symmetries yields (cf. Ref. [22])

$$Z_{\text{SP}} = i\zeta g \quad \text{and} \quad \tilde{Z}_{\text{SP}} = i\zeta g^{-1},$$

where $g \in \text{GL}(1|1)$. The domain of integration in the functional integral Eq. (4.13) is given by the following parameterization

$$Z_{ij} = i\zeta P_{ij} g_{ij} \quad \text{and} \quad \tilde{Z}_{ij} = i\zeta g_{ij}^{-1} P_{ij},$$

where $g_{ij} \in \text{GL}(1|1)$ and $P_{ij} \in \text{GL}(1|1)$ represent the massless modes (Goldstone modes) and massive modes, respectively. Taking into account the geometry of the integration manifold, Eqs. (4.10) and (4.11), the corresponding restrictions for the Goldstone and massive modes are given by

$$\begin{aligned} g_{ij,\text{bb}} &\in \text{GL}(1)/\text{U}(1) = \mathbb{R}^+, & g_{ij,\text{ff}} &\in \text{U}(1), \\ P_{ij,\text{bb}} &\in \text{U}(1), & P_{ij,\text{ff}} &\in \text{GL}(1)/\text{U}(1) = \mathbb{R}^+. \end{aligned}$$

Since the Goldstone modes describe the low-energy content of the theory whereas the massive modes govern the short-range physics, we now proceed by approximating the generating functional Eq. (4.13) in favor of an effective long-range field theory. There are three contributions to the effective action. The *fluctuation action*, S_{fl} , comes from an expansion of the action for $z = 0$ and $P = \mathbb{1}$ up to quadratic order and hence describes the quadratic fluctuations of the Goldstone modes around the spatially constant saddle point manifold. The *energy action*, S_{ϵ} , represents the presence of finite energy arguments. The third contribution is unusual in the sense, that it does not exist in the analogous field theories for the symmetry classes A, AI and AII. It is a speciality of systems with chiral symmetry which we call *Gade term*, S_{Gade} , since it was first derived by GADE in Ref. [13]. This term describes the interaction between Goldstone modes and massive modes. After the quadratic approximation this part is integrated over the massive modes. There is another peculiarity of chiral systems. It turns out that for finite systems a boundary term exists, which has the relevance of a *topological term*, S_{top} , and therefore has to be taken into account at all length scales. We will see that the existence of this term is responsible for the even-odd effect of the DoS. Having derived these different parts of the low-energy action we perform a continuum limit and finally end up with the following effective long-range generating functional

$$\mathcal{Z}[J] = \int \mathcal{D}g e^{-S[g,J]} \quad (4.15)$$

with the effective action

$$S_{\text{eff}}[g, J] = S_{\text{fl}}[g] + S_{\epsilon}[g, J] + S_{\text{Gade}}[g] + S_{\text{top}}[g],$$

where the contributions are given by

$$S_{\text{fl}}[g] = - \int d^d r \frac{N}{8d} a^{2-d} \text{str}[\partial g \partial g^{-1}], \quad (4.16a)$$

$$S_{\epsilon}[g, J] = -i \int d^d r \frac{N(2d-1)^{1/2} a^{2-d}}{4da^2} \text{str}[(g + g^{-1})(\epsilon^+ \mathbb{1}^{\text{bf}} + J\sigma_3^{\text{bf}})], \quad (4.16b)$$

$$S_{\text{Gade}}[g] = - \int d^d r \frac{C}{16d} a^{2-d} \text{str}^2(g^{-1} \partial g), \quad (4.16c)$$

$$S_{\text{top}}[g] = \frac{N}{2d} \sum_{s_1, \dots, s_d=0,1} \prod_{i=1}^d (-1)^{(N_i+1)s_i} \text{str} \ln g(s_1 L_1, \dots, s_d L_d). \quad (4.16d)$$

Here a is the lattice spacing and C a numerical constant of the order of unity. L_i denotes the length of the (hypercubic) system in the i -th direction and N_i the number of lattice sites in that direction. The measure is given by $\mathcal{D}g \equiv \lim_{K \rightarrow \infty} \prod_{i=1}^K dg_i$, where dg_i is the invariant measure on the supergroup $\text{GL}(1|1)$ we will calculate in Sec. 4.4.2.

4.4 Non-linear σ -Model for a Wire of AIII symmetry

4.4.1 Natural Formulation

Since we want to calculate the DoS of a (thick) wire, we focus on a quasi-1D system of length L from now on. Recall that by definition the channels play the role of inner degrees of freedom which are homogeneously coupled. Therefore, we can now identify the color degrees of freedom, introduced as arbitrary inner degrees of freedom in Eq. (4.4) with the N_c channels of the quasi-1D system. Thus we have $N = N_c$. Averaging over the whole unitary group $U(N)$ in the generating functional (cf. Eq. (4.7)) reflects the equality of all channels. We get for the effective action

$$S_{\text{eff}}[g, J] = - \int_0^L d\lambda (F_{\text{fl}}[g] + F_{\epsilon}[g] + F_J[g] + F_{\text{Gade}}[g]) + S_{\text{top}}[g], \quad (4.17)$$

with

$$F_{\text{fl}}[g] = c_{\text{fl}} \text{str}(\partial g \partial g^{-1}), \quad (4.18a)$$

$$F_{\epsilon}[g] = i c_{\epsilon} \epsilon^+ \text{str}(g + g^{-1}), \quad (4.18b)$$

$$F_J[g] = i c_{\epsilon} \text{str}[(g + g^{-1}) J \sigma_3^{\text{bf}}], \quad (4.18c)$$

$$F_{\text{Gade}}[g] = c_{\text{Gade}} \text{str}^2(g^{-1} \partial g), \quad (4.18d)$$

where the coupling constants will be identified below. From Eq. (4.16d) we obtain

$$S_{\text{top}}[g] = c_{\text{top}} \begin{cases} \text{str} \ln g(0) - \text{str} \ln g(L/\xi) & \text{for } N_s \text{ even,} \\ \text{str} \ln g(0) + \text{str} \ln g(L/\xi) & \text{for } N_s \text{ odd,} \end{cases} \quad (4.19)$$

where N_s denotes the number of sites in the longitudinal direction. Assuming open boundary conditions, i.e. coupling the wire to metallic leads, we can rewrite this term as an integral over a total derivative:

$$S_{\text{top}}[g] = - \int_0^L d\lambda F_{\text{top}}[g(\lambda)] \quad (4.20)$$

with

$$F_{\text{top}}[g] = c_{\text{top}} \text{str}(g^{-1} \partial g) = c_{\text{top}} \partial \text{str} \ln g. \quad (4.21)$$

We then obtain from Eq. (4.17)

$$S_{\text{eff}}[g, J] = - \int_0^L d\lambda F_{\text{eff}}[g, J] \quad (4.22)$$

with the "effective Lagrangian"

$$F_{\text{eff}}[g, J] = F_{\text{fl}}[g] + F_{\epsilon}[g] + F_J[g] + F_{\text{Gade}}[g] + F_{\text{top}}[g]. \quad (4.23)$$

We finally turn to the identification of the coupling constants in Eqs. (4.16). Since the coupling constant of the energy term has to be proportional to the bulk DoS (per volume), $\nu_0 = \rho_0/L$, we get from Eq. (4.16b) $\nu_0 = N_c/(2\pi a)$ and therefore

$$c_{\epsilon} = \frac{\pi}{2} \nu_0 \quad (4.24)$$

The coupling constant of the fluctuation term is then given by $N_c a/8 = \nu_0 \pi a^2/4$. Note that $E_c \propto v_F l_e/L^2 \propto a^2/L^2$, which can be seen as follows. Averaging over the whole unitary group in Eq. (4.7) corresponds to strong disorder. The mean

free path is minimal, i.e. of the order of the lattice spacing, $l_e \propto a$. Further, we have $v_F \propto a$ which results from the fact that all energies are measured in terms of the hopping matrix elements. Consequently, we have (cf. Sec. 2.1)

$$\frac{4}{\pi}c_{\text{fl}} \simeq \nu_0 D = \nu_0 E_c L^2 = gL \simeq N_c l_e \simeq \xi \quad (4.25)$$

For the remaining two coupling constants we read off:

$$c_{\text{Gade}} = \frac{C}{16} \quad \text{and} \quad c_{\text{top}} = \frac{N_c}{2}. \quad (4.26)$$

4.4.2 Coordinates and Invariant Measure on $\text{GL}(1|1)$

In this section we calculate the invariant measure dg (Haar measure) of the supergroup $\text{GL}(1|1)$ occurring in the generating functional Eq. (4.15). For future calculations it turns out to be convenient to introduce the *polar decomposition*³ on $G = \text{GL}(1|1)$. Let $\mathcal{G} = \mathfrak{gl}(1|1)$ be the super Lie algebra of G . Let further H be an element of the Cartan subalgebra⁴ \mathcal{T} of \mathcal{G} , $H \in \mathcal{T} \subset \mathcal{G}$, and K an element of the complement of \mathcal{G} w.r.t. \mathcal{H} , $K \in \mathcal{G} \setminus \mathcal{T}$. Then, $a \equiv \exp H \in T$, where T is the Cartan subgroup of G and $k = \exp K$ is an element of the coset space G/T . With these settings we can represent an element g of G in the following way (cf. Ref. [82]):

$$g = kak^{-1} = e^K e^H e^{-K} \quad (4.27)$$

with

$$H = \begin{pmatrix} x & \\ & iy \end{pmatrix} \quad \text{and} \quad K = \begin{pmatrix} & \eta_1 \\ \eta_2 & \end{pmatrix}, \quad (4.28)$$

where the radial coordinates are $x \in \mathbb{R}$, $y \in [0, 2\pi]$ and the angular coordinates η_1 and η_2 are Grassmann variables⁵.

In order to calculate the invariant measure within the polar decomposition we calculate the invariant 2-form $-\text{str}[dgdg^{-1}]$ on $\text{GL}(1|1)$ and identify the components of the metric tensor \mathfrak{g} ,

$$\sum_{i,j} \mathfrak{g}_{ij} dv_i \otimes dv_j = -\text{str}[dgdg^{-1}] = \text{str}[(dgg^{-1})^2]$$

³As usual, the introduction of special coordinates is motivated by symmetries, which result in invariance properties w.r.t. transformations within certain coordinate submanifolds. Here, we will have to deal with quantities which are rotationally invariant in superspace.

⁴The Cartan subalgebra of an algebra \mathcal{G} is the maximal abelian subalgebra of \mathcal{G} .

⁵Actually, with these restrictions of x and y we represent elements of the maximally Riemannian super space, which is contained in G .

where $\{v_1, \dots, v_4\}$ stands for the coordinates $\{x, iy, \eta_1, \eta_2\}$. We start with the calculation of the expression $dg g^{-1}$,

$$\begin{aligned} dg g^{-1} &= dk k^{-1} + k da a^{-1} k^{-1} - k a k^{-1} d k a^{-1} k^{-1} = dK + da a^{-1} - a dK a^{-1} \\ &= dK + d(e^H) e^{-H} - e^H dK e^{-H} = dK + dH - e^{\text{ad } H} dK \\ &= \begin{pmatrix} 0 & d\eta_1 \\ d\eta_2 & 0 \end{pmatrix} + \begin{pmatrix} dx & 0 \\ 0 & i dy \end{pmatrix} \\ &\quad - \cosh \alpha(H) \begin{pmatrix} 0 & d\eta_1 \\ d\eta_2 & 0 \end{pmatrix} - \sinh \alpha(H) \begin{pmatrix} 0 & d\eta_1 \\ -d\eta_2 & 0 \end{pmatrix}. \end{aligned}$$

The complex functions $\alpha(H) = (x - iy)$ are the (positive) roots of \mathcal{G} , i.e. the eigenvalues of the adjoint action of \mathcal{T} on \mathcal{G} (cf. App. A). Taking the square yields

$$(dg g^{-1})^2 = \begin{pmatrix} dx & 0 \\ 0 & i dy \end{pmatrix} + (2 - 2 \cosh(x - iy)) \begin{pmatrix} d\eta_1 d\eta_2 & 0 \\ 0 & -d\eta_1 d\eta_2 \end{pmatrix},$$

and we obtain

$$\begin{aligned} \text{str} [(dg g^{-1})^2] &= dx dx - dy dy - 2(1 - \cosh(x - y))(d\eta_2 d\eta_1 - d\eta_1 d\eta_2) \\ &= dx dx - dy dy + 4 \sinh\left(\frac{x - y}{2}\right) (d\eta_2 d\eta_1 - d\eta_1 d\eta_2). \end{aligned}$$

Thus, the metric tensor is given by

$$\mathbf{g} = \begin{pmatrix} 1 & 0 & 0 & 0 \\ 0 & 1 & 0 & 0 \\ 0 & 0 & 0 & -4 \sinh^2\left(\frac{x - iy}{2}\right) \\ 0 & 0 & 4 \sinh^2\left(\frac{x - iy}{2}\right) & 0 \end{pmatrix},$$

which yields for the density

$$\mathcal{J}(x, iy) = \sqrt{\text{sdet } \mathbf{g}} = \frac{1}{4} \sinh^{-2}\left(\frac{x - iy}{2}\right). \quad (4.29)$$

Thus, up to an arbitrary constant the integration measure for the polar decomposition on the supergroup manifold is given by

$$dg = \mathcal{J}(x, iy) dx dy d\eta_1 d\eta_2 = \sinh^{-2}\left(\frac{x - iy}{2}\right) dx dy d\eta_1 d\eta_2. \quad (4.30)$$

4.4.3 Formulation in Terms of EFETOV'S Q -Matrices

It turns out that for perturbation theoretical calculations the representation of the long-range modes by elements $g \in \text{GL}(1|1)$ is not very convenient. The supermatrices Q used in the formulation of the A, AI, and AII NL σ M by EFETOV

[81] are more qualified for that task, although they are of a higher dimension⁶. The relation between the supergroup elements g and the coset space elements Q is pointed out in App. D. Furthermore, this appendix contains the detailed calculations for the translation of the terms in the action. Changing only the argument in the notation the result is

$$F_{\text{eff}}[Q, J] = F_{\text{fl}}[Q] + F_{\epsilon}[Q] + F_J[Q] + F_{\text{Gade}}[Q] + F_{\text{top}}[Q]$$

with

$$F_{\text{fl}}[Q] = \frac{1}{2}c_{\text{fl}} \text{str}(\partial Q \partial Q), \quad (4.31a)$$

$$F_{\epsilon}[Q] = ic_{\epsilon} \epsilon^+ \text{str}(Q \sigma_3^{\text{AB}}), \quad (4.31b)$$

$$F_J[Q] = ic_{\epsilon} \text{str}(Q \sigma_3^{\text{AB}} J \sigma_3^{\text{bf}}), \quad (4.31c)$$

$$F_{\text{top}}[Q] = -\frac{1}{2}c_{\text{top}} \text{str}(Q \partial Q \sigma_2^{\text{AB}}), \quad (4.31d)$$

$$F_{\text{Gade}}[Q] = \frac{1}{4}c_{\text{Gade}} \text{str}^2(Q \partial Q \sigma_2^{\text{AB}}). \quad (4.31e)$$

4.5 From the NL σ M to the DoS

In this section we present the general expressions for the disorder averaged DoS in terms of the quasi-1D NL σ M. From Eqs. (3.9), (4.8), and (4.22) we get

$$\begin{aligned} \langle \rho(\epsilon^+) \rangle &= -\frac{1}{\pi} \text{Im} \text{tr} \langle G^+(\epsilon) \rangle = -\frac{1}{\pi} \text{Im} \int_0^L d\lambda \langle G^+(\lambda, \lambda; \epsilon) \rangle \\ &= \frac{1}{2\pi} \text{Im} \int_0^L d\lambda \left. \frac{\delta \langle \mathcal{Z}[J] \rangle}{\delta J(\lambda, \lambda)} \right|_{J=0} \\ &= \frac{1}{2\pi} \text{Im} \int_0^L d\lambda \int \mathcal{D}g F_{J=1}[g(\lambda)] e^{\int_0^L d\lambda' F_{\text{eff}}[g']}, \end{aligned} \quad (4.32)$$

where the pre-exponential factor is given by Eq. (4.18c). The functional integral in the last line of Eq. (4.32) can be interpreted as the propagation from one end of the wire to the other with a break at λ , where the integration over the source term is performed. Thus, it is quite natural to split the functional integral into a right propagator Y_{R} , an integration over the source term at λ , and a left

⁶More specific, the Q -matrices for the unitary class (AI) introduced by EFETOV are graded w.r.t. the advanced-retarded space. There is no such grading in our case.

propagator Y_L ,

$$\langle \rho(\epsilon^+) \rangle = \frac{1}{2\pi} \text{Im} \int_0^L d\lambda \int dg Y_R(a; \lambda) F_{J=1}[g(\lambda)] Y_L(a; L - \lambda) \quad (4.33)$$

where

$$Y_R(a; \lambda) \equiv Y_R(a; 0, \lambda) \equiv \int_{g'(\lambda)=g} \mathcal{D}g' e^{\int_0^\lambda d\lambda' F_{\text{eff}}(g')}$$

and

$$Y_L(a; L - \lambda) \equiv Y_L(a; 0, L - \lambda) \equiv \int_{g'(0)=g} \mathcal{D}g' e^{\int_0^{L-\lambda} d\lambda' F_{\text{eff}}(g')} = \int_{g'(\lambda)=g} \mathcal{D}g' e^{\int_0^L d\lambda' F_{\text{eff}}(g')}. \quad (4.34)$$

The integration has to be performed over all $g'(\lambda')$ except $g = g'(\lambda' = \lambda)$, and in the last line we have made use of the translational invariance of the propagation along the disordered wire. From that fact one could also conclude that the differentiation between right and left propagation is only artificial. That this is not true can be seen by considering the topological term, Eq. (4.21). Integration over the length yields

$$\int_0^\lambda d\lambda' c_{\text{top}} \partial \text{str} \ln g = \frac{N_c}{2} [x - iy + 2\pi i n(0)] \quad (4.35a)$$

and

$$\int_\lambda^L d\lambda' c_{\text{top}} \partial \text{str} \ln g = -\frac{N_c}{2} [x - iy + 2\pi i n(L)] \quad (4.35b)$$

where $x \equiv x(\lambda)$, $y \equiv y(\lambda)$, and we have used that $x(0) = x(L) = 0$ for open boundary conditions and $y(L) = 2\pi n(L)$ as well as $y(0) = 2\pi n(0)$ with $n(L), n(0) \in \mathbb{Z}$. As a consequence, the topological term influences the periodicity properties of $Y_{R,L}(a; \lambda)$ w.r.t. the compact sector of the group manifold: While for an even number of channels the periodicity of $Y_{R,L}$ remains unaffected the propagator becomes *anti-periodic* in y if N_c is odd. Hence, it is just the topological term which is responsible for the even-odd effect mentioned in the introduction. Furthermore, we have anticipated by the notation that the right and left propagator have the property $Y_{R,L}(g; \lambda) = Y_{R,L}(kak^{-1}; \lambda) = Y_{R,L}(a; \lambda)$,

i.e. they are rotationally invariant in superspace and therefore depend only on elements a of the radial sector T of $GL(1|1)$.

In this section we have derived expressions for the DoS in terms of the $NL\sigma M$. Introducing certain propagators the functional integration has been reduced to a single integration over the supergroup manifold. In the next chapter we will address the question how to calculate these propagators.

Chapter 5

Derivation of the Heat Equation

In chapter 4 we have derived a formula for the DoS of systems with AIII symmetry in terms of a supersymmetric effective long-range generating functional. Further, we have introduced a pair of propagators which allows us to reduce the functional integration to a single integration over the corresponding supergroup manifold. The question arises to what extent calculation is simplified, because the problem of the complicated functional integration is only shifted to the determination of the propagators. At this point, we take advantage of the fact that we are dealing with a quasi-1D system. In contrast to higher dimensional systems, here we have a powerful tool, namely the so-called *transfer matrix method*, which is introduced in the first section. Using this method we can reduce the determination of the propagators to the solution of a partial differential equation involving some generalized *Laplacian*. The terms of this differential operator correspond to the various contributions to the action and are explicitly calculated in the second section. In the last section the complete generalized heat equation is presented and discussed qualitatively.

5.1 Transfer Matrix Method

In this section we outline the general concept of the transfer matrix method. Following the strategy of Ref. [83] we go back to the discrete version of the functional integral and divide a (sub-)system of length λ into N pieces of length $\varepsilon = \lambda/N$, cf. Fig. 5.1. Then with

$$g'(\lambda') \longrightarrow g'_i \equiv g'(i\varepsilon) \quad \text{and} \quad \partial_{\lambda'} g' \longrightarrow \frac{g'_{i+1} - g'_i}{\varepsilon}, \quad i = 0, \dots, N-1,$$

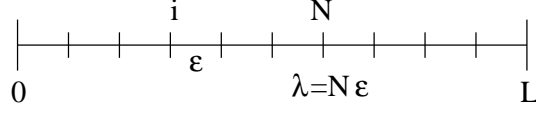


Figure 5.1: Discretization of the model

we have

$$\begin{aligned} \int_0^{\lambda+\varepsilon} d\lambda' F_{\text{eff}}[g'] &= \int_0^{\lambda} d\lambda' F_{\text{eff}}[g'] + \int_{\lambda}^{\lambda+\varepsilon} d\lambda' F_{\text{eff}}[g'] \\ &\rightarrow \varepsilon \sum_{i=0}^{N-1} F_{\text{eff}}[g'_i, g'_{i+1}; \varepsilon] + \varepsilon F_{\text{eff}}[g'_N, g'_{N+1}; \varepsilon], \end{aligned}$$

where $F_{\text{eff}}[g'_i, g'_{i+1}; \varepsilon]$ denotes the discretized form of the effective "Lagrangian", Eq. (4.23). Focusing on the right heat kernel for this chapter the change of $Y(a; \lambda) \equiv Y_{\text{R}}(a; \lambda)$ w.r.t. λ is given by

$$Y(g, \lambda + \varepsilon) - Y(g, \lambda) = \int dg' e^{\varepsilon F_{\text{eff}}[g', g; \varepsilon]} Y(g', \lambda) - Y(g, \lambda). \quad (5.1)$$

Here, we have relabeled $g'_N \rightarrow g'$ and $g'_{N+1} \rightarrow g$. Further, we have used the definition of $Y(a; \lambda)$ in Eq. (4.34). Introducing the polar decomposition (cf. Sec. 4.4.2) we get

$$g' = ka'k^{-1} = e^K e^{H'} e^{-K} \quad \text{and} \quad g = a = e^H, \quad (5.2)$$

where we have used that $S_{\mathfrak{h}}$ is invariant w.r.t. rotations of g . This can be seen as follows. With the above settings the discretized version of the fluctuation term Eq. (4.18a) is given by

$$F_{\mathfrak{h}} = c_{\mathfrak{h}} \text{str} (\partial g \partial g^{-1}) = c_{\mathfrak{h}} \text{str} [(g - g')(g^{-1} - g'^{-1})] = -c_{\mathfrak{h}} \text{str} [gg'^{-1} + g'g^{-1}].$$

Considering e.g. the term $\text{str}(g'g^{-1})$ and making the full ansatz $g' = \tilde{k}'a'\tilde{k}'^{-1}$ and $g = \tilde{k}^{-1}a\tilde{k}$ we get

$$\text{str}[(\tilde{k}'a'\tilde{k}'^{-1})(\tilde{k}^{-1}a^{-1}\tilde{k})] = \text{str}[ka'k^{-1}a^{-1}] = \text{str}[g'a^{-1}],$$

where we have set $k \equiv \tilde{k}\tilde{k}'$. Since large differences $g - g'$ are suppressed exponentially, we consider only small deviations δg from the maximum at $g'_{\text{max}} = g$. Thus, $H' = H + \delta H$ or in terms of the coordinates, $x' = x + \theta_x$ and $y' = y + \theta_y$, $dx' = d\theta_x$ and $dy' = d\theta_y$. The invariant measure is given by

$$dg' = \frac{1}{4} \mathcal{J}(\mathbf{x} + \boldsymbol{\theta}) d\theta_x d\theta_y d\eta_1 d\eta_2$$

with $\mathcal{J}(\mathbf{x})$ being the density, Eq. (4.29), $\mathbf{x} = (x, iy)$ and $\boldsymbol{\theta} = (\theta_x, i\theta_y)$. Expanding the right hand side of Eq. (5.1) up to linear order in ε we get a second order differential operator \mathfrak{L} which plays the role of a generalized *Laplacian*,

$$Y(\mathbf{x}; \lambda + \varepsilon) - Y(\mathbf{x}; \lambda) = \varepsilon \mathfrak{L}Y(\mathbf{x}; \lambda) + \mathcal{O}(\varepsilon^2).$$

Because of the rotational invariance of the heat kernel the Laplacian only depends on the radial coordinates and the derivatives w.r.t. them. Performing the continuum limit, $\varepsilon \rightarrow 0$, we obtain the partial differential equation

$$(\partial_\lambda - \mathfrak{L})Y(\mathbf{x}; s) = 0.$$

This differential equation has the formal structure of a diffusion or *heat equation*. Therefore, we will use this notion in the following. The propagator $Y(a; \lambda)$ determined by the heat equation acts as integral kernel in the theory of heat transport, which motivates the name *heat kernel*. Note that the procedure described above is quite similar to the derivation of the Schroedinger equation starting from Feynman's path integral formulation of quantum mechanics. The length of the quasi-1D wire plays the role of (imaginary) time, the heat kernel that of the quantum mechanical wave function and the heat equation corresponds to the Schroedinger equation.

5.2 Calculation of the Contributions

Now, we calculate the contributions to the Laplacian \mathfrak{L} , where we start with the term corresponding to $F_{\mathfrak{H}}[g]$. Containing a quadratic derivative this term yields expressions which are quadratic in the variables θ_x and θ_y . Thus, Eq. (5.1) becomes a Gaussian integral. The other terms are considered in combination with $F_{\mathfrak{H}}[g]$.

5.2.1 Laplacian corresponding to $F_{\mathfrak{H}}$

Let us consider $F_{\mathfrak{H}} = c_{\mathfrak{H}} \text{str}(\partial g \partial g^{-1})$. With the notation introduced in the previous section and in Sec. 4.4.2 we get

$$\begin{aligned} \text{str} \left[(g - g')(g^{-1} - g'^{-1}) \right] &= - \text{str} \left[gg'^{-1} + g'g^{-1} \right] \\ &= - \text{str} \left\{ \left[2 \cosh(\delta H) - e^{-\delta H} e^{-\text{ad} H} K - e^{\delta H} e^{\text{ad} H} K + \cosh(\delta H) K^2 \right] e^K \right\}. \end{aligned}$$

Expanding the exponential of the adjoint action according to Eq. (A.3)

$$\begin{aligned} e^{-\delta H} e^{-\text{ad} H} K + e^{\delta H} e^{\text{ad} H} K \\ = 2 [\cosh(\delta H) \cosh(x - iy) K + \sinh(\delta H) \sinh(x - iy) \sigma_3 K] \end{aligned}$$

we obtain

$$\begin{aligned} \text{str} \left[(g - g')(g^{-1} - g'^{-1}) \right] &= -4 \left\{ \frac{1}{2} (\cosh \theta_x - \cos \theta_y) \right. \\ &\quad \left. + \left[\cosh \left(\frac{\theta_x - i\theta_y}{2} \right) - \cosh \left(x + \frac{\theta_x}{2} - iy - i\frac{\theta_y}{2} \right) \right] \cosh \left(\frac{\theta_x + i\theta_y}{2} \right) \eta_1 \eta_2 \right\}. \end{aligned} \quad (5.3)$$

We now perform the integration over the Grassmann variables in Eq. (5.1). This yields a pre-exponential factor which equals $\mathcal{J}^{-1}(\mathbf{x} + \boldsymbol{\theta}/2)$ to quadratic order. Due to the normalization of the superintegral we can write

$$\begin{aligned} Y(\mathbf{x}; \lambda + \varepsilon) - Y(\mathbf{x}; \lambda) &= \frac{c_{\text{fl}}}{\varepsilon} \int \frac{d\boldsymbol{\theta}}{\pi} \frac{\mathcal{J}(\mathbf{x} + \boldsymbol{\theta})}{\mathcal{J}(\mathbf{x} + \boldsymbol{\theta}/2)} e^{-\frac{2c_{\text{fl}}}{\varepsilon} (\cosh \theta_x - \cos \theta_y)} [Y(\mathbf{x} + \boldsymbol{\theta}; \lambda) - Y(\mathbf{x}; \lambda)]. \end{aligned} \quad (5.4)$$

In the next step we expand both, the function in the exponent and the pre-exponential term to quadratic order in $\boldsymbol{\theta}$ yielding a Gaussian integral. The θ_y integration can then be extended over the whole real axis. Since ε is the width of the Gaussian integral the error we make within this approximation vanishes in the limit $\varepsilon \rightarrow 0$. With

$$\frac{\mathcal{J}(\mathbf{x} + \boldsymbol{\theta})}{\mathcal{J}(\mathbf{x} + \boldsymbol{\theta}/2)} \simeq 1 - \frac{1}{2} \coth \left(\frac{x - iy}{2} \right) (\theta_x - i\theta_y)$$

and

$$Y(\mathbf{x} + \boldsymbol{\theta}) = Y(\mathbf{x}) + \boldsymbol{\partial} Y(\mathbf{x}) \boldsymbol{\theta} + \frac{1}{2} \boldsymbol{\theta}^T \text{HY}(\mathbf{x}) \boldsymbol{\theta} + \mathcal{O}(\boldsymbol{\theta}^3),$$

where $\text{HY}(\mathbf{x})$ denotes the Hesse matrix of $Y(\mathbf{x})$, we obtain

$$\begin{aligned} Y(\mathbf{x}; \lambda + \varepsilon) - Y(\mathbf{x}; \lambda) &= \frac{c_{\text{fl}}}{2\varepsilon\pi} \int d\boldsymbol{\theta} \left[\theta_x^2 \partial_{xx}^2 + \theta_y^2 \partial_{yy}^2 - \coth \left(\frac{x - iy}{2} \right) (\theta_x^2 \partial_x - i\theta_y^2 \partial_y) \right] e^{-\frac{c_{\text{fl}}}{\varepsilon} \boldsymbol{\theta}^2} Y(\mathbf{x}; \lambda) \\ &= \varepsilon \mathcal{L}_{\text{fl}} Y(\mathbf{x}; \lambda). \end{aligned} \quad (5.5)$$

In the second line we have used that the integrals over mixed pre-exponential terms vanish. Performing the continuum limit we get

$$(\partial_\lambda - \mathcal{L}_{\text{fl}}) Y(\mathbf{x}; \lambda) = 0,$$

where the radial part of the Laplacian corresponding to the fluctuation action is given by

$$\mathcal{L}_{\text{fl}} = \frac{1}{4c_{\text{fl}}} \left[\partial_{xx}^2 + \partial_{yy}^2 - \coth \left(\frac{x - iy}{2} \right) (\partial_x - i\partial_y) \right] = \frac{1}{4c_{\text{fl}}} \mathbf{D}^2, \quad (5.6)$$

and $\mathbf{D} = (D_x, D_y)$ is the vector of the covariant derivatives

$$D_x = \partial_x - \frac{1}{2} \coth\left(\frac{x-iy}{2}\right) \quad \text{and} \quad D_y = \partial_y + \frac{i}{2} \coth\left(\frac{x-iy}{2}\right). \quad (5.7)$$

We would like to mention, that the Laplacian corresponding to the quadratic derivative term $F_{\mathfrak{fl}}[g]$ is just the radial part, i.e. the projection onto \mathcal{T} , of the Laplace-Beltrami operator on $\text{GL}(1|1)$,

$$\mathfrak{L}_{\mathfrak{fl}} = \mathfrak{L}^{\mathcal{T}} = \sum_{i=x,y} \mathcal{J}^{-1}(\mathbf{x}) \partial_i \mathcal{J}(\mathbf{x}) \partial_i. \quad (5.8)$$

5.2.2 Laplacian corresponding to $F_{\mathfrak{fl}} + F_{\epsilon}$

We additionally consider the energy term $F_{\epsilon}[g'] = ic_{\epsilon} \epsilon^+ \text{str}[g' + g'^{-1}]$. Since $g' \rightarrow g$ for $\epsilon \rightarrow 0$ we get

$$\begin{aligned} \text{str}(g' + g'^{-1}) &= \text{str}(a + a^{-1}) = \text{str}(e^H + e^{-H}) = 2 \text{str} \cosh H \\ &= 2 (\cosh x - \cos y). \end{aligned}$$

This expression does not depend on the integration variable. Expanding the exponential of this term up to linear order in ϵ we obtain from Eq. (5.5)

$$\begin{aligned} Y(\mathbf{x}; \lambda + \epsilon) &= \frac{c_{\mathfrak{fl}}}{\epsilon \pi} [1 + 2\epsilon c_{\epsilon} i \epsilon^+ (\cosh x - \cos y)] \int d\boldsymbol{\theta} \frac{\mathcal{J}(\mathbf{x} + \boldsymbol{\theta})}{\mathcal{J}(\mathbf{x} + \boldsymbol{\theta}/2)} Y(\mathbf{x} + \boldsymbol{\theta}) e^{-\frac{c_{\mathfrak{fl}}}{\epsilon} \boldsymbol{\theta}^2} \\ &= [\epsilon \mathfrak{L}_{\mathfrak{fl}} + 1 + 2\epsilon c_{\epsilon} i \epsilon^+ (\cosh x - \cos y)] Y(\mathbf{x}). \end{aligned}$$

Hence, we have $Y(\mathbf{x}; \lambda + \epsilon) - Y(\mathbf{x}; \lambda) = \epsilon \mathfrak{L}_{\mathfrak{fl}+\epsilon} Y(\mathbf{x}; \lambda)$ where the Laplacian corresponding to $F_{\mathfrak{fl}}$ and F_{ϵ} is given by

$$\mathfrak{L}_{\mathfrak{fl}+\epsilon} = \frac{1}{4c_{\mathfrak{fl}}} \mathbf{D}^2 + 2c_{\epsilon} i \epsilon^+ (\cosh x - \cos y). \quad (5.9)$$

5.2.3 Laplacian corresponding to $F_{\mathfrak{fl}} + F_{\text{top}}$

In order to implement the topological term $F_{\text{top}}[g] = c_{\text{top}} \text{str}(g^{-1} \partial g)$ into Eq. (5.4) we first note that

$$\begin{aligned} \text{str} [g'^{-1} (g - g')] &= \text{str} [a'^{-1} (a - a')] = \text{str} [e^{-H-\delta H} (e^H - e^{H+\delta H})] \\ &= \text{str}(e^{-\delta H}) = (e^{-\theta_x} - e^{-i\theta_y}) = -\theta_x + i\theta_y. \end{aligned} \quad (5.10)$$

Expanding again up to linear order in ε we obtain

$$\begin{aligned}
Y(\mathbf{x}; \lambda + \varepsilon) - Y(\mathbf{x}; \lambda) &= \frac{c_{\text{fl}}}{\varepsilon\pi} \int d\boldsymbol{\theta} \frac{\mathcal{J}(\mathbf{x} + \boldsymbol{\theta})}{\mathcal{J}(\mathbf{x} + \boldsymbol{\theta}/2)} e^{-\frac{c_{\text{fl}}}{\varepsilon}\boldsymbol{\theta}^2} e^{-c_{\text{top}}(\theta_x - i\theta_y)} [Y(\mathbf{x} + \boldsymbol{\theta}; \lambda) - Y(\mathbf{x}; \lambda)] \\
&= \varepsilon \mathfrak{L}_1 Y(\mathbf{x}; \lambda) - \frac{c_{\text{fl}}}{\varepsilon\pi} \int d\boldsymbol{\theta} e^{-\frac{c_{\text{fl}}}{\varepsilon}\boldsymbol{\theta}^2} c_{\text{top}}(\theta_x - i\theta_y) (\theta_x \partial_x + \theta_y \partial_y) Y(\mathbf{x}; \lambda) \\
&= \varepsilon \mathfrak{L}_{\text{fl}+\text{top}} Y(\mathbf{x}; \lambda).
\end{aligned}$$

where the Laplacian corresponding to F_{fl} and F_{top} is given by

$$\mathfrak{L}_{\text{fl}+\text{top}} = \frac{1}{4c_{\text{fl}}} \mathbf{D}^2 - \frac{1}{2} \frac{c_{\text{top}}}{c_{\text{fl}}} (\partial_x - i\partial_y) = \frac{1}{4c_{\text{fl}}} (\mathbf{D} - c_{\text{top}} \mathbf{A})^2, \quad (5.11)$$

with

$$\mathbf{A} \equiv \begin{pmatrix} 1 \\ -i \end{pmatrix}.$$

5.2.4 Laplacian corresponding to $F_{\text{fl}} + F_{\text{Gade}}$

Finally, we consider the fluctuation term together with the Gade term $F_{\text{Gade}}[g] = c_{\text{Gade}} \text{str}^2(g^{-1} \partial g)$. From Sec. 5.2.3 we obtain

$$\text{str}^2 [g'^{-1} (g - g')] = \text{str}^2 [a'^{-1} (a - a')] = (\theta_x - i\theta_y)^2. \quad (5.12)$$

From Eq. (5.4) we get the following expression for the heat kernel

$$Y(\mathbf{x}, \lambda + \varepsilon) = \frac{c_{\text{fl}}}{\pi\varepsilon} \int d\boldsymbol{\theta} e^{-\frac{1}{2}\boldsymbol{\theta}^T \mathbf{A} \boldsymbol{\theta}} \frac{\mathcal{J}(\mathbf{x} + \boldsymbol{\theta})}{\mathcal{J}(\mathbf{x} + \boldsymbol{\theta}/2)} [Y(\mathbf{x} + \boldsymbol{\theta}) - Y(\mathbf{x})], \quad (5.13)$$

where the matrix \mathbf{A} is given by

$$\mathbf{A} = \frac{2}{\varepsilon} (c_{\text{fl}} \mathbf{A}_1 + c_{\text{Gade}} \mathbf{A}_2)$$

with $\mathbf{A}_1 = \mathbb{1}$ and $\mathbf{A}_2 = (i\sigma_1 - \sigma_3)$. The determinant and the inverse are given by $\det \mathbf{A} = 4c_{\text{fl}}^2/\varepsilon^2$ and $\mathbf{A}^{-1} = \frac{\varepsilon}{2c_{\text{fl}}^2} (c_{\text{fl}} \mathbf{A}_1 - c_{\text{Gade}} \mathbf{A}_2)$, respectively. Expanding the

pre-exponential terms we obtain, using summation convention,

$$\begin{aligned}
Y(\mathbf{x}, \lambda + \varepsilon) &= \frac{c_{\text{fl}}}{\pi\varepsilon} \int d\boldsymbol{\theta} e^{-\frac{1}{2}\boldsymbol{\theta}^T \mathbf{A} \boldsymbol{\theta}} \frac{1}{2} [\partial_{ij}^2 Y(\mathbf{x}) \theta_i \theta_j + (\boldsymbol{\partial} \ln \mathcal{J} \cdot \boldsymbol{\theta}) (\boldsymbol{\partial} Y(\mathbf{x}) \cdot \boldsymbol{\theta})] \\
&= \frac{c_{\text{fl}}}{2\pi\varepsilon} \int d\boldsymbol{\theta} e^{-\frac{1}{2}\boldsymbol{\theta}^T \mathbf{A} \boldsymbol{\theta}} [\mathcal{J}^{-1} \partial_i (\mathcal{J} \partial_j Y(\mathbf{x})) \theta_i \theta_j] \\
&= \frac{c_{\text{fl}}}{2\pi\varepsilon} 2\pi \det \mathbf{A}^{-1/2} [\mathcal{J}^{-1} \partial_i (\mathbf{A}^{-1})_{ij} \mathcal{J} \partial_j] Y(\mathbf{x}) \\
&= \frac{\varepsilon}{4c_{\text{fl}}^2} [\mathcal{J}^{-1} \partial_i (c_{\text{fl}} \mathbf{A}_1 - c_{\text{Gade}} \mathbf{A}_2)_{ij} \mathcal{J} \partial_j] Y(\mathbf{x}) \\
&= \varepsilon \mathcal{L}_{\text{fl}} Y(\mathbf{x}) + \varepsilon \frac{c_{\text{Gade}}}{4c_{\text{fl}}^2} [\partial_i \partial_j + \mathcal{J}^{-1} (\partial_i \mathcal{J}) \partial_j] (\sigma_3 - i\sigma_1)_{ij} Y(\mathbf{x}) \\
&= \varepsilon \mathcal{L}_{\text{fl}+\text{Gade}} Y(\mathbf{x})
\end{aligned}$$

Since $\partial_y \mathcal{J} = -i\partial_x \mathcal{J}$, the terms linear in ∂_i cancel each other and we end up with

$$\mathcal{L}_{\text{fl}+\text{Gade}} = \frac{1}{4c_{\text{fl}}} \left[\mathbf{D}^2 + \frac{c_{\text{Gade}}}{c_{\text{fl}}} (\partial_x - i\partial_y)^2 \right]. \quad (5.14)$$

5.3 Discussion of the Generalized Heat Equation

After we have calculated the various contributions explicitly, we now combine all terms and obtain one of the main results, the generalized heat equation for systems of AIII symmetry,

$$(\partial_\lambda - \mathcal{L}) Y_{\text{R}}(\mathbf{x}; \lambda) = 0, \quad (5.15)$$

where the generalized Laplacian is given by

$$\mathcal{L} = \frac{1}{4c_{\text{fl}}} \left[(\mathbf{D} - c_{\text{top}} \mathbf{A})^2 + \frac{c_{\text{Gade}}}{c_{\text{fl}}} (\partial_x - i\partial_y)^2 \right] + 2ic_\varepsilon \varepsilon^+ (\cosh x - \cos y). \quad (5.16)$$

The heat equation Eq. (5.15) is subjected to the following constraints. As a partial differential equation it has to fulfill an initial condition. Let us consider the case where the wire is coupled to ideal leads. This corresponds to ideal sources/drains at its ends. According to Ref. [83] we get from Eqs. (4.34) and (5.3)¹

$$\lim_{\lambda \rightarrow 0} Y_{\text{R,L}}(\mathbf{x}, \lambda) = \delta(\mathbf{x}). \quad (5.17)$$

¹Note that

$$\lim_{\varepsilon \rightarrow 0} e^{\frac{c_{\text{fl}}}{\varepsilon} \text{str}[(g-g')(g^{-1}-g'^{-1})]} \longrightarrow \lim_{\varepsilon \rightarrow 0} e^{-\frac{c_{\text{fl}}}{\varepsilon} \text{str}(\cosh x - \cos y)}.$$

Further, the heat kernel has to be single-valued and therefore *periodic* w.r.t. the variable of the compact sector,

$$Y_{R,L}(x, iy; \lambda) = Y_{R,L}(x, i(y + 2\pi); \lambda). \quad (5.18)$$

As already mentioned at the beginning of this chapter the heat equation has the structure of an imaginary time Schroedinger equation. Since we know the explicit form of the Laplacian we can specify the formal analogies. The covariant derivative \mathbf{D} plays the role of the momentum and is responsible for the propagation in superspace. As we have seen in Eq. (5.8) the non-Euclidean structure of this term is directly related to the geometry of the integration manifold of the Goldstone fields, Eq. (4.30). However, it turns out that the non-Euclidean part of \mathfrak{L}_{fl} can be removed by applying a similarity transformation. Therefore, it is convenient to introduce new coordinates,

$$z = x + iy \quad \text{and} \quad \bar{z} = x - iy.$$

Using that $\partial_z = (\partial_x - i\partial_y)/2$ and $\partial_{\bar{z}} = (\partial_x + i\partial_y)/2$ the Laplacian reads

$$\mathfrak{L} = \frac{1}{c_{\text{fl}}} \left[\partial_{z\bar{z}} - \frac{\coth(\bar{z}/2)}{2} \partial_z - \frac{1}{2} c_{\text{top}} \partial_z + \frac{c_{\text{Gade}}}{c_{\text{fl}}} \partial_z^2 \right] + 4c_{\epsilon} i \epsilon^+ \sinh(z/2) \sinh(\bar{z}/2).$$

Consider the transformation

$$\mathfrak{L} \rightarrow \mathfrak{L}^{\text{E}} \equiv \mathcal{J}^{1/2}(\bar{z}) \mathfrak{L} \mathcal{J}^{-1/2}(\bar{z}), \quad (5.19)$$

where the "E" means Euclidean. With $\mathcal{J}(\bar{z}) = \sinh^{-2}(\bar{z}/2)$ we obtain

$$\mathfrak{L}_{\text{fl}}^{\text{E}} = \frac{1}{c_{\text{fl}}} \partial_{z\bar{z}} = \frac{1}{4c_{\text{fl}}} (\partial_{xx}^2 + \partial_{yy}^2), \quad (5.20)$$

i.e. the transformed Laplacian is indeed flat. In the complex coordinates it is to show that the other terms of \mathfrak{L} remain unchanged by the similarity transformation. Let us note that the procedure outlined above is not a special feature of our Laplacian. Rather, from the general theory of superanalysis (cf. [82]) it can be concluded that the similarity transformation Eq. (5.19) removes the terms of the (radial part of the) Laplace-Beltrami operator, which contain first order derivatives. Instead of this an effective potential occurs which is constant in the case of Lie supergroups. Furthermore, if the even and the odd sector of the supergroup have the same dimension, as is the case of $\text{GL}(1|1)$, this potential vanishes. The general form of the effective potential is calculated in App. B. Applying the similarity transformation Eq. (5.19) to the heat equation we get for the corresponding transformation of the heat kernel

$$Y_{R,L} \rightarrow \Psi_{R,L} \equiv \mathcal{J}^{1/2} Y_{R,L},$$

where we have omitted the arguments for notational transparency. It is important to note, that the periodicity of $Y_{R,L}$ w.r.t. y has changed to *anti-periodicity* of $\Psi_{R,L}$.

Let us now discuss the influence of the topological term. As already suggested by the notation, F_{top} results in a term \mathbf{A} analogous to a vector potential in the Schroedinger equation. Since \mathbf{A} is constant in superspace we can remove it by a gauge transformation of the heat kernel,

$$\Psi_{R,L} \rightarrow e^{\mp \frac{N_c}{2}(x-iy)} \Psi_{R,L} = \begin{cases} \Phi^e & \text{for } N_c \text{ even,} \\ \Phi^o & \text{for } N_c \text{ odd.} \end{cases} \quad (5.21)$$

Note that this relation is compatible with our previous findings, Eq. (4.35b). Particularly, it follows that there is no difference between a right and a left heat kernel any more. This is clear, since the absence of the vector potential corresponds to the absence of the topological term which just caused this difference. The crucial point is that the gauge transformation affects the periodicity properties depending on N being even (e) or odd (o). For an even number of channels the transformed function Φ^e fulfills the same anti-periodicity requirement as $\Psi_{R,L}$, whereas in the case of odd N_c the gauge transformed function sustains a repeated change and becomes a periodic function of y . While this discrimination was automatically included in $Y_{R,L}$ and $\Psi_{R,L}$ by the existence of the $e^{\pm \frac{N_c}{2}(x-iy)}$ term we now have to tag it explicitly by the superscripts "e" and "o". The transformed functions $\Phi^{e,o}(\mathbf{x}; \lambda)$ fulfill the heat equation

$$(\partial_\lambda - \mathfrak{L}^{\text{E,g}})\Phi^{e,o}(\mathbf{x}; \lambda) = 0,$$

where the similarity and gauge transformed Laplacian is given by

$$\mathfrak{L}^{\text{E,g}} = \frac{1}{4c_{\text{fl}}} \left(\partial_x^2 + \partial_y^2 + \frac{c_{\text{Gade}}}{c_{\text{fl}}} (\partial_x - i\partial_y)^2 \right) + 2ic_\epsilon \epsilon^+ (\cosh x - \cos y). \quad (5.22)$$

The differential equation Eq. (5.22) as it stands can not be solved analytically. The next step one could try is a solution of the problem in Fourier space. Thus, we expand the heat kernel in terms of eigenfunctions of the Laplacian. Let us for the time being neglect the impact of the topological term and the Gade term on the Laplacian. Let us further set $\epsilon = 0$, i.e. consider the heat equation corresponding to the Laplacian $\mathfrak{L}_{\text{fl}} = \frac{1}{4c_{\text{fl}}} \mathbf{D}^2$. Introducing the dimensionless length variable $s = L/\xi$ for convenience and using that $c_{\text{fl}} \propto \xi$ we get

$$\partial_s Y_{\epsilon=0}(\mathbf{x}; s) = \mathfrak{L}_{\text{fl}} Y_{\epsilon=0}(\mathbf{x}; s) \quad (5.23)$$

and the corresponding eigenvalue problem

$$\mathfrak{L}_{\text{fl}} \phi_\kappa(\mathbf{x}) = \beta_\kappa \phi_\kappa(\mathbf{x}), \quad (5.24)$$

where β_κ are the eigenvalues and κ stands for the variables in Fourier space. The eigenfunction decomposition of the initial condition is then given by

$$\delta(\mathbf{x}) = \int_{\kappa} \delta_\kappa \phi_\kappa(\mathbf{x}), \quad (5.25)$$

where \int_{κ} is a shorthand for the Fourier integration or summation. For the Fourier representation of the heat kernel we get

$$Y_{\mathfrak{H}}(\mathbf{x}; s) = \int_{\kappa} \delta_\kappa \phi_\kappa(\mathbf{x}) e^{-\beta_\kappa s}. \quad (5.26)$$

Although this approach is standard it turns out that we can not proceed. The reason is that Fourier transforming the delta function defined by Eq. (5.17) we get zero. This unusual behaviour results from the fact that $\delta(\mathbf{x})$ projects onto the origin of the supergroup if integrated with the measure dg , $\int dg \delta(\mathbf{x}) f(\mathbf{x}) = f(0)$. As a consequence of the perfect supersymmetry (equal number of commuting and Grassmann variables) the delta function Eq. (5.17) contains no normalization factor². Thus, the corresponding space is effectively zero-dimensional. Trying to Fourier transform this function on the two-dimensional radial sector of the supergroup results in an integral over an function of zero support, just yielding zero. We can find a remedy by the following modification [84]. Consider $\tilde{Y}_{\mathfrak{H}}(\mathbf{x}; s) \equiv Y_{\mathfrak{H}}(\mathbf{x}; s) - 1$ instead of $Y_{\mathfrak{H}}(\mathbf{x}; s)$. The heat kernel $\tilde{Y}_{\mathfrak{H}}$ also fulfills the heat equation, Eq. (5.23), but obeys the modified initial condition

$$\lim_{s \rightarrow 0} \tilde{Y}_{\mathfrak{H}}(\mathbf{x}; s) = -1. \quad (5.27)$$

The Fourier decomposition of the modified heat kernel is given by

$$\tilde{Y}_{\mathfrak{H}}(\mathbf{x}; s) = - \int_{\kappa} \mathbb{1}_\kappa \phi_\kappa(\mathbf{x}) e^{-\beta_\kappa s}, \quad (5.28)$$

where

$$\mathbb{1}_\kappa = \int d\mathbf{x} \mathcal{J}(\mathbf{x}) \bar{\phi}_\kappa(\mathbf{x}). \quad (5.29)$$

For the calculation of the eigenfunctions it is convenient to perform the similarity transformation Eq. (5.19) to Eq. (5.24). Then, evaluating $\mathbb{1}_\kappa$ we can solve the heat equation Eq. (5.23) in a small distance expansion, i.e. for $s \ll 1$. With H given by Eq. (4.28) and recalling that the dimensionless conductance is given by $g = \xi/L = 1/s$ it turns out that $Y(\mathbf{x}; s) \simeq 1 + \frac{1}{4s} \text{str} H^2 = 1 + g \text{str} H^2$. This is (apart from a sign) in agreement with a quite general calculation of the expansion of the heat kernel in powers of H [83].

²Recall that the cancellation of normalization factors is one of the most important properties of Gaussian superintegrals.

Chapter 6

Calculation of the DoS and Discussions

After the preparations we have made in the last chapters we are now able to start the investigations of the AIII DoS. In particular, with the heat equation derived in Ch. 5 we now have a tool at hand, which allows us to study the DoS of quasi-1D chiral systems on all relevant energy scales (cf. Sec. 2.1). Nevertheless, we will perform our calculations in the ergodic in diffusive regime without the aid of the heat kernel, the reason being that in these regimes the solution of the partial differential equation is not easier than starting directly from the NL σ M action. More concrete, the calculation in the ergodic regime is simplified by the fact that the fields can be assumed to be spatially constant. As a result it turns out that in this zero-dimensional limit the DoS reproduces results known from chiral RMT. Turning to the diffusive regime, the generic field of application of diagrammatic perturbation theory, actually no field theory is needed. But as we will see, the NL σ M allows for an elegant calculation of the loop contributions. Finally, in the last section we enter the localized regime $L \gg \xi$, which is manifestly non-perturbative. At this stage, where all other methods fail, the heat equation comes into operation. We will solve the heat equation and derive analytical expressions for the DoS on energy scales $\epsilon \ll \Delta_\xi$. As one of the main results we obtain the DoS to depend drastically on the parity of the channel number.

6.1 Ergodic Regime

Let us start our investigation of the DoS within the ergodic regime. Assuming that the localization length ξ is much larger than the length of the wire L the electrons cross the system very often. Thus, the ergodic regime is characterized by $\Delta \ll E_c$ and $\epsilon \ll E_c$ or, equivalently, times exceeding the diffusion time very much. We can imagine this case to be realized by very small systems (cf. Sec. 2.1).

As a consequence, the supermatrix fields $g(\lambda)$ of the σ -model action fluctuate only very slowly over the system length and hence can be treated as constant. Expressed in terms of Fourier modes in momentum space the ergodic regime corresponds to the *zero-mode approximation*.

6.1.1 Exact Calculation

Consider the general expression for the DoS given by Eq. (4.32). Within the zero-mode approximation the terms of the action containing derivatives, i.e. S_{fl} and S_{Gade} , can be neglected. Note, that this is not true for the topological term. Since we are dealing with very small systems we have to consider the global form $S_{\text{top}}[g]$ given by Eq. (4.19). Further, the fields are assumed to be independent of the length variable λ . We then obtain

$$\begin{aligned} \langle \rho_{0D}(\epsilon^+) \rangle &= \frac{L}{2\pi} \text{Im} \int dg F_{J=1}[g] e^{-(S_{\epsilon}[g] + S_{\text{top}}[g])} \\ &= \frac{L}{2\pi} \text{Im} \int dg F_{J=1}[g] e^{i\pi\rho_0\epsilon^+(\cosh x - \cos y)} f_{\text{top}}(x, y), \end{aligned} \quad (6.1)$$

where from Eq. (4.19) we get

$$f_{\text{top}}(x, y) = \begin{cases} 1 & \text{for } N_s \text{ even} \\ e^{-N_c(x-iy)} & \text{for } N_s \text{ odd.} \end{cases}$$

Alternatively, we could have started from the heat equation Eq. (5.15). Since $c_{\text{fl}} \propto E_c/\Delta$ and $c_{\epsilon} \propto \epsilon/\Delta$, the first term of Eq. (5.16) can be neglected. Hence, we end up with a simple ordinary differential equation for the heat kernel

$$\partial_{\lambda} Y(\mathbf{x}; \lambda) = i\pi\rho_0\epsilon^+(\cosh x - \cos y).$$

As can be seen easily, the product $Y(\mathbf{x}; \lambda)Y(\mathbf{x}; L - \lambda)$, which enters the formula for the DoS, Eq. (4.33), just reproduces the exponential function in Eq. (6.1).

In the next step we calculate the pre-exponential term $F_{J=1}[g]$ using the polar decomposition Eq. (4.27),

$$F_{J=1}[g] = ic_{\epsilon} \text{str}[(g + g^{-1})\sigma_3^{\text{bf}}] = ic_{\epsilon} \text{str}[(a + a^{-1})k^{-1}\sigma_3^{\text{bf}}k].$$

With

$$k^{-1}\sigma_3^{\text{bf}}k = \begin{pmatrix} 1 & 0 \\ 0 & -1 \end{pmatrix} + 2 \begin{pmatrix} 0 & \eta_1 \\ -\eta_2 & 0 \end{pmatrix} + 2 \begin{pmatrix} \eta_1\eta_2 & 0 \\ 0 & \eta_1\eta_2 \end{pmatrix},$$

we obtain

$$\text{str}[(g + g^{-1})\sigma_3^{\text{bf}}] = 2 [\cosh x + \cos y] + 4 [\cosh x - \cos y] \eta_1\eta_2.$$

Substituting this expression into Eq. (6.1) yields

$$\langle \rho_{0D}(\epsilon^+) \rangle = \frac{\rho_0}{2} \text{Im} i \int dg \left[(\cosh x + \cos y) + 2 (\cosh x - \cos y) \eta_1 \eta_2 \right] \\ \times e^{i\pi\rho_0\epsilon^+(\cosh x - \cos y)} f_{\text{top}}(x, y).$$

The integral over the first contribution contains no Grassmann variables but diverges at the origin o of the supergroup caused by the integration density. By a theorem of superanalysis (cf. Ref. [81]) the integral is given by the value of the integrand at $g = o$,

$$\frac{\rho_0}{2} \text{Re} \int dg (\cosh x + \cos y) e^{i\pi\rho_0\epsilon^+(\cosh x - \cos y)} = \rho_0. \quad (6.2)$$

Integrating the second contribution over the Grassmann variables we get for the total expression

$$\langle \rho_{0D}(\omega) \rangle = \rho_0 \left(1 + \frac{1}{8\pi} \text{Re} \int_{-\infty}^{\infty} dx \int_0^{2\pi} dy \frac{\cosh x - \cos y}{\sinh^2\left(\frac{x-iy}{2}\right)} e^{i\pi\omega^+(\cosh x - \cos y)} f_{\text{top}}(x, y) \right), \quad (6.3)$$

where we have introduced $\omega^+ \equiv \epsilon^+/\Delta = \epsilon^+\rho_0$ and the limit $\gamma \rightarrow 0$ is implicitly taken on the left hand side. The detailed calculation is presented in App. C for $\omega > 0$. Making use of the fact, that the energy spectrum is symmetric w.r.t. $\omega = 0$, the $0D$ DoS for an even number of sites is given by

$$\langle \rho_{0D}(\omega) \rangle = \frac{\pi^2}{2} \rho_0 |\omega| [J_0^2(\pi\omega) + J_1^2(\pi\omega)], \quad (6.4)$$

whereas for an odd number of sites and $N_c = 1$ we obtain

$$\langle \rho_{0D}(\omega) \rangle = \frac{\pi^2}{2} \rho_0 |\omega| [J_1^2(\pi\omega) - J_0(\pi\omega)J_2(\pi\omega)]. \quad (6.5)$$

A plot of both functions is shown in Fig. 6.1. The result is exact in the sense that it holds for all energy scales provided that $\epsilon \ll E_c$. Particularly, we notice that the zero-mode DoS resolves fluctuations on the scale of the mean level spacing Δ . Furthermore, for $\omega \rightarrow 0$ it drops down to zero, where an expansion of the Bessel functions yields for an even number of sites $\langle \rho_{0D}^{\omega \ll 1}(\omega) \rangle \simeq \rho_0 \omega$ whereas for odd N_s we get $\langle \rho_{0D}^{\omega \ll 1}(\omega) \rangle \simeq \rho_0 \omega^3$. It is remarkable that the DoS looks quite similar to the level-level correlation function for the symmetry class A plotted in Fig. 3.1. This results from the fact that the $AIII$ DoS has the complexity of coupled Green functions (cf. Eq. (3.12)).

Eqs. (6.4) and (6.5) reproduce calculations of the density of states within chiral RMT [16,17,67,85]. Cf. Ref. [86] for an overview. This is not surprising, since the

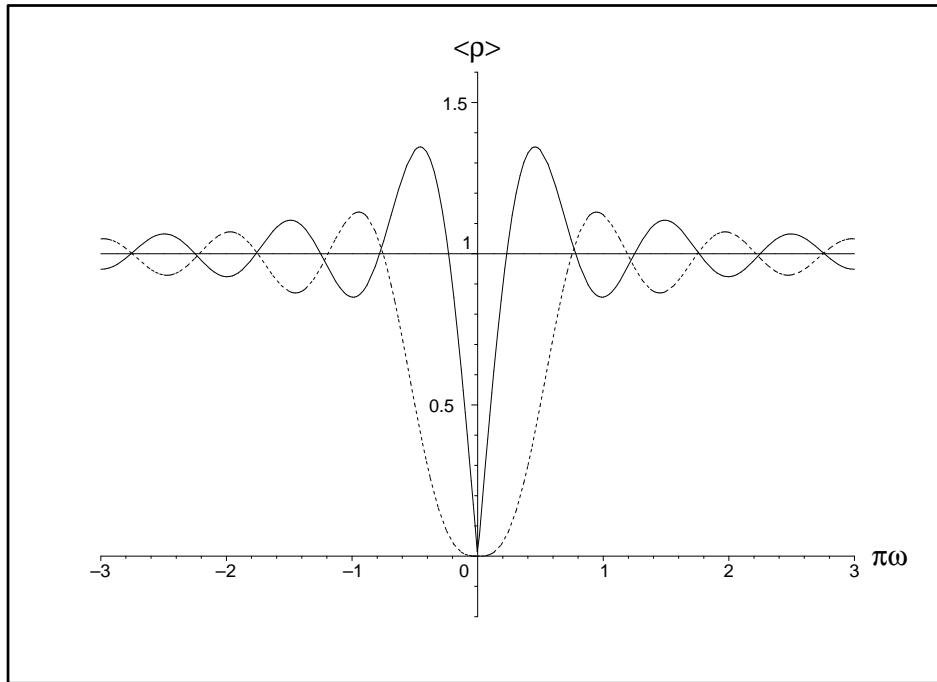


Figure 6.1: Plot of the average DoS in the ergodic regime for an even number of sites (solid curve) and an odd number of sites (dotted curve) ($\rho_0 = 1$).

zero-dimensional limit contains no information about microscopic details or the geometry of the system but is merely influenced by global symmetries. Note that this is not absolutely correct. In contrast to systems of standard symmetry here one microscopic detail, viz the number of sites, *has* an impact on the structure of the DoS. This fact is related to the topological character of the boundary term S_{top} occurring in the field theory.

6.1.2 Large Energy Asymptotics

We now turn to the large energy approximation of the exact zero-mode result, i.e. $\Delta \ll \epsilon \ll E_c$. We are interested in this limit for future checks of consistency. Using the large argument asymptotics of the Bessel functions we get

$$\langle \rho_{0D}^{\omega \gg 1}(\omega) \rangle \simeq \rho_0 \left(1 + \frac{1}{8\pi^2} \omega^{-2} - \frac{9}{128\pi^4} \omega^{-4} \right). \quad (6.6)$$

As can be seen in Fig. 6.2 the fluctuation on scales of the mean level spacing are smeared out. Instead, for $\epsilon \rightarrow 0$, i.e. leaving the range of validity of the present approximation, we get an algebraic divergency.

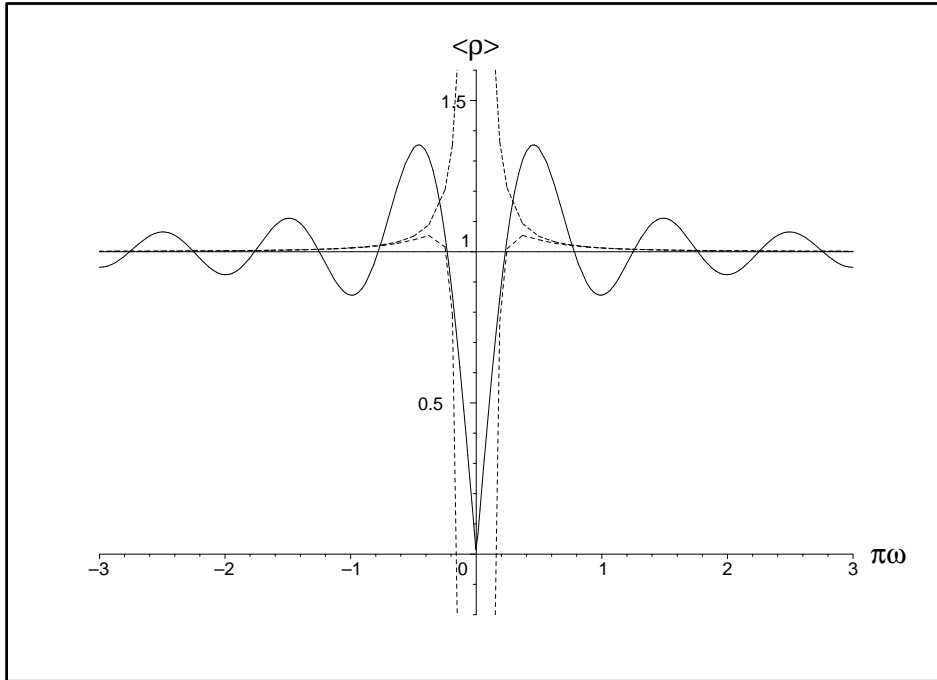


Figure 6.2: Plot of the average DoS in the ergodic regime for an even number of sites. The solid curve shows the exact RMT result, whereas the dashed curves are the first and second order approximation for $\epsilon \gg \Delta$.

6.2 Diffusive Regime

In this section we leave the universal zero-dimensional limit case and enter the regime of diffusive dynamics. Hence, we consider energies exceeding the Thouless energy, $\Delta \ll E_c \ll \epsilon$. Therefore, in quasi-1D, we have $\Delta/\sqrt{\epsilon E_c} \ll 1$ as small expansion parameter. Actually, we are entering the typical field of application of diagrammatic perturbation theory. Nevertheless, the NL σ M provides us a straightforward method for the perturbative expansion of the DoS, yielding contributions which correspond to certain diagrams. It turns out that it is much more convenient to switch to the σ -model formulation in terms of EFETOV's Q -matrices.

6.2.1 General Formulae

According to Ref. [81] we use the rational parameterization for the Q -matrices, which is with the settings in App. D given by

$$\begin{aligned} Q &= (1 - W \otimes \sigma_2^{\text{AB}})^{-1} \sigma_3^{\text{AB}} (1 - W \otimes \sigma_2^{\text{AB}}) \\ &= (1 - W \otimes \sigma_2^{\text{AB}})^{-1} (1 + W \otimes \sigma_2^{\text{AB}}) \sigma_3^{\text{AB}}, \end{aligned} \quad (6.7)$$

where the Pauli matrices σ_i^{AB} act in sublattice space. With the Taylor expansion

$$\begin{aligned} Q &= \left[1 + \sum_{n=1}^{\infty} 2(-1)^n (W \otimes \sigma_2^{\text{AB}})^n \right] \sigma_3^{\text{AB}} \\ &= \sigma_3^{\text{AB}} + 2\sigma_3^{\text{AB}} \sum_{n=1}^{\infty} (W \otimes \sigma_2^{\text{AB}})^n \end{aligned} \quad (6.8)$$

we get for the energy term $F_\epsilon[Q]$, Eq. (4.31b), and the pre-exponential source term $F_{J=1}[Q]$, Eq. (4.31c), up to quartic order in W

$$\begin{aligned} \text{str}[Q\sigma_3^{\text{AB}}] &\simeq 2 \text{str} \left[\frac{1}{2} \mathbb{1}^{\text{AB}} + \sum_{i=1}^4 (W \otimes \sigma_2^{\text{AB}})^i \right] \\ &= 2 \text{str} [W^2 \otimes \mathbb{1}^{\text{AB}} + W^4 \otimes \mathbb{1}^{\text{AB}}] = 4 \text{str} [W^2 + W^4] \end{aligned} \quad (6.9)$$

and

$$\text{str}[Q\sigma_3^{\text{AB}}\sigma_3^{\text{bf}}] \simeq 4 \text{str} \left[\frac{1}{2} \sigma_3^{\text{bf}} + W^2 \sigma_3^{\text{bf}} + W^4 \sigma_3^{\text{bf}} \right], \quad (6.10)$$

respectively. A similar calculation for the fluctuation term $F_{\text{fl}}[Q]$, Eq. (4.31a), yields

$$\begin{aligned} \text{str}[\partial Q \partial Q] &\simeq 4 \text{str} \left\{ [\sigma_3^{\text{AB}} \partial(W \otimes \sigma_2^{\text{AB}}) + \sigma_3^{\text{AB}} \partial(W \otimes \sigma_2^{\text{AB}})^2 + \sigma_3^{\text{AB}} \partial(W \otimes \sigma_2^{\text{AB}})^3]^2 \right\} \\ &= 4 \text{str} [(\partial W)^2 \otimes (-\mathbb{1}^{\text{AB}}) + 2(2(\partial W)^2 W^2 + (\partial W W)^2) \otimes (-\mathbb{1}^{\text{AB}}) \\ &\quad + (2(\partial W W)^2 + 2(\partial W)^2 W^2) \otimes \mathbb{1}^{\text{AB}}] \\ &= -8 \text{str} [(\partial W)^2 + 2(\partial W)^2 W^2], \end{aligned} \quad (6.11)$$

whereas it turns out that the topological term does not contribute. Concerning the Gade term, we note that its coupling constant is of the order of unity and hence much smaller than the coupling constants $c_{\text{fl}} \gg 1$ and $c_\epsilon \gg 1$. Therefore, this term is neglected. From Eq. (4.32) we obtain the DoS

$$\langle \rho(\epsilon) \rangle = \frac{\nu_0}{4} \text{Re} \int_0^L d\lambda \int \mathcal{D}Q \text{str} [Q(\lambda) \sigma_3^{\text{bf}} \sigma_3^{\text{AB}}] e^{-S_{\text{eff}}[Q]}. \quad (6.12)$$

Substituting the expansions, Eqs. (6.9) - (6.11), into Eq. (6.12), performing a Fourier transformation and expanding the exponential containing quartic powers

in W , we get

$$\begin{aligned}
\langle \rho_{\text{diff}}(\epsilon) \rangle &= \nu_0 \text{Re} \int_0^L d\lambda \int \mathcal{D}W \text{str} \left[\left(\frac{1}{2} + W^2 + W^4 \right) \sigma_3^{\text{bf}} \right] \\
&\quad \times e^{\pi\nu_0 \int_0^L d\lambda \text{str}[-2D(\partial W)^2 W^2 + 2i\epsilon W^4]} e^{\pi\nu_0 \int_0^L d\lambda \text{str}[-D(\partial W)^2 + 2i\epsilon W^2]} \\
&= \rho_0 \text{Re} \left\langle \text{str} \left[\left(\frac{1}{2} + \sum_k W_k W_{-k} + \sum_{l_1, l_2, l_3} W_{l_1} W_{l_2} W_{l_3} W_{-l_1-l_2-l_3} \right) \sigma_3^{\text{bf}} \right] \right. \\
&\quad \left. \times \left[1 + \pi \sum_{q_1, q_2, q_3} 2 \frac{Dq_1 q_2 + i\epsilon}{\Delta} \text{str} [W_{q_1} W_{q_2} W_{q_3} W_{-q_1-q_2-q_3}] \right] \right\rangle, \tag{6.13}
\end{aligned}$$

where

$$\langle \dots \rangle \equiv \int \mathcal{D}W (\dots) e^{-\sum_p c_p \text{str}[W_p W_{-p}]}, \tag{6.14}$$

$c_p \equiv \pi \frac{Dp^2 - 2i\epsilon}{\Delta}$ and $\mathcal{D}W$ denotes the flat functional measure, so that $\langle 1 \rangle = 1$. We now have to perform the Gaussian integral over all combinations in Eq. (6.13), i.e. certain contractions have to be calculated. Once having appropriate contraction rules derived this can be done quite easily. The derivation of the contraction rules and the calculation of the contributions to the DoS is presented in App. E. The terms can be classified according to the language of diagrammatic perturbation theory. Expressions containing n free momentum summations are called n -loop diagrams.

Representing the source σ_3^{bf} by a bullet and each momentum by a leg Eq. (6.13) can be visualized as follows:

$$\left[\bullet + \begin{array}{c} \diagup \\ \bullet \\ \diagdown \end{array} + \begin{array}{c} \diagup \\ \times \\ \diagdown \end{array} \right] \times \left[1 + \begin{array}{c} \diagup \\ \times \\ \diagdown \end{array} \right]$$

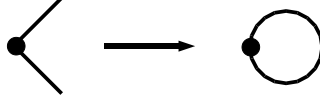
Each contraction then corresponds to the junction of two legs. Considering only diagrams up to 2-loop order we get the following five contributions

- Unperturbed part

•

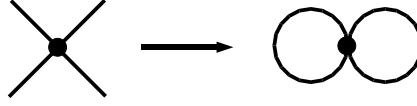
$$\langle \text{str}(\frac{1}{2}\sigma_3^{\text{bf}}) \rangle = \langle 1 \rangle = 1. \tag{6.15}$$

- 1-loop diagram



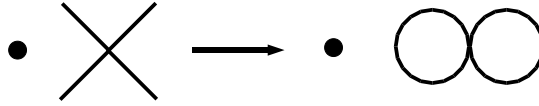
$$\sum_k \langle \text{str} [W_k W_{-k} \sigma_3^{\text{bf}}] \rangle = 0. \quad (6.16)$$

- 2-loop diagram A



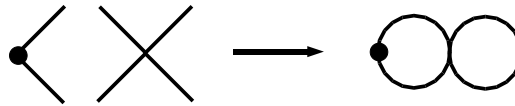
$$\sum_{l_1, l_2, l_3} \langle \text{str} [W_{l_1} W_{l_2} W_{l_3} W_{-l_1-l_2-l_3} \sigma_3^{\text{bf}}] \rangle = \frac{1}{2} \sum_{l_1, l_2} (c_{l_1})^{-1} (c_{l_2})^{-1} \quad (6.17)$$

- 2-loop diagram B



$$\sum_{q_1, q_2, q_3} \frac{Dq_1 q_2 + i\epsilon}{\Delta} \langle \text{str}(\frac{1}{2} \sigma_3^{\text{bf}}) \text{str} [W_{q_1} W_{q_2} W_{q_3} W_{-q_1-q_2-q_3}] \rangle = 0 \quad (6.18)$$

- 2-loop diagram C



$$\begin{aligned} \sum_{k, q_1, q_2, q_3} \frac{Dq_1 q_2 + i\epsilon}{\Delta} \langle \text{str} [W_{-k} \sigma_3^{\text{bf}} W_k] \text{str} [W_{q_1} W_{q_2} W_{q_3} W_{-q_1-q_2-q_3}] \rangle \\ = \frac{i\omega}{2} \sum_{q_1, q_2} [(c_{q_1})^{-2} (c_{q_2})^{-1} + (c_{q_1})^{-1} (c_{q_2})^{-2}] \quad (6.19) \end{aligned}$$

Thus, there is no 1-loop contribution and only two of the 2-loop diagrams yield a non-vanishing result. Finally, we obtain the DoS in the diffusive regime,

$$\begin{aligned}
\langle \rho_{\text{diff}}(\epsilon) \rangle &= \rho_0 \operatorname{Re} \left\{ 1 + \frac{1}{2} \sum_{l_1, l_2} (c_{l_1})^{-1} (c_{l_2})^{-1} \right. \\
&\quad \left. + i\omega\pi \sum_{q_1, q_2} [(c_{q_1})^{-2} (c_{q_2})^{-1} + (c_{q_1})^{-1} (c_{q_2})^{-2}] \right\} \\
&= \rho_0 \left\{ 1 + \frac{\Delta^2}{2\pi^2} \operatorname{Re} \sum_{p, q} \frac{1}{(Dp^2 - 2i\epsilon)(Dq^2 - 2i\epsilon)} \right. \\
&\quad \left. + \frac{4i\epsilon}{(Dp^2 - 2i\epsilon)^2 (Dq^2 - 2i\epsilon)} \right\} \\
&= \rho_0 \left\{ 1 + \frac{\Delta^2}{2\pi^2} \operatorname{Re} \sum_{p, q} \frac{Dp^2 + 2i\epsilon}{(Dp^2 - 2i\epsilon)^2 (Dq^2 - 2i\epsilon)} \right\}.
\end{aligned} \tag{6.20}$$

6.2.2 Zero-Mode Approximation

Before summing up all momenta let us consider the zero-dimensional limit of Eq. (6.20), i.e. the case of slowly varying fields, or $\epsilon \ll E_c$. Then, we can restrict the momentum sum to the zero-mode $p = q = 0$ and get

$$\langle \rho_{\text{diff}}^{\text{0D}}(\omega) \rangle = \rho_0 \left[1 + \frac{\Delta^2}{2\pi^2} \operatorname{Re} \frac{2i\epsilon}{-(2i\epsilon)^2 2i\epsilon} \right] = \rho_0 \left(1 + \frac{1}{8\pi^2} \omega^{-2} \right), \tag{6.21}$$

which reproduces the high energy limit of the exact zero-mode result in Eq. (6.6).

6.2.3 Large System Approximation

In the next step we consider the regime $\xi > L \gg (D/\omega)^{1/2}$, which corresponds to energies $\omega \gg E_c$. This is the regime of weak localization, where the diffusion constant in the common systems of *A*, *AI*, and *AII* symmetry is renormalized by mechanisms of quantum interference. Consequently, we should expect to get algebraic corrections in the small parameter ω^{-1} . Since for $L \rightarrow \infty$ the discrete momenta pass over to a continuum we can approximate the sums by integrals: $\sum_p \rightarrow \frac{L}{2\pi} \int dp$. With

$$\int \frac{1}{ap^2 + b} dp = \frac{\pi}{\sqrt{ab}} \quad \text{and} \quad \int \frac{1}{(ap^2 + b)^2} dp = \frac{\pi}{2\sqrt{ab^3}} \tag{6.22}$$

we obtain from Eq. (6.20)

$$\langle \rho_{\text{diff}}(\epsilon) \rangle = \rho_0 \left\{ 1 + \frac{\Delta^2}{2\pi^2} \operatorname{Re} \frac{L^2}{4} \left[\frac{-1}{2iD\epsilon} + \frac{2i\epsilon}{D(-2i\epsilon)^{3/2}(-2i\epsilon)^{1/2}} \right] \right\} = \rho_0. \tag{6.23}$$

Thus, there are *no perturbative corrections* to the DoS in the diffusive regime up to three loop order. Before discussing this result let us consider the exact summation and show how to recover the results obtained in this and the previous subsection.

6.2.4 Exact Momentum Summation

Indeed, it is possible to perform the momentum summation in Eq. (6.20) exactly, i.e. to calculate the DoS for $\epsilon \gg \Delta$ on all length scales assumed that $\epsilon \gg E_c$ and $\xi \gg L$. Let us first outline the general recipe how to perform a sum $\sum_{n=-\infty}^{\infty} f(q_n)$, where $f(q_n)$ is some function depending on a discrete set of arguments $\{q_i\}_i$.

- Introduce a auxiliary function $g(z)$ with simple poles at q_n , for all n , such that $f(z)g(z) \rightarrow 0$ for $|z| \rightarrow \infty$.
- Consider the contour integral $\int_C dz f(z)g(z)$ over a contour C , that encloses all poles of the integrand (e.g. a circle of infinite radius).
- Since the integral vanishes we get an representation of the sum of the following form:

$$\sum_n f(q_n) = \sum \text{Res}(fg)(z) \Big|_{\text{Poles of } f} = - \sum \text{Res}(fg)(z) \Big|_{\text{Poles of } g}. \quad (6.24)$$

Now, we apply this recipe to the sum

$$\sum_q \frac{1}{Dq^2 - 2i\epsilon} = \sum_n f(\sqrt{D}q_n) \quad (6.25)$$

with

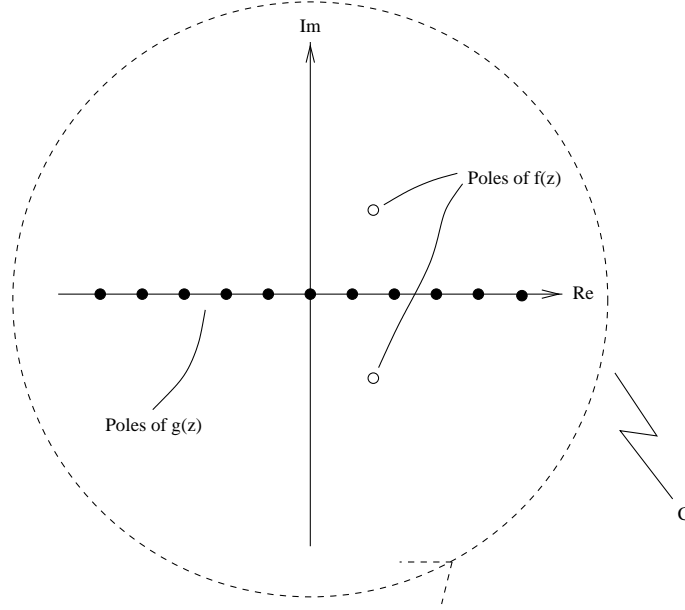
$$f(z) \equiv \frac{1}{z^2 - 2i\epsilon} = \frac{1}{(z + \sqrt{2i\epsilon})(z - \sqrt{2i\epsilon})}. \quad (6.26)$$

As auxiliary function we choose

$$g(z) = \frac{\alpha}{e^{\alpha z} - 1}, \quad \text{with } \alpha \equiv iL/\sqrt{D}. \quad (6.27)$$

The (simple) poles of $g(z)$ are located at $z_n = n\frac{2\pi}{L}\sqrt{D} = \sqrt{D}q_n$ as demanded, whereas $f(z)$ has poles at $\pm\sqrt{2i\omega}$ (cf. Fig. 6.3). After a careful verification of $\lim_{|z| \rightarrow \infty} f(z)g(z) = 0$ we conclude

$$0 = \int_C dz f(z)g(z) = 2\pi i \left[\sum_n \text{Res}(fg)(z) \Big|_{z=\sqrt{D}q_n} + \sum_{s=1,-1} \text{Res}(fg)(z) \Big|_{z=s\sqrt{2i\epsilon}} \right] \quad (6.28)$$

Figure 6.3: Poles of f and g

The first residuum turns out to be given by

$$\text{Res}(fg)(z)|_{z=z_n} = f(z_n) = \frac{1}{Dq_n^2 - 2i\epsilon}, \quad (6.29)$$

and we obtain

$$\begin{aligned} \sum_q \frac{1}{Dq^2 - 2i\epsilon} &= -\text{Res}(fg)(z)|_{z=\sqrt{2i\epsilon}} - \text{Res}(fg)(z)|_{z=-\sqrt{2i\epsilon}} \\ &= -\frac{\alpha}{2\sqrt{2i\epsilon}} \coth\left(\frac{\alpha}{2}\sqrt{2i\epsilon}\right). \end{aligned} \quad (6.30)$$

We turn now to the second sum in Eq. (6.20)

$$\sum_q \frac{1}{(Dq^2 - 2i\epsilon)^2} = \sum_n h(\sqrt{D}q_n), \quad (6.31)$$

where

$$h(z) \equiv \frac{1}{(z^2 - 2i\epsilon)^2} = \frac{1}{(z + \sqrt{2i\epsilon})^2} \frac{1}{(z - \sqrt{2i\epsilon})^2}. \quad (6.32)$$

With the second order residua of hg at $\pm\sqrt{2i\epsilon}$ given by

$$\begin{aligned} \text{Res}(hg)(z)|_{z=\pm\sqrt{2i\epsilon}} &= \frac{d}{dz} \left(z \pm \sqrt{2i\epsilon} \right)^{-2} \Big|_{z=\pm\sqrt{2i\epsilon}} \\ &= \mp \frac{2}{(2\sqrt{2i\epsilon})^3} \frac{\alpha}{e^{\pm\alpha\sqrt{2i\epsilon}} - 1} - \frac{1}{(2\sqrt{2i\epsilon})^2} \frac{\alpha^2 e^{\pm\alpha\sqrt{2i\epsilon}}}{(e^{\pm\alpha\sqrt{2i\epsilon}} - 1)^2} \end{aligned} \quad (6.33)$$

we derive

$$\sum_q \frac{1}{(Dq^2 - 2i\epsilon)^2} = \frac{\alpha}{4(2i\epsilon)^{3/2}} \coth\left(\frac{\alpha}{2}\sqrt{2i\epsilon}\right) + \frac{\alpha^2}{16i\epsilon} \frac{1}{\sinh^2\left(\frac{\alpha}{2}\sqrt{2i\epsilon}\right)}. \quad (6.34)$$

Finally, the "exact" DoS in the diffusive regime, denoted by a superscript Σ , is given by

$$\begin{aligned} \langle \rho_{\text{diff}}^{\Sigma}(\epsilon) \rangle &= \rho_0 \left[1 - \text{Re} \left(\frac{\nu_0 L}{2\pi^2} \frac{\alpha^3}{8\sqrt{2i\epsilon}} \frac{\cosh\left(\frac{\alpha}{2}\sqrt{2i\epsilon}\right)}{\sinh^3\left(\frac{\alpha}{2}\sqrt{2i\epsilon}\right)} \right) \right] \\ &= \rho_0 \left[1 + \text{Re} i \frac{\Delta^2}{16\pi^2 \sqrt{2i\epsilon} E_c^3} \frac{\cosh\left(\frac{1}{2}\sqrt{2i\epsilon/E_c}\right)}{\sinh^3\left(\frac{1}{2}\sqrt{2i\epsilon/E_c}\right)} \right]. \end{aligned} \quad (6.35)$$

As expected this expression contains no (purely) algebraic contributions, which is in agreement with our previous results. In conclusion, we consider the limits $\epsilon \ll E_c$ corresponding to the zero-mode regime and $\epsilon \gg E_c$ corresponding to the thermodynamic limit. Starting with the former case we obtain

$$\begin{aligned} \langle \rho_{\text{diff}}^{\Sigma,0D}(\epsilon) \rangle &= \rho_0 \left[1 + \text{Re} i \frac{\Delta^2}{16\pi^2 \sqrt{2i\epsilon} E_c^3} \frac{1}{-\frac{i}{2} \left(\sqrt{2i\epsilon/E_c}\right)^3} \right] \\ &= \rho_0 \left[1 + \frac{1}{8\pi^2 \omega^2} \right], \end{aligned} \quad (6.36)$$

which reproduces Eq. (6.6) whereas in the latter case we get

$$\langle \rho_{\text{diff}}^{\Sigma,\epsilon \gg E_c}(\epsilon) \rangle = \rho_0 \left[1 - \frac{\sqrt{2}}{16\pi^2} \frac{\Delta^2}{\sqrt{\epsilon} E_c^3} e^{-\sqrt{\epsilon/E_c}} \sin\left(\sqrt{\epsilon/E_c} + \frac{\pi}{4}\right) \right], \quad (6.37)$$

which in the limit $L \rightarrow \infty$, i.e. $E_c \rightarrow 0$, yields our former result, $\langle \rho_{\text{diff}}(\epsilon) \rangle = \rho_0$ from Eq. (6.23).

6.2.5 Perturbation Theory with the Replica σ -model

At the end of this section we now point out an alternative to the *supersymmetric* version of the NL σ M. As already mentioned the so-called *replica trick* also provides a method, which allows to circumvent inconvenient determinants. Particularly, it turns out that starting from a replica NL σ M it is even easier to estimate whether a perturbative contribution vanishes or not. Thus, although yielding no new results this subsection is motivated by a methodical point of view. Recall that

$$\rho(\epsilon^+) = -\frac{1}{\pi} \text{Im tr} \langle G^+(\epsilon) \rangle. \quad (6.38)$$

Considering the $J = 0$ generating functional in Eq. (4.1) with fermionic fields we obtain for the Green function

$$\left\langle \text{tr} \frac{1}{\epsilon^+ - H} \right\rangle = \langle \text{tr} \partial_\epsilon \ln(\epsilon^+ - H) \rangle = \partial_\epsilon \langle \ln \det(\epsilon^+ - H) \rangle = \partial_\epsilon \langle \ln \mathcal{Z} \rangle. \quad (6.39)$$

Thus, in order to get the DoS we have to calculate the disorder average of the *logarithm* of the original generating functional. At first view, this task seems to be even more complicated but it is managed by the replica trick. We consider the partition sum of an n -fold replicated system, $\langle \mathcal{Z}^n \rangle$. This is related to the logarithm of the single generating functional by the following identity

$$\langle \ln \mathcal{Z} \rangle = \lim_{n \rightarrow 0} \frac{\langle \mathcal{Z}^n \rangle - 1}{n}. \quad (6.40)$$

Consequently, the DoS is given by the expression

$$\rho(\epsilon^+) = \frac{1}{\pi} \text{Im} \partial_\epsilon \lim_{n \rightarrow 0} \left(\frac{\langle \mathcal{Z}^n \rangle - 1}{n} \right). \quad (6.41)$$

Applying a similar procedure as in Ch. 4 one can derive a NL σ M. Formulated in terms of Q -matrices (elements of the corresponding coset space) this has nearly the same form as in the supersymmetric case. The only difference is that the matrices W (cf. Eq. (6.7)) are now *Hermitean* $n \times n$ -matrices and the supertrace is substituted by the common trace:

$$\langle \mathcal{Z}^n \rangle = \int \mathcal{D}Q e^{-S_{\text{eff}}[Q]} \quad (6.42)$$

with the effective action

$$S_{\text{eff}}[Q] = -\frac{\pi\nu_0}{2} \int_0^L \frac{D}{4} \text{tr}[\partial Q \partial Q] + i\epsilon \text{tr} [Q \sigma_3^{\text{AB}}]. \quad (6.43)$$

Expanding the Q -matrices according to Eq. (6.8) we obtain

$$\mathrm{tr}[Q\sigma_3^{\mathrm{AB}}] = 2n + 4 \mathrm{tr}[W^2 + W^4] \quad (6.44)$$

and

$$\mathrm{tr}[\partial Q \partial Q] = -8 \mathrm{tr}[(\partial W)^2 + 2(\partial W)^2 W^2]. \quad (6.45)$$

After a Fourier transformation and an expansion of the exponential function containing the quartic terms we end up with the following expression for the generating functional of the replicated system:

$$\langle \mathcal{Z}^n \rangle = \left\langle 1 + 2\pi \sum_{q_1, q_2, q_3} \frac{Dq_1 q_2 + i\epsilon}{\Delta} \mathrm{tr}[W_{q_1} W_{q_2} W_{q_3} W_{-q_1 - q_2 - q_3}] \right\rangle_W \quad (6.46)$$

where

$$\langle \dots \rangle_W \equiv e^{i\pi\rho_0\epsilon^+ n} \int \mathcal{D}W(\dots) e^{-\sum_p c_p \mathrm{tr}[W_p W_{-p}]}, \quad (6.47)$$

$c_p \equiv \pi(\frac{Dp^2 - 2i\epsilon}{\Delta})$, and the measure is given in App. E.3. Before we start to calculate the contributions let us note that all odd loop diagrams vanish by a general reason. Focusing on the zero mode regime each power of W^2 yields a factor ϵ^{-1} after integration. Hence, $\epsilon \langle (W^2)^k \rangle \propto \epsilon^{-k+1}$ ($k \in \mathbb{N}$) and differentiation w.r.t. ϵ yields $(-k+1)\epsilon^{-k}$, i.e. each odd loop order contribution is of odd order in ϵ . But since the DoS is an even function of ϵ , all diagrams with an odd number of loops must vanish.

Substituting Eq. (6.46) into Eq. (6.41) for the DoS we get the following contributions. From

$$\langle 1 \rangle = e^{i\pi\rho_0\epsilon^+ n} \quad (6.48)$$

which corresponds to the unperturbed part we get

$$\frac{1}{\pi} \mathrm{Im} \partial_\epsilon \lim_{n \rightarrow 0} \frac{e^{i\pi\rho_0\epsilon^+ n} - 1}{n} = \frac{1}{\pi} \mathrm{Im} \partial_\epsilon (i\pi\rho_0\epsilon^+) = \rho_0. \quad (6.49)$$

By means of the contraction rules derived in cf. App. E.3 we find

$$\begin{aligned} \langle \rho_{\mathrm{diff}}(\epsilon) \rangle &= \rho_0 \left(1 + 2 \mathrm{Im} \partial_\epsilon \lim_{n \rightarrow 0} \sum_{p, q} \frac{(Dpq + i\epsilon) \langle \mathrm{tr} W_q \mathrm{tr} W_{-q} \rangle_W}{2c_p n} \right) \\ &= \rho_0 \left(1 + 2 \mathrm{Im} \partial_\epsilon \lim_{n \rightarrow 0} \sum_{p, q} \frac{(Dpq + i\epsilon) \mathrm{tr} \mathbb{1}_n}{4c_p c_q n} \right) \\ &= \rho_0 \left(1 + \frac{\Delta^2}{2\pi^2} \mathrm{Im} \partial_\epsilon \sum_{p, q} \frac{i\epsilon}{(Dp^2 - 2i\epsilon)(Dq^2 - 2i\epsilon)} \right) \\ &\simeq \rho_0 \left(1 - \frac{\Delta^2}{2\pi^2} \mathrm{Im} \frac{L^2}{4} \partial_\epsilon \frac{1}{2D} \right) = \rho_0, \end{aligned} \quad (6.50)$$

where in the last line we have again performed the thermodynamic limit. Thus, we have again verified the result that all perturbative corrections to the DoS of quasi-1d system with AIII symmetry vanish at least up to three loop order.

6.2.6 Discussion

In conclusion we have calculated the perturbative corrections to the AIII DoS using a diagrammatic perturbation scheme generated by the NL σ M. Both within the supersymmetric and the replica version of the quasi-1D NL σ M we do not find perturbative contributions up to three loop order. The question arises, whether *all* perturbative corrections vanish or whether there exists a loop order which yields a non-vanishing contribution. The four-loop corrections are the next which come into question but their calculation is quite involved and out of the scope of this work. Since we do not find a simple argument for the absence of all contributions, the four-loop contributions may exist. A definitive answer to this problem is still lacking.

6.3 Quantum Regime

We now turn to the most interesting case, the localized quantum regime. Here, the system length is much larger than the localization length, $g = \xi/L \ll 1$. The relevant energy scale in this regime is the mean level spacing corresponding to a localization volume, $\Delta_\xi = \frac{L}{\xi}\Delta$, not the mean level spacing itself. The limit of small energies is then characterized by, $\epsilon \ll \Delta_\xi$ or $\omega \ll 1$, where $\omega \equiv \epsilon/\Delta_\xi$. This corresponds to such large times that the electron wave function decays exponentially around some center due to strong localization, i.e. due to destructive quantum interference. Since the quantum regime corresponds to extended systems sizes and since it is manifestly non-perturbative (formally $\Delta^2 \gg E_c\epsilon$), the methods of the previous sections can not be applied. Instead, the heat equation comes into operation. With the preparations made in the last section of Ch. 5 we solve the heat equation in the limit of small energies and calculate the DoS in this limit by means of Eq. (4.33).

6.3.1 Calculation without Gade Term

Let us for the time being neglect the influence of the Gade term, thus setting $c_3 = 0$. The originator for our calculations is the similarity and gauge transformed heat equation, Eq. (5.22), which after multiplication with the factor $4c_{\text{fl}}$ reads

$$\partial_s \Phi^{e,o}(\mathbf{x}; s) = [\partial_x^2 + \partial_y^2 - \eta(\cosh x - \cos y)] \Phi^{e,o}(\mathbf{x}; s). \quad (6.51)$$

Here we have introduced the small parameter $\eta \equiv -i\epsilon^+ 8c_1 c_2 = -i\epsilon^+/\Delta_\xi$. The next step is to apply the Fourier expansion scheme outlined in Sec. 5.3. Since we are interested in the DoS for large $s = L/\xi$, i.e. in the bulk of the wire, far away from the boundaries, it is sufficient to consider the zero-mode eigenfunction. That this is justified can be seen by looking at the general expansion, Eq. (5.28). For large s the main contribution to the Fourier integral comes from the zero-mode $\beta_0 = 0$. Denoting the zero-mode eigenfunction by $\phi^{e,o}(\mathbf{x})$ the problem is reduced to the solution of the differential equation

$$[\partial_x^2 + \partial_y^2 - \eta(\cosh x - \cos y)] \phi^{e,o}(\mathbf{x}) = 0, \quad (6.52)$$

Let us start with the case $\eta = 0$. Note that Eq. (6.52) is solved by each function $f = f(x - iy)$. But the solutions must obey the initial condition, Eq. (5.17), and the periodic boundary condition Eq. (5.18). Consider the following solutions¹ of Eq. (6.52),

$$\phi_{\eta=0}^e(\mathbf{x}) = -\sinh^{-1}\left(\frac{x - iy}{2}\right) \quad \text{and} \quad \phi_{\eta=0}^o(\mathbf{x}) = -\coth\left(\frac{x - iy}{2}\right). \quad (6.53)$$

They fulfill both, anti-periodicity/periodicity and the initial condition

$$\lim_{x,y \rightarrow 0} \left[-\sinh\left(\frac{x - iy}{2}\right) e^{\mp N_c(x-iy)/2} \phi^{e,o}(\mathbf{x})_{\eta=0} \right] = -1. \quad (6.54)$$

Note that the large x asymptotics are given by

$$\begin{aligned} \phi_{\eta=0}^e(\mathbf{x}) &\xrightarrow{|x| \gg 1} -2 e^{-\chi(x-iy)/2}, \\ \phi_{\eta=0}^o(\mathbf{x}) &\xrightarrow{|x| \gg 1} -1 - 2 e^{-\chi(x-iy)} \xrightarrow{|x| \rightarrow \infty} -1, \end{aligned} \quad (6.55)$$

where $\chi \equiv \text{sgn } x$. In the next step we turn to the solution for $0 < \eta \ll 1$ (cf. App. F for more details). It turns out that due to $\eta \ll 1$ the solution for $x = \mathcal{O}(1)$ does not contribute. Thus, we can restrict our calculations to large values of the non-compact variable, $|x| \gg 1$. The differential equation Eq. (6.52) decouples and can be solved by the separation ansatz

$$\phi^{e,o}(\mathbf{x}) = \phi_1^{e,o}(x) \phi_2^{e,o}(y), \quad (6.56)$$

where for large $|x|$ the factors on the right hand side satisfy the differential equations

$$\left[\partial_x^2 - \frac{\eta}{2} e^{|x|} - C^{e,o} \right] \phi_1^{e,o}(x) = 0 \quad (6.57)$$

¹We anticipated here, that other solutions, especially those which decrease faster than the expressions in Eq. (6.53), lead to contributions to the DoS, which vanish in the limit $\eta \rightarrow 0$.

and

$$[\partial_y^2 + \eta \cos y + C^{e,o}] \phi_2^{e,o}(y) = 0 \quad (6.58)$$

with $C^e = 1/4$ and $C^o = 0$. We first solve the y -equation perturbatively in η . It appears that already the zero order term yields the leading contributions to the DoS (cf. App. F). Thus, we have

$$\phi_{2,\eta=0}^e(y) = e^{i\chi \frac{y}{2}} \quad \text{and} \quad \phi_{2,\eta=0}^o(y) = 1. \quad (6.59)$$

In order to solve the x equation we substitute

$$u \equiv (2\eta)^{1/2} e^{|x|/2} \quad (6.60)$$

into Eq. (6.57) and get

$$[u^2 \partial_u^2 + u \partial u - (\nu^2 + u^2)] \phi_1^{e,o}(u) = 0, \quad (6.61)$$

with $\nu = 0$ for odd N_c and $\nu = 1$ for even N_c . This equation is solved by Bessel functions of the second kind. Hence, the general solution is given by a superposition of $K_\nu(u)$ and $I_\nu(u)$. But the functions $I_\nu(u)$ grow exponentially and hence are not integrable. Thus, we keep only the Bessel functions $K_\nu(u)$. Determining the normalization factors by the $\eta \rightarrow 0$ asymptotics we finally get for the heat kernel in the limit of small η

$$\phi^e(\mathbf{x}) = -2(2\eta)^{1/2} K_1(u) e^{i\chi y/2} \quad \text{and} \quad \phi^o(\mathbf{x}) = \frac{2}{\ln \eta} K_0(u). \quad (6.62)$$

Calculating the pre-exponential factor analogously to Eq. (6.3) we obtain from Eq. (4.33)

$$\langle \rho_{\text{quant}}(\epsilon^+) \rangle^{e,o} = \rho_0 \left(1 + \text{Re} \frac{1}{4\pi} \int_{-\infty}^{\infty} dx \int_0^{2\pi} dy \frac{1}{2} (\cosh x - \cos y) \phi^{e,o,2}(\mathbf{x}) \right). \quad (6.63)$$

Since $K_\nu(u)$ decays exponentially for large arguments and $u \simeq 1$ for $x \simeq -\ln \eta$ we introduce $\mp \ln \eta$ as an upper/lower cut-off for the x -integration. Then the argument of the Bessel function is smaller than 1 and we can use the expansion for small arguments. After an analytic continuation $\eta \rightarrow -i(\omega + i\gamma/\Delta_\xi)$ with $\omega \equiv \epsilon/\Delta_\xi$ and performing the limit $\gamma \rightarrow 0$ we finally get for the DoS in the quantum regime

$$\langle \rho_{\text{quant}}(\omega) \rangle^e \propto -\rho_0 |\omega| \ln |\omega| \quad \text{for } N_c \text{ even} \quad (6.64)$$

and

$$\langle \rho_{\text{quant}}(\omega) \rangle^o - \rho_0 \propto \frac{\rho_0}{|\omega \ln^3 |\omega||} \quad \text{for } N_c \text{ odd.} \quad (6.65)$$

Thus, the DoS in the small energy limit, $\epsilon \ll \Delta_\xi$, of the deep quantum regime dramatically depends on the parity of the number of channels in the quasi-1D AIII system, cf. Fig. 6.4. For an even number of channels the DoS vanishes for $\epsilon \rightarrow 0$. Being unusual in system of standard symmetry, this behaviour is a direct consequence of the underlying chiral symmetry. As we have seen in Sec. 3.1 by formal arguments, eigenvalues of a chiral Hamiltonian appear pairwise with opposite sign. The corresponding modes influence each other resulting in level repulsion, which is the stronger the closer the levels are. As a consequence, there is no state at the exceptional point $\epsilon = 0$. For an odd number of channels the situation changes drastically. There is one mode left which does not have a partner. Hence, this state is able to become extended mode.

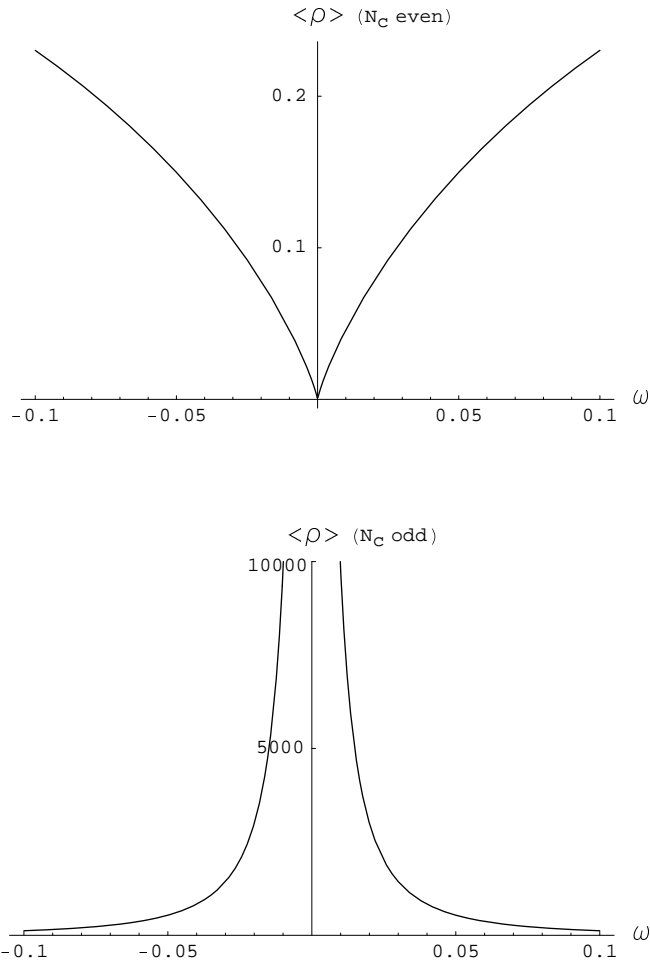


Figure 6.4: Average DoS in the quantum regime ($\omega = \epsilon/\Delta_\xi \ll 1$ and $L \gg \xi$). For even N_c (top) the DoS exhibits a gap at the band center, whereas for odd N_c (bottom) it diverges.

6.3.2 Influence of the Gade Term

Finally, adding the Gade term to Eq. (6.52) and get

$$[\partial_x^2 + \partial_y^2 + \zeta(\partial_x - i\partial_y)^2 - \eta(\cosh x - \cos y)] \phi^{e,o}(\mathbf{x}) = 0, \quad (6.66)$$

where $\zeta \equiv c_3/c_1$. Note that for $\eta = 0$ each solution of Eq. (6.52) also solves Eq. (6.66), which can easily be seen by rewriting Eq. (6.66) using complex variables. Unfortunately, for finite η Eq. (6.66) does not decouple in x and y . Hence, we can not follow the same procedure as in the previous section. Instead of this, we make a series ansatz in both, $e^{x/2}$ and $e^{y/2}$. Recall that the x depending part of the $\zeta = 0$ heat equation is solved by Bessel functions. Hence, we use the following generalization of the series representation of $K_\nu(u)$ as an ansatz for the solution of Eq. (6.66),

$$\phi(u, v) = u^{-1} \sum_{l=0}^{\infty} b_l v^l + \sum_{k,l=0}^{\infty} a_{kl} u^k v^l \ln u.$$

Here we have introduced

$$u \equiv (2\eta)^{1/2} e^{x/2} \quad \text{and} \quad v \equiv e^{iy/2}.$$

Substituting the ansatz into Eq. (6.66) yields

$$\begin{aligned} \left[(1 + \zeta) (u^2 \partial_u^2 + u \partial_u) + 2\zeta uv \partial_u \partial_v - (1 - \zeta) (v^2 \partial_v^2 + v \partial_v) \right. \\ \left. - u^2 + 2\eta(u^2 + v^{-2}) \right] \phi(u, v) = 0 \end{aligned}$$

and therefore

$$\begin{aligned} u^{-1} \sum_l \{ [1 - l^2 + \zeta(1 - l)^2] b_l + 2\eta(b_{l-2} + b_{l+2}) \} v^l + \sum_{kl} [2k + 2\zeta(k + l)] a_{kl} u^k v^l \\ + \ln u \sum_{kl} \{ [k^2 - l^2 + \zeta(k + l)^2] a_{kl} - a_{k-2,l} + 2\eta(a_{k,l-2} + a_{k,l+2}) \} u^k v^l \\ - u \sum_l b_l v^l = 0. \end{aligned}$$

Comparing the coefficients we obtain the following relations

$$\begin{aligned} [1 - l^2 + \zeta(1 - l)^2] b_l + 2\eta(b_{l-2} + b_{l+2}) &= 0, \\ [2k + 2\zeta(k + l)] a_{kl} - b_l &= 0 \quad (k = 1), \\ [2k + 2\zeta(k + l)] a_{kl} &= 0 \quad (k \neq 1), \\ [k^2 - l^2 + \zeta(k + l)^2] a_{kl} - a_{k-2,l} + 2\eta(a_{k,l-2} + a_{k,l+2}) &= 0. \end{aligned} \quad (6.67)$$

Anticipating that for odd N_c the Gade term has no impact on the result we concentrate on the case of even N_c . Reflecting that for $\eta = 0$ the solution of Eq. (6.52) also solves Eq. (6.66) we conclude from the $\eta \rightarrow 0$ asymptotics (cf. Eq. (6.55)) that $\lim_{\eta \rightarrow 0} \phi(u, v) = -2\sqrt{2\eta}u^{-1}v$. Therefore, we have

$$b_1 = -2\sqrt{2\eta},$$

and Eq. (6.67) yields

$$a_{11} = \frac{b_1}{2(1+2\zeta)}.$$

Up to second order in η the heat kernel is given by

$$\phi^e(u, v) = -2\sqrt{2\eta} \left[u^{-1} + \frac{1}{2(1+2\zeta)} u \ln u + \mathcal{O}(u^3 \ln u) \right] v.$$

Finally, we obtain for the DoS in the case of an even channel number

$$\langle \rho_{\text{quant}}^{\text{Gade}}(\omega) \rangle^e \propto \frac{\rho_0}{1+2\zeta} |\omega \ln |\omega||, \quad (6.68)$$

whereas for odd N_c the DoS in the quantum regime is unaffected by the Gade term, $\langle \rho_{\text{quant}}^{\text{Gade}}(\omega) \rangle^o = \langle \rho_{\text{quant}}(\omega) \rangle^o$.

Part II

Localization-Delocalization Transition in 2D Systems of *AI* symmetry

Chapter 7

Systems of AII Symmetry

In the second part of this work we investigate the localization-delocalization transition in two-dimensional systems belonging to the symmetry class AII. The present chapter gives an introduction into the peculiarities of AII symmetry. Further, we present the basic concepts of the scattering theoretical network model, within which we perform our investigations. In the second section an survey of the scaling theory of localization is given.

7.1 Introduction and Motivation

Recently, localization-delocalization (LD) transitions in 2D disordered electron systems in the absence of a magnetic field were observed by several groups [30–36]. These results are in contrast with the scaling theory for non-interacting electrons of ABRAHAMS ET AL. [9], which predicts that all states are localized in 2D and in the absence of spin-orbit interaction. Now, a new discussion has started on this topic with the emphasis on the effects of electron-electron interaction and spin-orbit interaction [37–42].

It is known that both types of interactions could be responsible for the existence of an LD transition. In the case of spin-orbit interaction, general arguments [43] and perturbation theoretical calculations in the weakly disordered regime [44,45] yield a positive correction to the conductance. This quantum interference effect requiring time reversal invariance is known as weak anti-localization. In the present work we focus on the detailed examination of a 2D non-interacting electron system with spin-orbit interaction. We perform the investigations within a scattering theoretical network model approach.

In a recent paper [46] it was shown that scattering theoretical network models (NWMs) are well suited to describe mesoscopic disordered electron systems. In general such a NWM can represent any system of coherent waves propagating

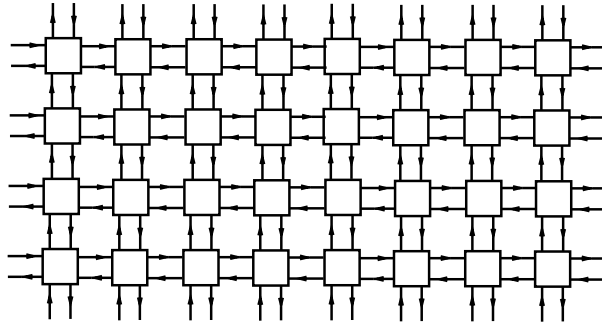


Figure 7.1: Topology of a general network model. Squares are scatterers and lines are bonds.

through disordered media. It consists of a network of unitary scatterers connected by bonds. The arrangement of scatterers and bonds defines the topology of the NWM, which can be described by a connectivity matrix. In this work we choose a simple case, where the scatterers are located on the sites of a quadratic grid, so each of them has four nearest neighbors, as is sketched in Fig. 7.1. Each bond consists of $2n$ links, n for each direction, where $n = 1$ for waves without and $n > 1$ for waves with internal degrees of freedom, e.g. spin. In the case of electron waves a complex number is attached to each link representing the probability amplitude at this position. The set of all amplitudes defines the quantum mechanical state $\Psi(t)$ at time t . One step of time evolution is then given by a unitary operator \mathcal{U} ,

$$\Psi(t + 1) = \mathcal{U}\Psi(t).$$

This time evolution operator is determined by all the scatterers in the NWM. Each scatterer maps $4n$ incoming channels to $4n$ outgoing channels conserving the current and is therefore represented by a unitary $4n \times 4n$ -matrix. The disorder is in general simulated in two ways: first by multiplying the amplitude on each link with a complex random phase factor $e^{i\phi}$ with ϕ randomly chosen from $[0, 2\pi[$ simulating the random distances between the scatterers and secondly by taking random values for the parameters that parameterize the matrix representation of the scatterers simulating the random strengths of the scatterers. Of course, both random choices have to be compatible with the symmetry properties of the system. NWMs for systems with (AI) and without (A) time-reversal symmetry have been examined in [87]. There a reflection, a transmission and a deflection coefficient were introduced, which parameterize the scattering matrices. Furthermore an elastic mean free path could be defined in terms of these coefficients. It was concluded that in both cases all states are localized, in correspondence to the scaling theory of localization.

In this part of the work we focus on a NWM with conserved time-reversal but broken spin-rotational invariance, in order to investigate the localization behaviour

of systems with AII symmetry. We therefore implement additionally spin scatterers in the NWM defined in Ref. [87]. This introduces a further parameter governing the spin scattering strength. By means of the transfer matrix method we calculate the renormalized localization length Λ for a strip geometry. This quantity serves as scaling variable. We determine a phase diagram in the three-dimensional parameter space. Towards a characterization of the LD transition we first construct a scaling function in order to verify the assumption of one-parameter scaling. Then we calculate the critical exponent ν of the correlation length and the critical value of the scaling variable, Λ^* . In the literature the critical value of the scaling variable is simply read-off from plots in most cases. As we will see, ν depends drastically on small variations of Λ^* . Therefore, the determination of both, the scaling function and the critical values, is performed by means of a numerical fit procedure adopted from Ref. [47], in order to get reliable results. Additionally, the confidence of the fits is estimated by a χ^2 -test.

7.2 Localization-Delocalization Transition

The central subject of the present part is the LD transition in 2D systems of AII symmetry. In this section we describe the general phenomenology of this critical phenomenon and show how the existence of such a transition for the AII symmetry class can be concluded from simple scaling arguments.

As a second order transition (cf. [88]) the LD transition is characterized by scaling invariance and algebraical decay of correlations at the critical point. Recalling that the correlation function of a local order parameter field, $\varphi(\mathbf{r})$, has the general form $\chi(r) = \langle \varphi(\mathbf{r}_1)\varphi(\mathbf{r}_2) \rangle \propto e^{-r/\xi_c} r^{-\tilde{\eta}}$, where $r \equiv |\mathbf{r}_1 - \mathbf{r}_2|$, we see that algebraical decay at the critical point comes along with the divergence of the correlation length,

$$\xi_c(s) \propto |s - s^*|^{-\nu}. \quad (7.1)$$

Here s is some system parameter, s^* its critical value and ν the critical exponent of the correlation length. From rescaling $r \rightarrow \tilde{r} = br$ then follows $\chi(r) \propto r^{-\tilde{\eta}} = (\tilde{r}/b)^{-\tilde{\eta}}$, which means that there is no preferred length scale. Furthermore, the mean order parameter, $\langle \phi(\mathbf{r}) \rangle$, should vanish at the critical point (and in one of the two phases). In [48] it was shown that the *typical local density of states* (LDOS) is an appropriate choice for the order parameter of the LD transition,

$$\rho_{\text{typ}} := e^{\langle \ln \rho(\epsilon, \mathbf{r}) \rangle} \propto |s - s^*|^{\beta_\rho}, \quad (7.2)$$

where $\rho(\epsilon, \mathbf{r}) = |\psi(\epsilon, \mathbf{r})|^2 / \Delta(\epsilon)$, energy ϵ and level spacing $\Delta(\epsilon)$. β_ρ is the critical exponent of the order parameter. Moreover, ρ_{typ} shows power law scaling at the critical point,

$$\rho_{\text{typ}} \propto L^{d-\alpha_0}, \quad (7.3)$$

where L^d is the volume of a d -dimensional cube and α_0 is a scaling exponent, which is known from multifractal analysis of critical wave functions.

In 2D, i.e. for a square system, this scaling exponent is linked to the critical value of the quasi-1D RLL by a conformal mapping argument [48],

$$\Lambda^* = \frac{1}{\pi(\alpha_0 - 2)}. \quad (7.4)$$

With the knowledge of ν and α_0 the critical exponent of the LDOS is given by

$$\beta_\rho = \nu(\alpha_0 - 2). \quad (7.5)$$

Extending our interest from the critical region to the whole phase space we can ask for the existence of a global scaling variable. At first glance, the dimensionless conductance $g = (h/e^2)G$ seems to be the only suitable candidate for a scaling variable. Based on this *one-parameter scaling* hypothesis ABRAHAMS ET AL. developed in a celebrated paper [9] a complete qualitative picture of the LD transition only by scaling arguments. More precisely, they constructed the qualitative form of the β -function, which in the case of one-parameter scaling depends only on g (not explicitly on L or other parameters),

$$\beta(\ln g(L)) = \frac{d \ln g(L)}{d \ln L}. \quad (7.6)$$

For smooth β this is a one-parameter flow equation, also called *renormalization group equation*. Due to Ohm's law, $G = \sigma L^{d-2}$ with conductivity σ , the limiting value of β for large g is $d-2$, whereas in the regime of strong localization, $g \ll 1$, we have $\beta(\ln g) = \ln g \ll -1$. As a consequence we find the β -function always to be negative for 1D, which means that the system flows towards the attractive *localization fixed point* under renormalization. This corresponds to $g(d=1) = 0$ in the thermodynamic limit. Fig. 7.2 shows a qualitative picture of the β -function for $d = 1, 2, 3$. For 3D there exists (at least) one point with $\beta = 0$, where the conductance becomes independent of the system length. This critical point is a repulsive fixed point. It separates the localized regime from the delocalized regime, where in the thermodynamic limit g tends to the *delocalization fixed point* $g = \infty$. At the critical point we have $g = g^* = \mathcal{O}(1)$. Thus, the 3D system exhibits an LD transition. The two-dimensional case finally is more delicious. Here it depends strongly on the sign of the leading weak localization correction to the conductance, whether an LD transition is possible or not. As mentioned in the introduction the perturbative corrections to the conductance are negative for the symmetry classes A and AI yielding always localization. Whereas there is evidence for the existence of a delocalized phase in systems of AII symmetry, where the weak anti-localization correction yields a positive conductance for large system sizes. Thus, similar as in 3D we should expect an LD transition. We now

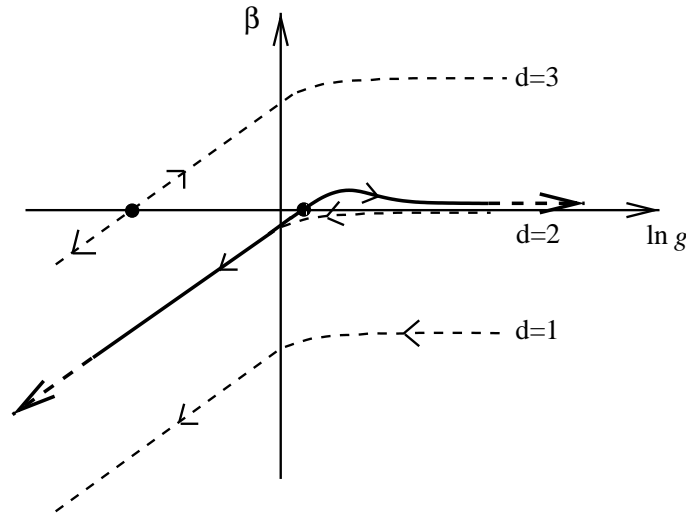


Figure 7.2: Qualitative picture of the β -function for $d = 1, 2, 3$. In the 2D case there can be a transition due to weak anti-localization.

ask, how to make progress towards a more quantitative characterization of this critical phenomenon. At this stage we make use of the important fact, that the derivative of the β -function at the critical point is *universal*, i.e. depending only on the symmetry and dimensionality of the system, and is just given by the inverse of the critical exponent ν of the correlation length

$$\beta'(\ln g) \Big|_{g=g^*} = \frac{1}{\nu}. \quad (7.7)$$

In Ch. 9 we will see, how ν can be calculated by means of a numerical method taking advantage of the scaling behaviour.

For completeness let us mention that later it was questioned whether the dimensionless conductance g is a good choice for a scaling variable, because of the universal conductance fluctuations mentioned in the introduction. As a consequence of UCF, the corresponding conductance distribution is far away from being Gaussian and the mean value $\langle g \rangle$ is not necessary a typical value for the conductance of the system. There can be a large influence of far tails of the distribution. Therefore, it was proposed¹ to consider the *geometric mean* $g_{\text{typ}} = e^{\langle \ln g \rangle}$ instead of $\langle g \rangle$ (cf. Ref. [2]), and indeed it turns out that formulated in terms of g_{typ} the scaling theory remains valid.

¹This proposition is based on the observation, that due to general results from the theory of random numbers the *logarithm* of g turns out to be Gaussian distributed. This distribution is also called a *log-normal distribution*.

Chapter 8

Network Model

In this chapter we introduce the scattering theoretical NWM for systems of AII symmetry. After the description of its topology we explicitly present the parameterization of the involved scattering matrices appropriate to the underlying symmetry. Finally, we discuss the structure of the corresponding parameter space.

8.1 Topology

The basic idea is to describe a 2D disordered mesoscopic system by a regular quadratic grid of unitary scattering matrices, which model the disorder potential of a real sample (cf. Fig. 7.1). These *potential scatterers* (PSs) map four incoming to four outgoing complex amplitudes, which symbolize electron waves. This allows a parameter dependent change of their direction, where the unitarity of the scatterers ensures conservation of the probability current. Between two scatterers electrons propagate freely, but a random phase factor is attached to the corresponding amplitudes modelling the random distances. So far, we have a NWM at hand, which allows us to describe mesoscopic systems of symmetry AI or A depending on the system being time-reversal invariant or not. This NWM has been investigated in Refs. [87,46]. In order to get a network model for AII symmetry we have to introduce spin degrees of freedom and to provide it with an additional mechanism of spin scattering. This can be realized by doubling each channel corresponding to spin-up and spin-down, and inserting *spin scatterers* (SSs) between each pair of PSs (cf. Fig. 8.1). The spin scatterers act only in spin space and are not able to change the direction of the propagating electrons. Of course, the most general case had been to implement spin scattering in the PSs. But it turns out that the simpler version of separated scatterers, which is easier to handle, is sufficient to explore the phenomenology of system with AII symmetry.

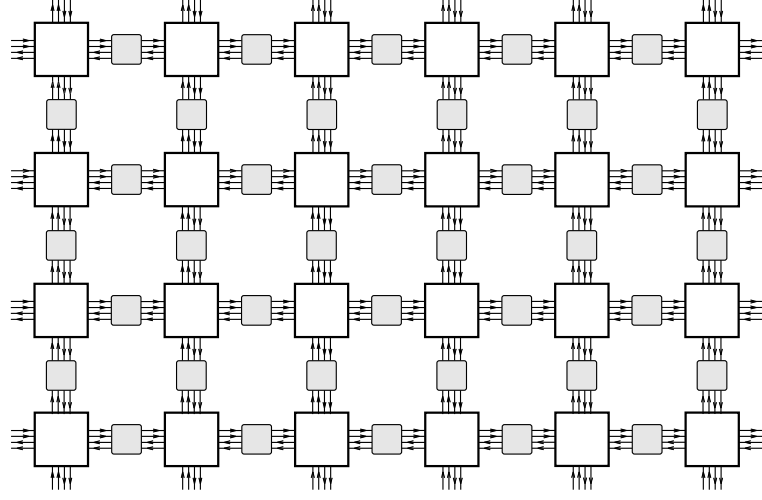


Figure 8.1: Topology of the network. The potential scatterers (white) change the direction, the spin scatterers (grey) the spin of the electrons.

8.2 Potential Scatterers

After doubling of the channels the PSs in the AII-NWM are now specified as follows: Each scatterer maps *eight* incoming amplitudes I_i^σ to *eight* outgoing amplitudes O_i^σ , where $\sigma \in \{+, -\}$ and $i \in \{1, 2, 3, 4\}$. Consequently, they can be represented by a 8×8 -matrix \mathbf{S}_{pot} . With the labeling of the channels defined according to Fig. 8.2 the mapping is specified by

$$\mathbf{O} = \mathbf{S}_{\text{pot}} \mathbf{I} \quad \text{with} \quad \mathbf{I} = \begin{pmatrix} I_1^+ \\ I_1^- \\ \vdots \\ I_4^+ \\ I_4^- \end{pmatrix} \quad \text{and} \quad \mathbf{O} = \begin{pmatrix} O_1^+ \\ O_1^- \\ \vdots \\ O_4^+ \\ O_4^- \end{pmatrix}. \quad (8.1)$$

Due to the constraint of current conservation,

$$\sum_{i,\sigma} |I_i^\sigma|^2 = \sum_{i,\sigma} |O_i^\sigma|^2, \quad (8.2)$$

each scattering matrix has to be unitary, $\mathbf{S}_{\text{pot}} \cdot \mathbf{S}_{\text{pot}}^\dagger = \mathbb{1}_8$, where $\mathbb{1}_8$ denotes the 8×8 identity matrix. Additionally, the scatterers are time reversal invariant. Both properties yield the matrix to be symmetric,

$$\mathbf{S}_{\text{pot}} = \mathbf{S}_{\text{pot}}^T. \quad (8.3)$$

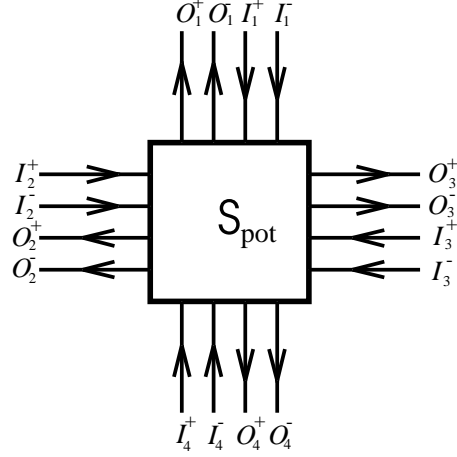


Figure 8.2: Potential scatterer: The eight incoming channels I_i^σ are mapped to the eight outgoing channels O_i^σ .

For convenience we choose the potential scatterers to be isotropic, i.e. they are invariant under rotations by multiple angles of $\pi/2$. This reduces the number of independent parameters by a factor four, without restricting the phenomenological content. With these constraints each scattering matrix S_{pot} can be parameterized in the following way [87]:

$$S_{\text{pot}} = \Phi \tilde{S}_{\text{pot}} \Phi, \quad (8.4)$$

where

$$\tilde{S}_{\text{pot}} = \begin{pmatrix} re^{i\phi_r} & d & d & te^{i\phi_t} \\ d & re^{i\phi_r} & te^{i\phi_t} & d \\ d & te^{i\phi_t} & re^{i\phi_r} & d \\ te^{i\phi_t} & d & d & re^{i\phi_r} \end{pmatrix} \otimes \mathbb{1}_2 \quad (8.5)$$

and

$$\Phi = \begin{pmatrix} e^{i\phi_1} & 0 & 0 & 0 \\ 0 & e^{i\phi_2} & 0 & 0 \\ 0 & 0 & e^{i\phi_3} & 0 \\ 0 & 0 & 0 & e^{i\phi_4} \end{pmatrix} \otimes \mathbb{1}_2. \quad (8.6)$$

Here $\mathbb{1}_2$ denotes the 2×2 identity matrix (in spin space). The real parameters r, t, d denote the *reflection*, *transmission*, and *deflection coefficient* (or *strength*), respectively. In Fig. 8.3 the meaning of the three parameters is visualized. For an incoming wave (bold line) the reflection and transmission coefficient are defined as usual. Additionally, our scatterers allow for left and right deflection, which are controlled by the *same* parameter d . We should note that the equality of left and

right scattering is *not* for convenience but specifies the present NWM to belong to a class of models *without handedness*. This is a crucial symmetry property which is e.g. not fulfilled in the Chalker-Coddington NWM.

It turns out that the constraints for S_{pot} allow for the choice of only two independent strengths and four phases. Let us chose r and t as independent, then the phases ϕ_r , ϕ_t and the deflection coefficient d are related to them due to unitarity and time reversal symmetry by

$$\begin{aligned} r^2 + 2d^2 + t^2 &= 1, \\ rd \cos \phi_r &= -td \cos \phi_t, \\ rt \cos(\phi_r - \phi_t) &= -d^2. \end{aligned} \tag{8.7}$$

The four phases ϕ_1, \dots, ϕ_4 which are randomly chosen from the interval $[0, 2\pi[$ model the spatial disorder. They can be interpreted as the phase factors $e^{i\phi_i}$ picked up during the propagation from one scatterer to the next one. Consequently, Altogether, we have *six* independent parameters for the PSs, from which only r and t govern the macroscopic properties, as localization behavior. For convenience we choose them to be equal for all PSs in the network, whereas the phases ϕ_1, \dots, ϕ_4 are randomly taken for each scatterer. We should expect that this is still enough randomness and that all crucial quantum interference effects are modelled. Hence, the partition in Eq. (8.4) can be interpreted by a constant center matrix taking into account the symmetries of the system and outer phase factors providing the interference effects.

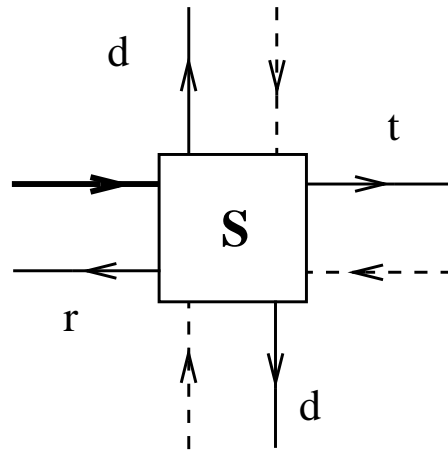


Figure 8.3: Definition of the reflection coefficient r , the transmission coefficient t and the deflection coefficient d .

8.3 Spin Scatterers

As already mentioned, each SS is located between a pair of PSs (cf. 8.1). Consequently, it has two incoming and two outgoing channels on the left and on the right, as is shown in Fig. 8.4. Hence, the SSs can be represented by 4×4 -matrices \mathbf{S}_{sp}

$$\mathbf{O} = \mathbf{S}_{\text{sp}} \mathbf{I} \quad \text{with} \quad \mathbf{I} = \begin{pmatrix} I^+ \\ I^- \\ \tilde{I}^+ \\ \tilde{I}^- \end{pmatrix} \quad \text{and} \quad \mathbf{O} = \begin{pmatrix} O^+ \\ O^- \\ \tilde{O}^+ \\ \tilde{O}^- \end{pmatrix}. \quad (8.8)$$

Conservation of probability current and time reversal symmetry result in (cf. [89])

$$\mathbf{S}_{\text{sp}} = \mathbf{D}^T \mathbf{S}_{\text{sp}}^T \mathbf{D} \quad (8.9)$$

and

$$\mathbf{S}_{\text{sp}} = \mathbf{D}^T \mathbf{K} \mathbf{S}_{\text{sp}}^{-1} \mathbf{K} \mathbf{D} = \mathbf{D}^T (\mathbf{S}_{\text{sp}}^{-1})^* \mathbf{D}, \quad (8.10)$$

respectively. Here the asterisk denotes complex conjugation and $\mathbf{K} \mathbf{D}$ is the time-reversal operator with complex conjugation operator \mathbf{K} and

$$\mathbf{D} = \begin{pmatrix} -\tau_2 & 0 \\ 0 & -\tau_2 \end{pmatrix}, \quad (8.11)$$

where τ_2 is one of the basis quaternions $(\tau_0, \boldsymbol{\tau}) = (\tau_0, \tau_1, \tau_2, \tau_3)$ given by

$$\tau_0 = \mathbb{1}_2 \quad \text{and} \quad \boldsymbol{\tau} = -i\boldsymbol{\sigma}, \quad (8.12)$$

and $\boldsymbol{\sigma} = (\sigma_1, \sigma_2, \sigma_3)$ is the vector of the Pauli matrices. The symmetries (8.9) and (8.10) suggest the following parameterization of the spin scattering matrix,

$$\mathbf{S}_{\text{sp}} = \begin{pmatrix} 0 & e^{i\varphi} q \\ e^{i\varphi} \bar{q} & 0 \end{pmatrix}, \quad (8.13)$$

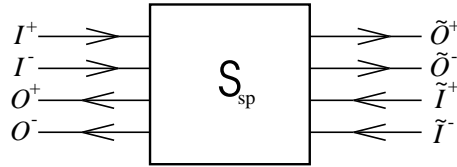


Figure 8.4: Spin scatterer: The four incoming channels $I^\sigma, \tilde{I}^\sigma$ are mapped to the eight outgoing channels $O^\sigma, \tilde{O}^\sigma$.

where

$$q = \sum_{k=0}^3 q_k \tau_k = \begin{pmatrix} q_0 - iq_3 & -q_2 - iq_1 \\ q_2 - iq_1 & q_0 + iq_3 \end{pmatrix} \in SU(2), \quad (8.14)$$

is a general *quaternion real* matrix and the bar denotes the quaternion conjugation,

$$\bar{q} = q_0 \tau_0 - \sum_{k=1}^3 q_k \tau_k. \quad (8.15)$$

Due to conservation of current the real coefficients q_i must fulfill the constraint $\sum_{k=0}^3 q_k^2 = 1$. It is now convenient to introduce a *spin scattering strength* by

$$s = \sqrt{1 - q_0} = \sqrt{q_1^2 + q_2^2 + q_3^2} \in [0, 1]. \quad (8.16)$$

While s is fixed for the whole network, the vector (q_1, q_2, q_3) is homogeneously taken from a 2-sphere of radius s . For $s = 0$ we then have $q = \bar{q} = \mathbb{1}_2$ and there is no spin scattering at all, whereas for the maximum value, $s = 1$, we have $q_0 = 0$, and in each scattering event the spin is changed. In average this corresponds to a complete randomization of the spin after only one scattering process. The phase φ is randomly taken from $[0, 2\pi[$.

8.4 Parameter space

In conclusion there are three independent strength $(r, t, s) \in [0, 1] \times [0, 1] \times [0, 1]$ building up the three dimensional parameter space (or phase space) of the AII-NWM. While s can take all values in the interval $[0, 1]$ the (r, t) subspace is restricted by further constraints. Fig. 8.5 shows a cross-section of the phase space at some arbitrary value of s . From Eqs. (8.7) follows that

$$r^2 + t^2 \leq 1 \quad \text{and} \quad r + t \geq 1. \quad (8.17)$$

The first inequation resulting from the unitarity of the PSs restricts the possible values to a quarter of a circle of radius 1, the second one corresponding to time-reversal invariance allows only values on the right of the secondary diagonal. As a consequence only values in the grey region are admitted. This area is just the accessible parameter space of a NWM for systems of symmetry class AI. Thus, setting $s = 0$, which means switching off the spin scattering, we leave the AII symmetry class and cross-over to AI. Note further, that abandoning the second constraint in Eq. (8.17) we get the parameter space of an A-NWM. But note that in the case of A symmetry, the PSs have less symmetry, which must be taken into account in order to realize an A-NWM.

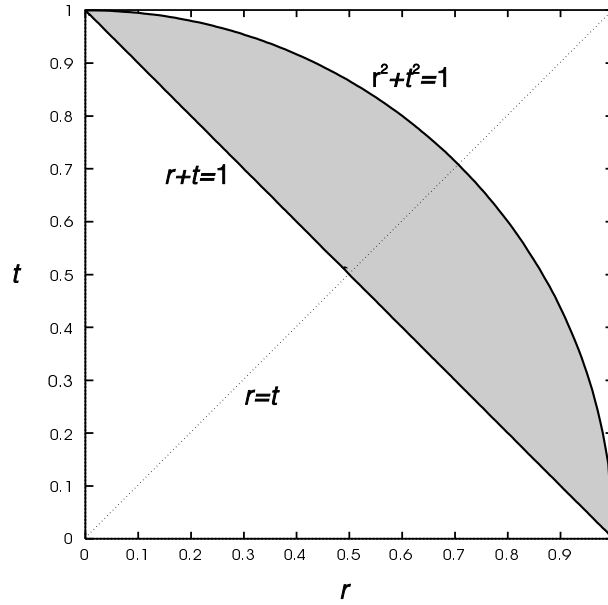


Figure 8.5: Cross-section of the parameter space at some fixed s . Only the grey area is accessible in the AII-NWM.

There are three exceptional points in the phase space, marked by bullets in Fig. 8.5: The point $(r, t) = (0, 1)$ is the *delocalization fixed point*, where there is no disorder, and the electron waves propagate freely. At the opposite side of the phase space, $(r, t) = (1, 0)$, we have the *localization fixed point*, where all incoming waves are strictly reflected, prohibiting any transport. The point $r = t = 0$ is the *Chalker-Coddington fixed point* [90], which corresponds to the critical point of a quantum Hall system. Here all waves are scattered with equal probability either to the right or to the left. Note further, that on the line $r^2 + t^2 = 1$ the deflection coefficient vanishes due to Eq. (8.7). Thus, the system splits into two uncoupled 1D subsystems, which without fail yields strong localization.

Chapter 9

Finite-Size Scaling

In the introduction to this part we have seen that the flow of the dimensionless conductance g under renormalization of the system size characterizes the system to be localized or not. In order to investigate the LD transition in (quadratic) 2D systems of AII symmetry we now could try to calculate g and study its system size dependence. But as likewise pointed out in the introduction the conductance fluctuates very strongly due to the effect of UCF and is therefore not very suited for this task. Instead, let us now consider a quasi-1D system of *finite*¹ width M and length L and calculate the so-called *quasi-1D localization length* $\xi = \xi(M)$ which turns out to be a self-averaging quantity². Particularly, ξ can be calculated with high precision by means of the transfermatrix method [91,92] based on the NWM. This method yields a sequence of Lyapunov exponents in decreasing order, where the inverse of the smallest positive Lyapunov exponent determines the quasi-1D LL. It is always finite due to the finite width of the system. Furthermore, it turns out that the ratio $\xi(M)/M$ provides us with a well-suited scaling variable, whose M dependence allows us to explore the localization behaviour of the system. The *finite size scaling* method is one of the most powerful tools for the numerical investigation of scaling behaviour (cf. Ref. [93]). In the context of NWM it has already been applied to the symmetry classes A and AI (cf. Ref. [94,46,87]) and the Chalker-Coddington-NWM (cf. Ref. [90,95]).

In the first section we show how the quasi-1D LL can be calculated by means of a numerical transfer matrix method. Then the definition and parameterization of the transfer matrices in the AII-NWM are given. In the last section we explicitly present the fit methods used for the elaboration of the LD transition. Further, we show how these fits can be verified by confidence tests.

¹Of course, for numerics we always have to consider finite systems. But finite here means that in contrast to a 2D system the width M is much smaller than the (even finite but considered as infinite) length L .

²This means that fluctuations around the mean value die out for $L \rightarrow \infty$.

In Ref. [87] an elastic mean free path is defined by the expression

$$l_e := \frac{1}{2} \frac{t^2 + d^2}{r^2 + d^2}. \quad (9.1)$$

The factor $1/2$ is a consequence of the diagonal arrangement, which is shown in Fig. 9.2. l_e is measured in units of a lattice constant.

9.1 Transfer Matrix Method

In this section we sketch how to get the quasi-1D LL by means of the (numerical) transfer matrix method. In analogy to the derivation of the heat equation in the first part of this thesis, we therefore divide the whole quasi-1D strip into N small vertical slices of length $\epsilon = L/N$. To each of these slices a $2P \times 2P$ -dimensional *strip transfer matrix* \mathbb{T}_k is assigned³, which in contrast to the scattering matrices defined in the foregoing chapter maps amplitudes on the left to amplitudes on the right. Thus, composition of two such matrices results in the transfer operator for a system of doubled slice length, i.e. the transfer matrices are *multiplicative*. This allows us to formulate the transfer matrix of the total quasi-1D system by the product

$$\mathbb{T}(N) = \prod_{k=1}^N \mathbb{T}_k. \quad (9.2)$$

Note that the Landauer-Büttiker formula for the conductance (cf. e.g. Ref. [2]),

$$g = \text{tr} \frac{2}{\mathbb{T}(N)\mathbb{T}^\dagger(N) + (\mathbb{T}(N)\mathbb{T}^\dagger(N))^{-1} + 2}, \quad (9.3)$$

basically depends on the product $\mathbb{T}\mathbb{T}^\dagger$. By a theorem of the theory of random matrices (cf. Ref. [91]) the limit matrix $\lim_{N \rightarrow \infty} (\mathbb{T}(N)\mathbb{T}^\dagger(N))^{\frac{1}{2N}}$ exists and can be diagonalized yielding P pairs⁴ of eigenvalues $(e^{\lambda_i}, e^{-\lambda_i})$, where the P positive numbers $\lambda_P > \dots > \lambda_1$ are called *Lyapunov exponents*. In the case of time-reversal invariance and spin-orbit scattering, each eigenvalue appears twice as a consequence of Kramers degeneracy (cf. Ref. [89]). Entering the eigenvalues into Eq. (9.3) it turns out that the dimensionless conductance decreases exponentially on a length scale $\xi \propto 1/\lambda_1$ justifying the name localization length for ξ .

Numerically, the calculation of the p largest Lyapunov exponents can be realized as follows: Interpret the index k as discrete time and generate at $k = 1$ a system

³The value of P depends on the number of channels per width unit and will be specified for the AII-NWM in the next section

⁴This is a consequence of the conservation of probability current.

of p vectors $\mathbf{z}_1(1), \dots, \mathbf{z}_p(1) \in \mathbb{C}^{2P}$. Then $\mathbf{z}_l(k+1) = \mathbb{T}_k \mathbf{z}_l(k)$, and the sum of the p largest Lyapunov exponents is given by (cf. [96,91])

$$\lambda_P + \dots + \lambda_{P-p+1} = \lim_{N \rightarrow \infty} \frac{1}{N} \ln \frac{\text{Vol}[\mathbb{T}(N)\mathbf{z}_1(1), \dots, \mathbb{T}(N)\mathbf{z}_p(1)]}{\text{Vol}[\mathbf{z}_1(1), \dots, \mathbf{z}_p(1)]} \quad (9.4)$$

where $\text{Vol}[\mathbf{z}_1, \dots, \mathbf{z}_p]$ denotes the volume of the spar spanned by the vectors $\mathbf{z}_1, \dots, \mathbf{z}_p$. Starting with $p = 1$ this method should yield the Lyapunov exponents in descending order. But we are faced with a problem. The length of the vectors grows very rapidly in the direction of the eigenvector corresponding to the largest Lyapunov exponent, which causes a memory overflow and strongly decreasing accuracy after only a few transfer steps. These problemes can be surmounted by the following trick. One decomposes the total system into n subsystems with transfer matrices $\mathbb{T}(j)$, $j = 1, \dots, n$, where each subsystem consists of m slices with transfer matrices $\mathbb{T}_k(j)$, $k = 1, \dots, m$ (cf. Fig. (9.1)). Consequently, the

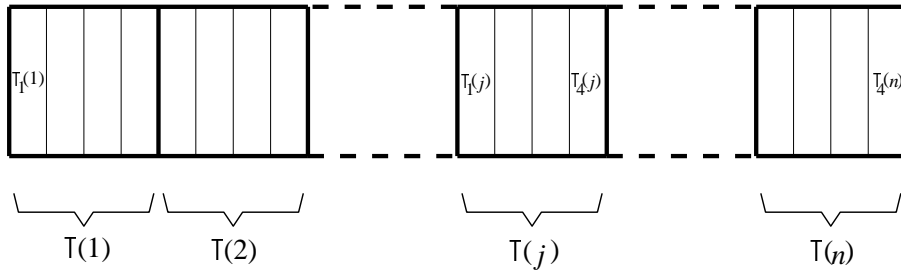


Figure 9.1: Decomposition of the quasi-1D system.

transfer matrix of the total system is given by

$$\mathbb{T}(N) = \prod_{j=1}^n \mathbb{T}(j), \quad \text{where } \mathbb{T}(j) = \prod_{k=1}^m \mathbb{T}_k(j). \quad (9.5)$$

In order to prohibit the problems mentioned above after each m steps corresponding to a subsystem we perform a Gram-Schmidt orthonormalization to the vectors $\{\mathbf{z}_1(j), \dots, \mathbf{z}_p(j)\}$, yielding a new system $\{\mathbf{z}'_1(j), \dots, \mathbf{z}'_p(j)\}$. Here m has to be small enough, so that we stay within the computational accuracy. Before each renewed orthonormalization we store the growing factors of each of the p vectors obtained by the foregoing orthonormalization. These factors are given by

$$b_i(j) = \left| \mathbf{z}_i(j) - \sum_{l=1}^{i-1} \alpha_l(j) \mathbf{z}'_l(j) \right|, \quad i = 1, \dots, p, \quad (9.6)$$

with expansion coefficients $\alpha_l(j) = \mathbf{z}'_l(j) \cdot \mathbf{z}_i(j)$. We finally end up with the following expression for the i -th Lyapunov exponent

$$\lambda_i = \lim_{n \rightarrow \infty} \frac{1}{n} \sum_{j=1}^n \frac{\ln b_i(j)}{m}. \quad (9.7)$$

This expression is exact. For real calculations we of course have to introduce a cut-off for n , which will depend on the desired accuracy of the result. With the available computational power we can demand $\Delta\lambda < 1\%$, where the mean error of the average is given by

$$\Delta\lambda_i = \frac{1}{\sqrt{n}} \sqrt{\frac{\frac{1}{n} \sum_{j=1}^n [\ln b_i(j)]^2 - \left[\frac{1}{n} \sum_{j=1}^n \ln b_i(j) \right]^2}{m^2}}. \quad (9.8)$$

9.2 Transfer Matrices of the AII Network Model

With the labels defined in Fig. 8.2 and Fig. 8.4 the transfer matrices of the AII-NWM corresponding to \mathbf{S}_{pot} and \mathbf{S}_{sp} are defined by

$$\begin{pmatrix} O_3^+ \\ O_3^- \\ I_3^+ \\ I_3^- \\ O_4^+ \\ O_4^- \\ I_4^+ \\ I_4^- \end{pmatrix} = \mathbf{T}_{\text{pot}} \begin{pmatrix} I_1^+ \\ I_1^- \\ O_1^+ \\ O_1^- \\ I_2^+ \\ I_2^- \\ O_2^+ \\ O_2^- \end{pmatrix} \quad (9.9)$$

and

$$\begin{pmatrix} \tilde{O}^+ \\ \tilde{O}^- \\ \tilde{I}^+ \\ \tilde{I}^- \end{pmatrix} = \mathbf{T}_{\text{sp}} \begin{pmatrix} I^+ \\ I^- \\ O^+ \\ O^- \end{pmatrix}, \quad (9.10)$$

respectively. From this definition a diagonal arrangement of the network results as is shown in Fig. 9.2. The natural width unit in this arrangement is given by a *pair* of diagonally neighboured transfer matrices. This corresponds to a channel number⁵ of $N_c = 4$. Therefore the bold printed part of the picture represents a *strip transfer matrix* of width $M = 2$, i.e. channel number $N_c = 8$, and unit length $L = 1$. The arrows at the top and the bottom of the figure symbolize periodic boundary conditions. In terms of the transfer matrices the conservation of current density becomes a *pseudo-unitarity* relation

$$\mathbf{T}_{\text{pot}} \Sigma_3 \mathbf{T}_{\text{pot}}^\dagger = \Sigma_3 \quad (9.11)$$

and

$$\mathbf{T}_{\text{sp}} \Sigma'_3 \mathbf{T}_{\text{sp}}^\dagger = \Sigma'_3 \quad (9.12)$$

⁵Note that one incoming wave and its outgoing partner count as one channel.

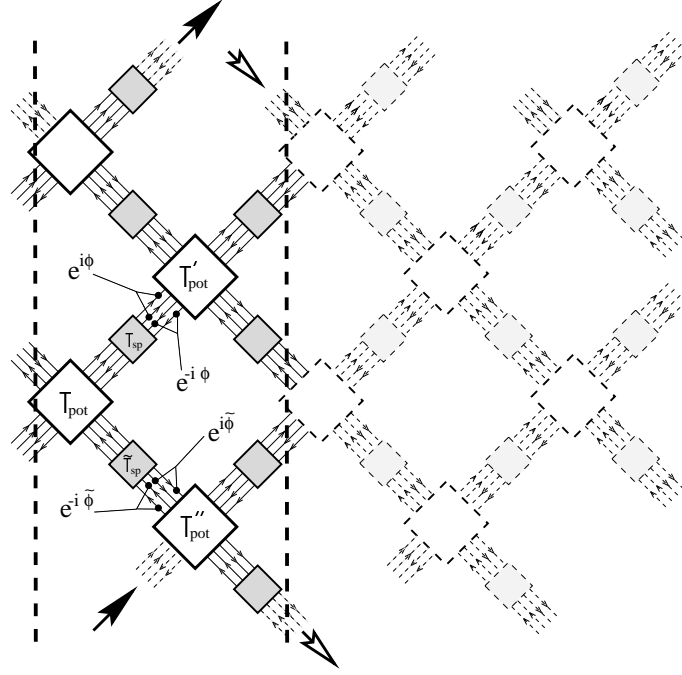


Figure 9.2: Definition of the strip transfer matrix for $M = 2$. The arrows indicate the periodic boundary conditions.

for PSs and SSs, respectively, where $\Sigma_3 = \mathbb{1}_4 \otimes \sigma_3$ and $\Sigma'_3 = \mathbb{1}_2 \otimes \sigma_3$. Furthermore, time reversal invariance yields

$$\mathsf{T}_{\text{pot}} = \begin{pmatrix} 0 & \mathsf{D} \\ \mathsf{D} & 0 \end{pmatrix}^T \mathsf{T}_{\text{pot}}^* \begin{pmatrix} 0 & \mathsf{D} \\ \mathsf{D} & 0 \end{pmatrix} \quad (9.13)$$

and

$$\mathsf{T}_{\text{sp}} = \mathsf{D}^T \mathsf{T}_{\text{sp}}^* \mathsf{D}, \quad (9.14)$$

where D is given by Eq. (8.11). A parameterization of S_{pot} compatible with these constraints is given by (cf. Ref. [87])

$$\mathsf{T}_{\text{pot}} = \begin{pmatrix} \alpha^* & \gamma & \beta^* & \delta \\ -\gamma & \alpha & -\delta & \beta \\ \beta^* & \delta & \alpha^* & \gamma \\ -\delta & \beta & -\gamma & \alpha \end{pmatrix} \otimes \mathbb{1}_2, \quad (9.15)$$

where

$$\begin{aligned}\alpha &= \frac{d}{\Delta}, & \beta &= -\frac{te^{i\phi_t}}{\Delta}, \\ \gamma &= \frac{(re^{i\phi_r} - te^{i\phi_t})d}{\Delta}, & \delta &= \frac{d^2 - re^{i\phi_r}te^{i\phi_t}}{\Delta}, \\ \Delta &= d^2 - (te^{i\phi_t})^2.\end{aligned}\tag{9.16}$$

For T_{sp} we find

$$T_{\text{sp}} = \begin{pmatrix} e^{i\varphi\bar{q}} & 0 \\ 0 & e^{-i\varphi\bar{q}} \end{pmatrix}\tag{9.17}$$

It turns out that the four outer phase factors ϕ_1, \dots, ϕ_4 of S_{pot} can be absorbed in a *single* phase φ on the links, which we have included in S_{sp} . Note that due to time-reversal symmetry the phase factors of an incoming and the corresponding outgoing amplitude are related by complex conjugation (cf. Fig. 9.2).

9.3 LD Transition in the AII-NWM

In the following we point out how finite-size scaling method can be applied to the AII-NWM. We have seen in Sec. 9.1 that the inverse of the smallest Lyapunov exponent plays the role of the quasi-1d LL,

$$\xi(M) = \frac{1}{\lambda_1}.\tag{9.18}$$

Within the NWM this quantity generally depends on all free parameters (r, t, s) of the transfer matrices, but in what follows we will fix two of these parameters. Let us denote the free parameter by $\tau \in r, t, s$. Then we $\xi(M) = \xi(M; \tau)$, where we suppress the τ in the notation, if specification is not necessary for the context. In the thermodynamic limit we have $\lim_{M \rightarrow \infty} \xi(M; \tau) = \xi(\infty; \tau)$ if we start in the localized and $\lim_{M \rightarrow \infty} \xi(M; \tau) = \infty$ if we start in the delocalized phase. At the critical point, where the system is scale independent, we should expect $\xi(M; \tau) \propto M$. This motivates the introduction of the *renormalized localization length* (RLL) (cf. Ref. [92])

$$\Lambda(M; \tau) = \frac{\xi(M; \tau)}{M}.\tag{9.19}$$

Let M_1 and M_2 be system widths with $M_1 < M_2$. Then the LD transition can be characterized by the behaviour of $\Lambda(M; \tau)$ under renormalization:

$$\left\{ \begin{array}{l} \Lambda(M_2) < \Lambda(M_1) \\ \Lambda(M_2) = \Lambda^* = \Lambda(M_1) \\ \Lambda(M_2) > \Lambda(M_1) \end{array} \right\}, \quad \text{if the system is} \quad \left\{ \begin{array}{l} \text{in the localized phase} \\ \text{at the critical point} \\ \text{in the delocalized phase} \end{array} \right\}.\tag{9.20}$$

In the thermodynamic limit we obtain

$$\lim_{M \rightarrow \infty} \Lambda(M) = \begin{cases} 0 & \text{at the localization fixed point} \\ \Lambda^* & \text{at the critical point} \\ \infty & \text{at the delocalization phase} \end{cases}. \quad (9.21)$$

Thus, we obtain exactly the same behaviour as for the conductance (cf. Sec. 7.2) and can therefore use the RLL as a scaling variable.

Now the question arises whether $\Lambda(M; \tau)$ is the *only* scaling variable, i.e. whether one-parameter scaling is valid. If this is the case the β -function for the RLL should depend only on Λ itself. It turns out that equivalently we can ask for the existence of a *scaling function*, which depends only on the *ratio* of the correlation length ξ_c and the system width M ,

$$\Lambda(M; \tau) = \tilde{f}\left(\frac{\xi_c(\tau)}{M}\right) \quad (9.22)$$

or logarithmically

$$\ln \Lambda(M; \tau) = f\left(\ln M - \ln \xi_c(\tau)\right). \quad (9.23)$$

Within our transfer matrix approach the correlation length ξ_c is now defined as the fictitious system width up to which the system is in the critical regime, where critical regime means the range of validity for the linearization of the β -function. Thus, for the localized regime we just have $\xi_c = \xi(\infty; \tau)$, whereas at the critical point the correlation length diverges as demanded. Eq. (9.23) tells us that a whole set of data $\Lambda(M; \tau)$, which can be obtained by the transfer matrix method described in Sec. 9.1, has to fall onto one curve, if one-parameter scaling is valid. Note that one can also predict the qualitative form of the scaling function. Since in the localized regime the RLL decreases with increasing system width, whereas it increases in the delocalized regime this function has two independent branches. These branches tend to the same value $\ln \Lambda^*$ at one side and diverge in opposite directions on the other side.

The existence of a one-parameter scaling function is an inevitable condition for the applicability of the methods we use later for the calculation of ν . Hence, we should spend some effort for a preferably reliable answer to the question whether one-parameter scaling is valid or not. Therefore, we do not use the method of shifting data on transparencies, reading off the shift and calculating $\xi_c(\tau)$ from these values. Rather, we use a numerical fit procedure and apply a confidence test to the fit in order to obtain an optimal result. The same idea is used for the subsequent calculation of the critical exponent. The next section is dedicated to a detailed presentation of the numerical fit and test methods.

9.4 Methods of evaluation

The methods presented in the following are based on Ref. [47], where the scaling function for a quantum Hall system was fitted and tested by a χ^2 test.

9.4.1 Fit Procedure for the Scaling Function

According to Eq. (9.23) we want to fit the scaling function f to the logarithms of the RLLs, which we assume to depend on n_M system widths $\{M_1, \dots, M_{n_M}\}$ and n_r system parameters $\{r_1, \dots, r_{n_r}\}$. Thus, we have $n_\Lambda = n_M \cdot n_r$ data points $\{\Lambda_1, \dots, \Lambda_{n_\Lambda}\}$. The parameters are the reflection strength in the transfer matrices of the NWM. Let us introduce the following vectors,

$$\mathbf{Y} := \begin{pmatrix} \ln \Lambda_1 \\ \vdots \\ \ln \Lambda_{n_\Lambda} \end{pmatrix}, \quad \tilde{\mathbf{X}} := \begin{pmatrix} \ln M_1 - \ln \xi_c(r_1) \\ \vdots \\ \ln M_{n_M} - \ln \xi_c(r_{n_r}) \end{pmatrix} \quad (9.24)$$

and

$$\mathbf{E} := \begin{pmatrix} \Delta \ln \Lambda_1 \\ \vdots \\ \Delta \ln \Lambda_{n_\Lambda} \end{pmatrix}, \quad (9.25)$$

the latter being the vector containing the errors of the average according to Eq. (9.8). Assuming the data to be statistically independent the corresponding correlation matrix \mathbf{C}_Λ given by

$$(\mathbf{C}_\Lambda)_{ij} := \langle E_i \cdot E_j \rangle \quad (9.26)$$

is diagonal. Here $\langle \dots \rangle$ denotes the mean value.

We now make an ansatz for the scaling function by a linear combination of Chebyshev polynomials,

$$F(x_i) = \frac{c_0}{2} + \sum_{k=1}^N c_k T_k(X_i), \quad (9.27)$$

which gives a polynomial of degree N . Omitting the tilde over the X_i indicates the argument to be rescaled to the interval $[-1, 1]$. In this interval the Chebyshev polynomials are orthogonal and have simple behavior at the edges.

The smallest of the parameters $\ln \xi_c$ is fixed by requiring $\ln \xi_c(r_1) \equiv 0$ for the delocalized branch and $\ln \xi_c(r_{n_r}) \equiv 0$ for the localized branch, respectively. Thus,

we have $n_{\Theta} = n_r + N$ parameters

$$\Theta := \begin{pmatrix} \ln \xi_c(r_1) \\ \vdots \\ \ln \xi_c(r_{n_r-1}) \\ c_0 \\ \vdots \\ c_N \end{pmatrix}, \quad (9.28)$$

for the localized and

$$\Theta := \begin{pmatrix} \ln \xi_c(r_2) \\ \vdots \\ \ln \xi_c(r_{n_r}) \\ c_0 \\ \vdots \\ c_N \end{pmatrix}, \quad (9.29)$$

for the delocalized branch, respectively. These parameters have to be fitted with respect to the data \mathbf{Y} . Hence, the n_{Λ} values of the fit function can be written as

$$\mathbf{F}(\mathbf{X}; \Theta) := \begin{pmatrix} F(X_1; \Theta) \\ \vdots \\ F(X_{n_{\Lambda}}; \Theta) \end{pmatrix}. \quad (9.30)$$

Using the method of the least-squares fit we have to minimize the sum S_{Θ} of the weighted quadratic deviations, which means solving the equation

$$\frac{\partial S_{\Theta}}{\partial \Theta} = \mathbf{0} \quad (9.31)$$

with

$$S_{\Theta} = \left(\mathbf{Y} - \mathbf{F}(\mathbf{X}; \Theta) \right)^{\top} \mathbf{C}_{\Lambda}^{-1} \left(\mathbf{Y} - \mathbf{F}(\mathbf{X}; \Theta) \right). \quad (9.32)$$

Since \mathbf{F} is non-linear in the parameters Θ this procedure yields a system of n_{Θ} coupled non-linear equations. Therefore S_{Θ} is minimized directly by a numerical method. Starting with some estimated initial values for the logarithms of the correlation lengths we successively optimize the c_i and the $\ln \xi_c(r_i)$. If the data are compatible we will have convergence, and thus we can stop when a chosen accuracy is reached. The result then is a set of coefficients c_i which defines the fit function and a set of optimized values for the correlation lengths.

According to Ref. [97] the correlation matrix of the parameters is given by

$$\mathbf{C}_{\Theta} = \left(\mathbf{F}_{\Theta}^{\top} \mathbf{C}_{\Lambda}^{-1} \mathbf{F}_{\Theta} \right)^{-1}, \quad (9.33)$$

where F_{Θ} is the Jacobian of \mathbf{F} with respect to Θ ,

$$F_{\Theta} := \frac{\partial \mathbf{F}}{\partial \Theta}. \quad (9.34)$$

Usually, as errors of the parameters one takes the diagonal elements of the error matrix \mathbf{E} , which is defined by

$$\mathbf{E}_{\Theta} = \frac{S_{\Theta}}{n_{\Lambda} - n_{\Theta}} \mathbf{C}_{\Theta}. \quad (9.35)$$

9.4.2 Testing the Fit of the Scaling Function

A converging fit procedure does not guarantee that the errors of the numerical data are actually compatible with the obtained fit function. Therefore, in addition to this fit procedure we apply a χ^2 test to estimate the confidence of the fit. We make the essential assumption that the data y_i are *normally* distributed about $f(x_i; \Theta)$ with variances e_i^2 . Consequently, the quantity S_{Θ} has to be distributed as χ^2 with $n_{\Lambda} - n_{\Theta}$ degrees of freedom. This distribution has the estimated value $n_{\Lambda} - n_{\Theta}$ and the variance $2(n_{\Lambda} - n_{\Theta})$. A suitable measure for the confidence of the fit then is the normalized deviation of S from the estimated value

$$\Delta_{\Theta} = \frac{S_{\Theta} - (n_{\Lambda} - n_{\Theta})}{\sqrt{2(n_{\Lambda} - n_{\Theta})}}. \quad (9.36)$$

If $|\Delta_{\Theta}| \lesssim 1$ it is safe to assume that the fit is trustworthy. But if $|\Delta_{\Theta}|$ takes values much larger than 1 it is very unlikely that the data Y_i are normally distributed about $F(X_i; \Theta)$ which indicates systematic errors. In this case the fit has failed, we have to give up the assumption of one-parameter scaling and further calculations, e.g. of the critical exponent, do not make much sense.

It should be noticed that rescaling of the variance matrix \mathbf{S} by a factor b , $\tilde{\mathbf{S}} = b \cdot \mathbf{S}$, results in the reciprocal rescaling of S_{Θ} , $\tilde{S}_{\Theta} = b^{-1} S_{\Theta}$. Since Δ_{Θ} depends sensitively on S_{Θ} , especially if n_{Λ} is small, one should carefully consider, how to determine the errors of the raw data.

9.4.3 Fit for the Critical Exponent ν

In order to determine the critical exponent of the correlation length we apply the same idea as before with respect to Eq. (7.1). Particularly, we simultaneously deal with both branches of the scaling function, i.e. we assume the critical value r^* and the critical exponent ν to be the same in the localized and the delocalized regime. Only the prefactor can take different values, which will be denoted as

$\xi_c^{0,\text{loc}}$ and $\xi_c^{0,\text{deloc}}$ for the localized and the delocalized regime, respectively. Taking the logarithm Eq. (7.1) writes as

$$\ln \xi_c(r_i) = \ln \xi_c^{0,\text{loc}} - \nu \ln |r_i - r^*| \quad (9.37a)$$

and

$$\ln \xi_c(r_i) = \ln \xi_c^{0,\text{deloc}} - \nu \ln |r_i - r^*| \quad (9.37b)$$

for r_i in the localized and delocalized regime, respectively. The n_r values $\ln \xi_c(r_i)$ are the results of the foregoing optimization, the arguments are the values $\ln |r_i - r^*|$ and the four parameters that have to be optimized are $\xi_c^{0,\text{loc}}$, $\xi_c^{0,\text{deloc}}$, ν and r^* . Introducing the vectors

$$\mathbf{y} := \begin{pmatrix} \ln \xi_c(r_1) \\ \vdots \\ \ln \xi_c(r_{n_r}) \end{pmatrix}, \quad \mathbf{x} := \begin{pmatrix} \ln |r_1 - r^*| \\ \vdots \\ \ln |r_{n_r} - r^*| \end{pmatrix} \quad (9.38)$$

$$\boldsymbol{\theta} := \begin{pmatrix} \ln \xi_c^{0,\text{loc}} \\ \ln \xi_c^{0,\text{deloc}} \\ \nu \\ r^* \end{pmatrix} \quad \text{and} \quad \tilde{\boldsymbol{\theta}} := \begin{pmatrix} \ln \xi_c^{0,\text{loc}} \\ \ln \xi_c^{0,\text{deloc}} \\ \nu \end{pmatrix} \quad (9.39)$$

and comparing them with Eq. (9.37) the fit function can be written as

$$\mathbf{f}(\mathbf{x}; \boldsymbol{\theta}) = \mathbf{W}(\mathbf{x}) \tilde{\boldsymbol{\theta}}, \quad (9.40)$$

with

$$\mathbf{W} := \begin{pmatrix} 1 & 0 & -\ln |r_1 - r^*| \\ \vdots & \vdots & \vdots \\ 1 & 0 & -\ln |r_{n_r,\text{loc}} - r^*| \\ 0 & 1 & -\ln |r_{n_r,\text{loc}+1} - r^*| \\ \vdots & \vdots & \vdots \\ 0 & 1 & -\ln |r_{n_r} - r^*| \end{pmatrix}. \quad (9.41)$$

Here $n_{r,\text{loc}}$ is the number of values r_i which belong to the localized regime. The correlation matrix \mathbf{C}_{ξ_c} of the data y_i is the upper left $n_r \times n_r$ submatrix of \mathbf{C}_Θ in Eq. (9.33) obtained by the fit of the scaling function. Thus, the sum of the quadratic deviations is

$$S_\theta = \left(\mathbf{y} - \mathbf{f}(\mathbf{x}; \boldsymbol{\theta}) \right)^\top \mathbf{C}_{\xi_c}^{-1} \left(\mathbf{y} - \mathbf{f}(\mathbf{x}; \boldsymbol{\theta}) \right). \quad (9.42)$$

Since the fit function is a *linear* function in the argument \mathbf{x} , we can analytically solve the minimization problem

$$\frac{\partial S_\theta}{\partial \tilde{\boldsymbol{\theta}}} = \mathbf{0}, \quad (9.43)$$

which yields

$$\tilde{\boldsymbol{\theta}} = (\mathbf{W}^T \mathbf{C}_{\xi_c}^{-1} \mathbf{W})^{-1} \mathbf{W}^T \mathbf{C}_{\xi_c}^{-1} \mathbf{y}. \quad (9.44)$$

In contrast to that the parameter r^* has to be optimized numerically since it appears non-linearly in Eq. (9.37). Giving some starting value for r^* one iteration step consists of successively optimizing $\tilde{\boldsymbol{\theta}}$ and r^* . The 4×4 correlation matrix of the four parameters is given by

$$\mathbf{C}_\theta = (\mathbf{F}_\theta^T \mathbf{C}_{\xi_c}^{-1} \mathbf{F}_\theta)^{-1}, \quad (9.45)$$

where

$$\mathbf{F}_\theta \equiv \frac{\partial \mathbf{f}}{\partial \boldsymbol{\theta}}. \quad (9.46)$$

Finally we get the error matrix

$$\mathbf{E}_\theta = \frac{S_\theta}{n_r - 4} \mathbf{C}_\theta. \quad (9.47)$$

As in Eq. (9.36) we use the quantity

$$\Delta_\theta = \frac{S_\theta - (n_r - 4)}{\sqrt{2(n_r - 4)}}. \quad (9.48)$$

to test the confidence of the fit. $|\Delta_\theta|$ should take values of about 1 or smaller to verify the assumption that the values y_i are normally distributed about the fit function, which is a straight line in this case. Note that it is important to take the correlations between the $\xi_c(r_i)$ introduced by the previous fit procedure into account in the present analysis. Thus, a simple linear regression will not give the correct results.

9.4.4 Determination of Λ^*

The fit procedures introduced in Secs. 9.4.1 and 9.4.3 are not the most direct way to determine ν from the raw data. Instead, one can fit the RLLs as functions of $|r - r^*|$ with a width dependent scaling factor $M^{1/\nu}$

$$\Lambda(M; r) = h(M^{1/\nu} |r - r^*|), \quad (9.49)$$

which is a consequence of Eqs. (9.22) and (7.1). This procedure leads to a continuous curve, because there is no splitting in two branches as in the logarithmic case. Fitting the scaling function in this manner allows a direct evaluation of Λ^* . Since at $r = r^*$ the argument of h is zero, one only has to calculate this value,

$$\Lambda^* = h(0). \quad (9.50)$$

Following the law of propagation of errors we get for the error of the critical RLL

$$\Delta\Lambda^* = \Delta\Lambda|_{r=r^*} = M^{1/\nu} \Delta h'(0)r^*, \quad (9.51)$$

where h' denotes the first derivative of h with respect to the argument.

Chapter 10

Results and Discussions

In this chapter the results of our investigations of the AII-NWM are presented. In the first section RLLs depending on the system width and several choices for the parameters are shown. Furthermore, we determine a phase diagram for the total three-dimensional phase space. The second section presents the scaling function, which we have obtained by the fit procedure described in the foregoing chapter. In the last section finally, the values for the critical exponent and the critical RLL are given.

10.1 Localization Lengths and Phase Diagram

We calculated quasi-1D LLs for system widths from $M = 2$ up to $M = 32$, which corresponds to channel numbers from $N_c = 16$ to $N_c = 256$. The corresponding errors $\Delta\Lambda$ are the errors of the mean value given by Eq. (9.8), which vanish for $L \rightarrow \infty$. We have chosen system lengths from $2 \cdot 10^4$ ($M = 32$) to $2 \cdot 10^5$ ($M = 2$), so that the relative errors $\Delta\Lambda/\Lambda$ take values of about 0.1 % ($M = 2$) to 1 % ($M = 32$). Let us now consider some selected cases.

The first example, cf. Fig. 10.1, shows the RLLs for $r = 0.8$ and $t = 0.4$. The values decrease with increasing M for all possible values of the spin scattering strength, indicating that the system is in the localized regime for these values of the parameters. This matches with the fact that the mean free path, Eq. (9.1), takes a value of $l_e \simeq 0.35$ in units of the lattice constant. Thus, reflection is too strong to allow for the existence of extended states.

In contrast to this, the next example corresponding to $r = 0.55$ and $t = 0.6$, i.e. $l_e \simeq 1.1$, exhibits a LD transition as can be seen in Fig. 10.2. While for $s < s^* \simeq 0.3$ the system turns out to be localized, we find that the RLLs grow up with increasing M for larger spin scattering strength. Obviously, the effect of weak anti-localization causes the existence of extended states, if s is

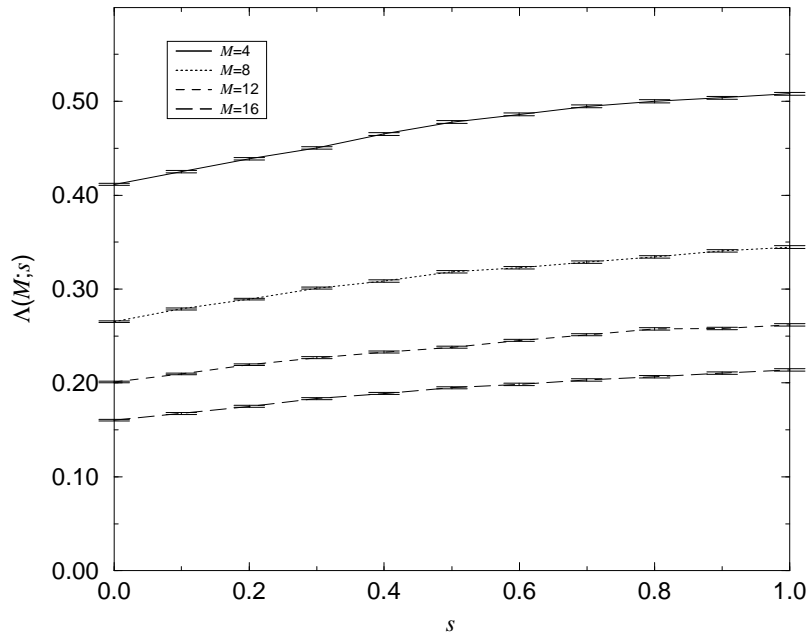


Figure 10.1: RLL for strong disorder, $r = 0.8$, $t = 0.4$ which corresponds to $l_e \simeq 0.35$, depending on the spin scattering strength s and the system width M .

strong enough. The intersection of the curves clearly indicates the LD transition. However, their slope is rather small compared to the error bars preventing an accurate scaling analysis close to the critical point. Let us now consider a really bad example.

Fig. 10.3 shows RLLs corresponding to $t = 0.8$ and $s = 0.4$, where now r varies in a small interval from $r = 0.48$ to $r = 0.56$. Although curves for different system widths M intersect, the points of intersection do not match. Rather, they systematically depend on the width. The larger M is the closer are the points of intersection for curves of neighboring values of M . It is obvious that there exists a limiting point, which would be the true critical point. The observed deviations are the consequence of so-called *finite-size effects*, which have the typical form (cf. Ref. [89])

$$\ln \left(\frac{\Lambda(M; \tau^*)}{\Lambda^*(M = \infty; \tau^*)} \right) \propto \left(\frac{M}{\xi_{\text{irr}}} \right)^{-y_{\text{irr}}}. \quad (10.1)$$

This formula describes the deviations of the RLL at the critical value of the parameter and for *finite* system size, $\Lambda(M; \tau^*)$, from the true critical value of the

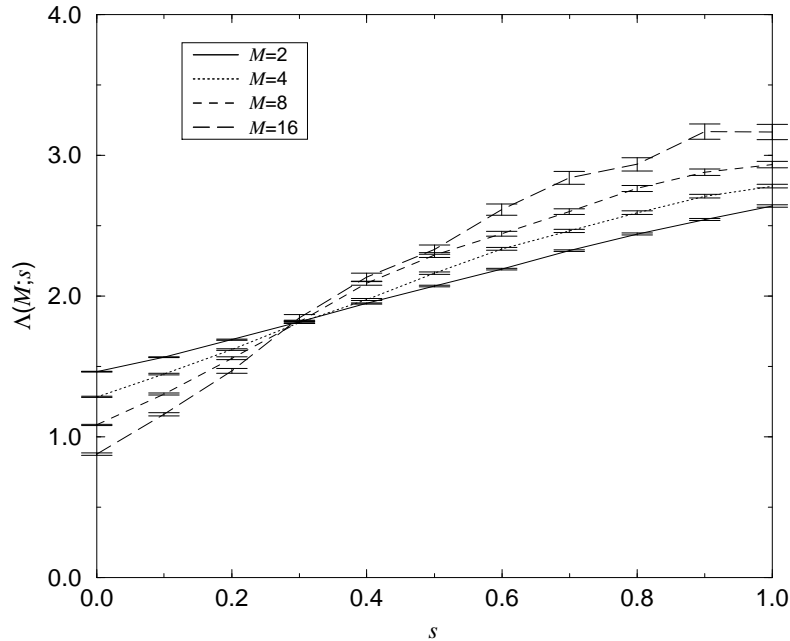


Figure 10.2: RLL for $r = 0.55$, $t = 0.6$ which corresponds to $l_e \simeq 1.1$, depending on the spin scattering strength s and the system width M .

RLL in the thermodynamic limit, $\Lambda^*(M = \infty; \tau^*)$. ξ_{irr} denotes some length scale, which is called *irrelevant*, because the finite-size correction vanishes algebraically with the critical exponent y_{irr} in the thermodynamic limit. Obviously, for regions in phase space corresponding to more delocalized systems such finite-size effects are more important than for regions which correspond to more localized systems. For a reliable analysis of the critical region we have to find a more suited area in the phase space, i.e. a region where the finite-size effects are very small and the RLL depends stronger on the selected parameter as compared to the foregoing example. Actually, there is only a small area in parameter space that is suitable for a quantitative analysis of the LD transition. We will come back to this in Sec. 10.2.

Now we turn to the phase diagram for the LD transition, which we determined using the scaling behavior of the RLL. More precisely, we calculated $\Lambda(M_1 = 4)$ and $\Lambda(M_2 = 8)$ for a lot of pairs (r, t) with $s = 0.01, 0.02, 0.05, 0.1, 0.4$ and 1 . In order to get the critical line in the (r, t) -subspace with fixed s we decided the point (r, t, s) to be in the localized and delocalized regime, if

$$\Lambda(M_1) - \Delta\Lambda(M_1) > \Lambda(M_2) + \Delta\Lambda(M_2) \quad (10.2)$$

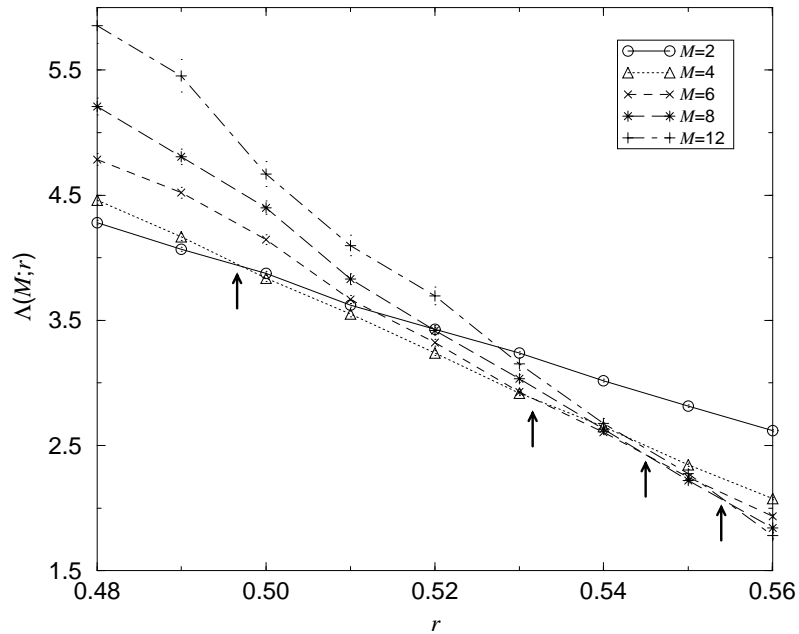


Figure 10.3: RLL in the vicinity of the localization-delocalization transition, $t = 0.8$, $s = 0.6$ which corresponds to $l_e \simeq 2$, depending on the reflection coefficient r and the system width M . The arrows mark the section of curves corresponding to neighbored values of M .

and

$$\Lambda(M_2) - \Delta\Lambda(M_2) > \Lambda(M_1) + \Delta\Lambda(M_1), \quad (10.3)$$

respectively. In the case that both conditions failed, we considered the point in the parameter space to be critical. By that procedure we got a critical *region*, i.e. the separating line had some finite width. Fig. 10.4 shows the resulting phase diagrams for some intersections of the parameter space at the above declared fixed values of s . The white area marks the localized the grey one the delocalized phase. The drawn critical line is the interpolated center line of the critical region.

The region of the metallic phase shrinks with decreasing spin scattering strength. This is due to the fact that weak anti-localization then becomes less effective in preventing Anderson localization. At $s = 0$ the system changes universality class from AII to AI, a fact that could be verified by comparing the values of the localization lengths with those in Ref. [87]. On the other hand even a very small value of s gives rise to a certain delocalized phase, if r is small and t is large

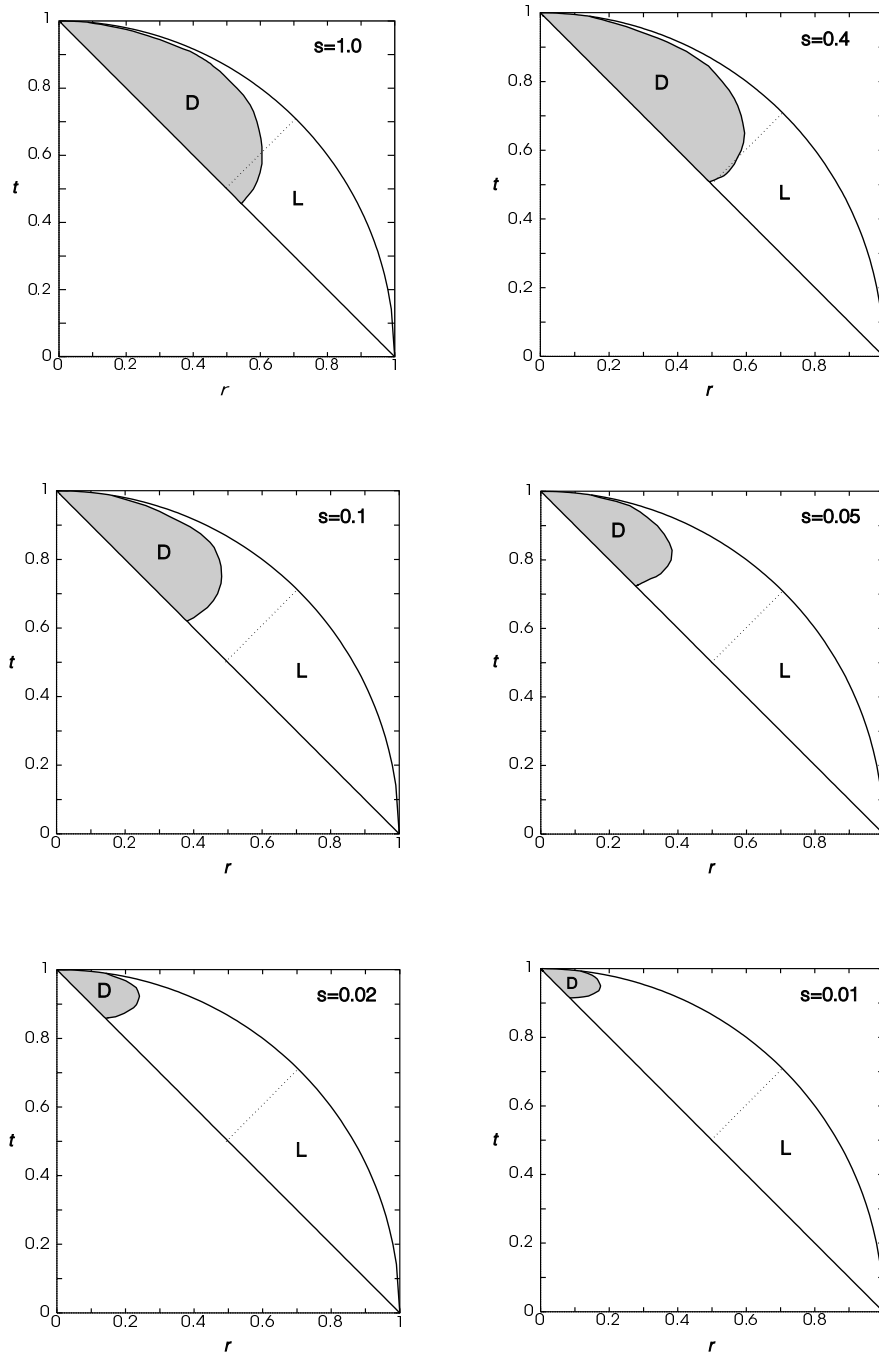


Figure 10.4: Phase diagrams for the localization-delocalization transition for cross-sections at $s = 1, 0.4, 0.1, 0.05, 0.02, 0.01$. The grey area shows the delocalized, the white the localized regime. The dotted line corresponds to $r = t$.

enough. Of course, the larger l_e , i.e. the larger t and smaller r , the more easily extended states occur. But even in the presence of full spin scattering only about

the half of the area of the parameter space belongs to the metallic phase. This is due to the fact that parameter values (r, t) belonging to the localized phase correspond to too strong disorder resulting in too strong localization to be broken by weak anti-localization.

It should be noticed, that for $t \gtrsim 0.6$ the shape of the phase boundary is influenced by finite-size effects. So the phase diagram can only serve as a qualitative picture of the LD transition. In order to improve on the phase diagram, one has to consider much larger systems, which is very computer time consuming taking such a large number of data points into account. Nevertheless, the lower part of the boundary, i.e. the region close to the line $r = t$ (dotted line in the figure), is suitable for quantitative investigations, as will be shown in the following.

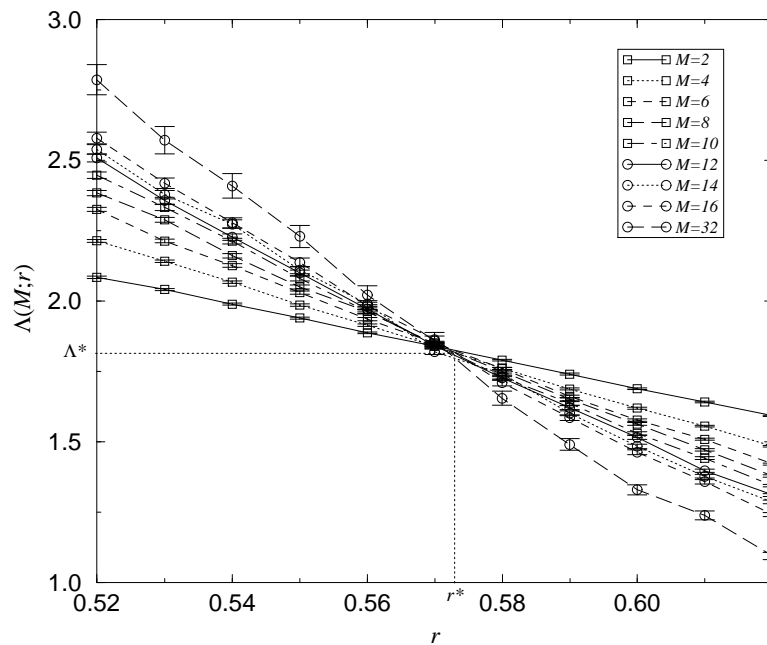


Figure 10.5: Renormalized localization length for $t = 0.6$, $s = 0.4$ which corresponds to $l_e \simeq 1$, depending on the reflection coefficient r and the system width M .

10.2 Scaling Function

We determined the scaling function by the fitting procedure described in Sec. 9.4.1 for $t = 0.6$, $s = 0.4$ and $r \in [0.52, 0.62]$. In this small region of the phase

space the corresponding curves $\Lambda(M; r)$ (cf. Fig. 10.5) are very well suitable for a quantitative analysis, because of their strong r dependence and the absence of noticeable finite-size effects ($l_e \simeq 1$). Fig. 10.6 shows the scaling function with the upper branch belonging to the metallic and the lower branch belonging to the localized regime. The curves represent the fitted Chebyshev polynomials. The data points are the raw data shifted by the fitted values of $\xi_c(r)$. We omitted the data with $M = 2$ in the localized and $M = 2$ and $M = 4$ in the delocalized regime, because these values showed systematic deviations due to finite-size effects. Also data that are too close to the critical point were omitted. For the remaining data the confidence test of the fit gives

$$\Delta_{\Theta} = -0.30 \quad \text{for the localized branch and} \quad (10.4)$$

$$\Delta_{\Theta} = 0.27 \quad \text{for the delocalized branch} \quad (10.5)$$

Thus, the assumption of one-parameter scaling is very well confirmed. Fixing the fit parameters $\ln \xi_c$ by setting $\ln \xi_c(r = 0.52) = 0$ for the delocalized and $\ln \xi_c(r = 0.62) = 0$ for the localized branch (circles in Fig. 10.6) the procedure has converged with an accuracy of 0.1% after about 50 iterations. The starting values have a radius of convergence of about 5. Hence, a rough estimate is sufficient for convergence. The Chebyshev polynomials we have used are of fourth order.

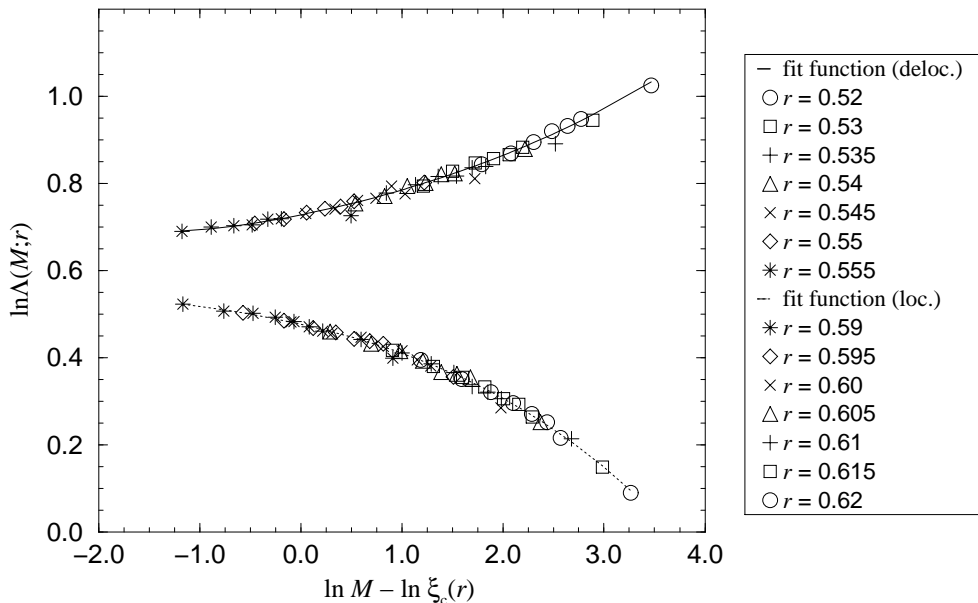


Figure 10.6: Scaling function for the localization-delocalization transition. The upper branch corresponds to the delocalized and the lower to the localized phase.

With a lower order it is impossible to fit the curves (as indicated by the figure of merit Δ_Θ), whereas with an order higher than 6 the fitted curves start to follow the fluctuations of the data points, which results in a non-physical behavior of the scaling function. With an order between four and six there is no significant difference in the results.

10.3 Critical Exponent ν and Critical RLL Λ^*

In order to determine the critical exponent ν of the correlation length we used the fit procedure presented in Sec. 9.4.3. With a starting value $r^* \in [0.53, 0.59]$ the procedure converges. After about 10 iterations the corrections are smaller than 1%. The results of the fit are

$$\nu = 2.51 \pm 0.18 \quad \text{and} \quad r^* = 0.571 \pm 0.002. \quad (10.6)$$

The prefactors take the values

$$\ln \xi_c^{0,\text{loc}} = -7.55 \pm 0.42 \quad (10.7a)$$

and

$$\ln \xi_c^{0,\text{deloc}} = -7.50 - \pm 0.43. \quad (10.7b)$$

The confidence test of the fit gives $\Delta_\theta = -0.47$, showing its high quality. It is very important to stress, that the given errors (cf. Eq. (9.47)) are *not independent*. They have to be interpreted considering the correlation matrix

$$C_\theta = \begin{pmatrix} 0.0310 & -0.0737 & -0.0739 & -0.0004 \\ -0.0737 & 0.1782 & 0.1766 & 0.0009 \\ -0.0739 & 0.1766 & 0.1853 & 0.0009 \\ -0.0004 & 0.0009 & 0.0009 & 5.5 \cdot 10^{-6} \end{pmatrix}, \quad (10.8)$$

which shows that the different values are highly correlated.

Several reference values for ν have been published in the last years [98,99,70,100]. The most recent calculations yield $\nu = 2.75 \pm 0.1$ [101], $\nu = 2.5 \pm 0.3$ [102] and $\nu = 2.32 \pm 0.14$ [103]. Within the errors our value agrees with these. We note that ν is very sensitive to slight variations of r^* . This is seen by fitting ν for fixed values of r^* . As is shown in Fig. 10.7 ν changes by 30% if r^* changes by about 3%. The difficulties in obtaining a credible value for ν were a further reasons to employ an numerical fit procedure.

In order to determine the critical RLL we used Eqs. (9.49) and (9.50). The result is

$$\Lambda^* = 1.83 \pm 0.03. \quad (10.9)$$

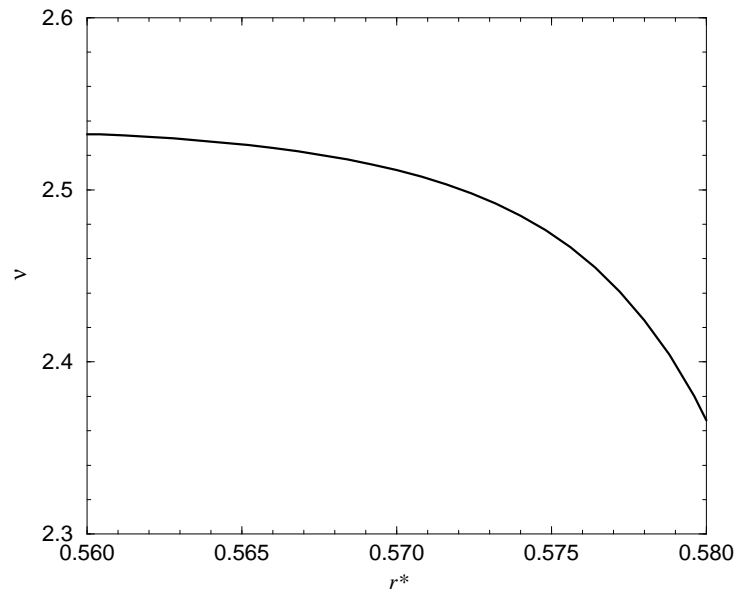


Figure 10.7: Dependence of ν on the assumed value of r^* . The best estimate is found for $r^* = 0.571$

Finally, Eq. (7.4) yields the value for the scaling exponent of the typical LDOS

$$\alpha_0 = 2.174 \pm 0.003. \quad (10.10)$$

This value agrees well with the result of Schweitzer [104], $\alpha_0 = 2.19 \pm 0.03$ obtained for a Hamiltonian model.

Chapter 11

Real-Space RG for the Manhattan Model

11.1 Introduction

In the foregoing chapters we have investigated the scaling behaviour of the RLL in the AII-NWM by means of the finite-size scaling approach and the transfer matrix method. In principle, this method is able to yield a qualitative as well as quantitative correct characterization of the LD transition in terms of critical exponents. But it makes great demands on the computational resources. Thus, one may be forced to reduce the system size without having reached the desired accuracy. In this sense the finite-size scaling method can be denoted as large scale numerics.

In the present chapter we shortly want to present another numerical approach to the LD transition by means of a scattering theoretical NWM, which is called *real-space renormalization group* (real-space RG) (cf. Ref. [49]). It allows us to obtain a qualitative overview about the localization behaviour with very little computational effort. Considering the scattering matrix corresponding to a 2D system of size L^2 one may ask, how this matrix renormalizes under rescaling of the (linear) system length, $L \rightarrow bL$. Repeated rescaling generates a RG flow of the reflection and transmission coefficient, r and t , which parameterize the scattering matrix (cf. Sec. 8.2). The scaling behaviour of these coefficients directly answers the question, whether the delocalization fixed point is repulsive (localized phase) or attractive (deocalized phase).

Since the calculation of the scattering matrix elements corresponding to an arbitrary large system still involves large computational effort, we neglect some of the informations about the exact topology of the network and consider a so-called *hierarchical* NWM. The idea is to connect a few elementary scatterers of an original NWM in such a way, that the resulting system globally looks as any of the

elementary scatterers. Cf. Fig. 11.1 for an example. Interpreting the composed scatterer on its part as new building block this process can be called an *RG step*. We then can build up a system of a certain size by repeating this RG step sufficiently often. A composed scatterer consisting of b^2 sites and V non-trivial

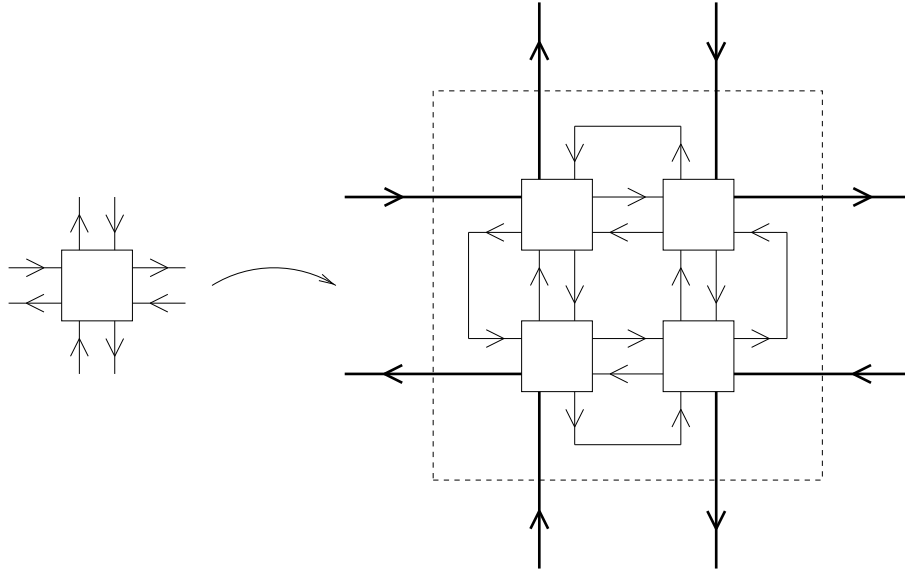


Figure 11.1: Defining building block of the $A[2/4]$ -NWM.

elementary scatterers¹ defines a hierarchical NWM, which we denote as $[b/V]$ -NWM. The example in Fig. 11.1 shows a composed scatterer for a hierarchical NWM of A symmetry (cf. Sec. 8). Since all of the $b^2 = 4$ sites are occupied it is the $A[2/4]$ NWM. In general, if $V = b^2$ there is no difference in the number of scatterers between the hierarchical NWM after some RG steps and the original model of the corresponding size. But note that the topology represented by the connectivity matrix is still different (cf. the short cuts in Fig. 11.1). If $V < b^2$ the hierarchical model is additionally sparser equipped with scatterers than the original one. To be more specific it is a fractal with fractal dimension $D^{[b/V]} = \ln V / \ln b$. For the example the fractal dimension coincides with the spatial dimension, $D^{[2/4]} = d = 2$.

If there are not too many elementary matrices involved in the defining RG step, the relation between the reflection and transmission coefficients of the composed matrix and those of the building blocks can be calculated analytically. Once this relation is known, we can iteratively perform the RG step until the desired system size is reached.

The model we use for our investigations is a derivative of the CC-NWM and is

¹We denote a scatterer as trivial if all transmission coefficients are 1.

expected to show always localized behaviour. We want to verify this statement by a real-space RG analysis. After the calculation for the change of parameters in one RG step, in the third section we explicitly point out the employed algorithm for the calculation of the RG flow of the transmission coefficient and show the results.

11.2 Manhattan Model

Noticing that the CC-NWM does not fall in the class of vertex models which are treatable and solvable by the quantum Yang-Baxter equation, M.R. ZIRNBAUER introduced in Ref. [105] a slightly modified NWM which fulfils this requirement. Fig. 11.2 shows a picture of both models, where each node represents a scatterer. In contrast to the CC-NWM the new model allows at each node transmission and deflection to only one side as is specified in the figure. As a consequence the direction in each line does not change, which motivates us to call it *Manhattan model* (MM). The MM can not be interpreted by microscopic mechanisms as in the case of the CC-NWM. But while we are in interested only in the critical behaviour of the system which is basically determined by the equality of left and right deflections we should expect the MM to be adequate. However, as is argued in Ref. [105] the MM is *not* able to describe the critical point of a quantum Hall system. Instead it shows always localization. It is the aim of the present section to verify this statement by numerical calculations.

In order to investigate the MM by means of the real-space RG we have to define an RG step, i.e. we have to determine how many elementary scatterers are connected in the composed scatterer and in which manner. The smallest composed scatterer with the same arrangement of incoming and outgoing channels as the building blocks is of size 3×3 and contains five non-trivial scatterers, cf. Fig. 11.3. Thus,

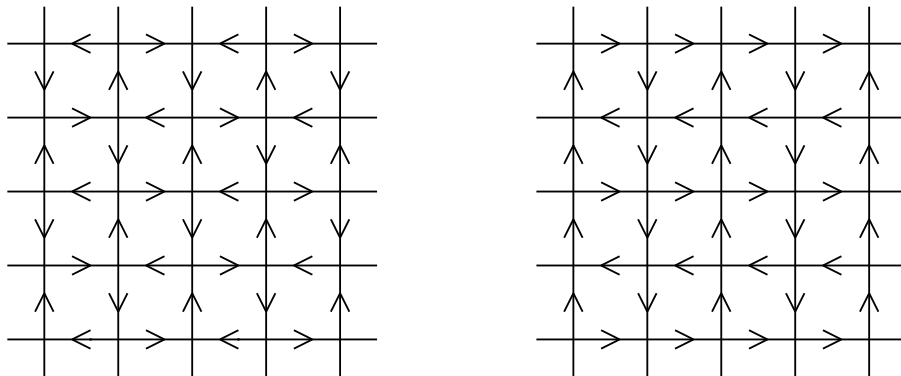


Figure 11.2: left: Chalker-Coddington NWM, right: Manhattan model.

the fractal dimension of this MM[3/5] is given by $D^{[3/5]} \approx 1.46$. The black and grey bullet indicate the corresponding links to be connected. In the following we outline how to get the algebraical expression for the transmission coefficient of the composed scatterer in terms of the five building blocks. Each elementary scatterer is represented by a 2×2 matrix mapping incoming amplitudes i_k and i'_k to outgoing amplitudes o_k and o'_k (cf. also Fig. 11.3)

$$\begin{pmatrix} o_k \\ o'_k \end{pmatrix} = \begin{pmatrix} r_k & t'_k \\ t_k & r'_k \end{pmatrix} \begin{pmatrix} i_k \\ i'_k \end{pmatrix}, \tag{11.1}$$

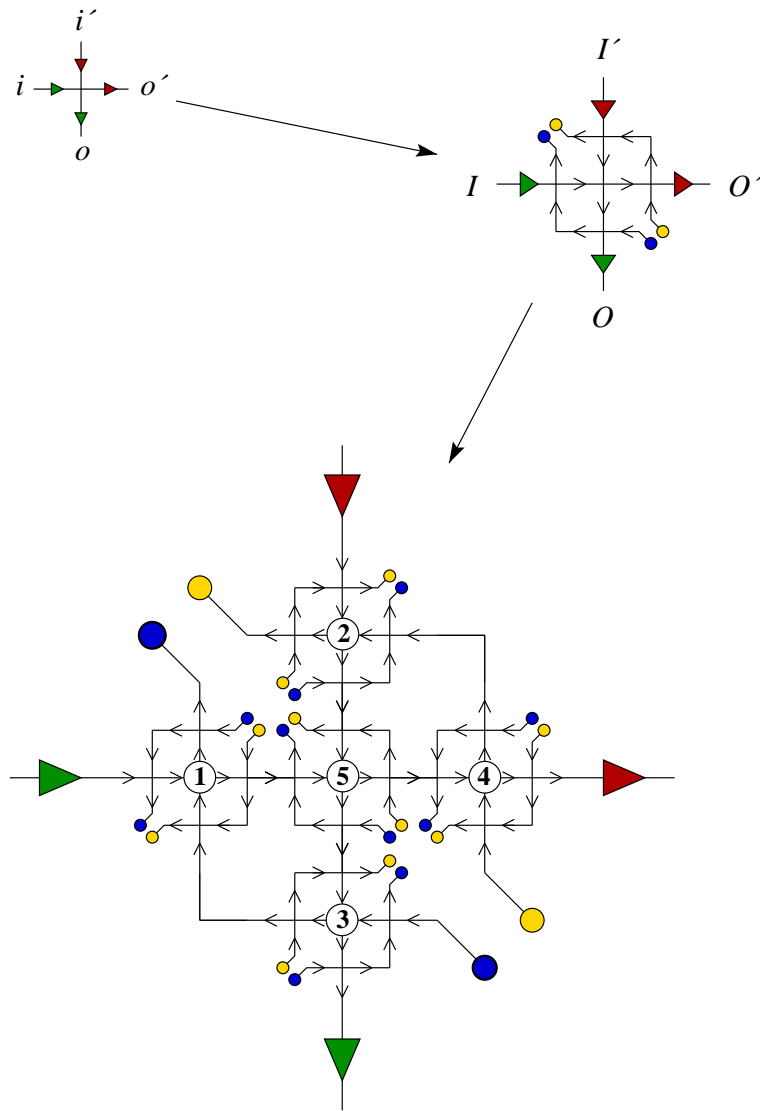


Figure 11.3: Definition of the hierarchical MM[3/5]. Here two renormalization steps are drawn.

where $k = 1, \dots, 5$. Writing the complex entries in polar representation the unitarity of the scattering matrix results in

$$\begin{aligned} |t_k|^2 + |r_k|^2 &= 1, \\ |t_k| &= |t'_k|, \\ |r_k| &= |r'_k|, \\ e^{i(\varphi_{t_k} + \varphi_{t'_k})} &= -e^{i(\varphi_{r_k} + \varphi_{r'_k})}. \end{aligned} \quad (11.2)$$

For the composed scatterer we have

$$\hat{O} \equiv \begin{pmatrix} O \\ O' \end{pmatrix} = S \begin{pmatrix} I \\ I' \end{pmatrix} \equiv \hat{I}, \quad (11.3)$$

where the 2×2 scattering matrix is given by

$$S = \begin{pmatrix} r & t' \\ t & r' \end{pmatrix}. \quad (11.4)$$

With the numbering of the elementary scatterers defined in Fig. 11.3 we read off the *outer* amplitudes to be $I = i_1$, $I' = i'_3$, $O = o_2$, and $O' = o'_4$. Let further

$$\overset{\circ}{I} = \begin{pmatrix} i'_1 \\ i_2 \\ i'_2 \\ i_3 \\ i_4 \\ i'_4 \\ i_5 \\ i'_5 \end{pmatrix} \quad \text{and} \quad \overset{\circ}{O} = \begin{pmatrix} o_1 \\ o'_1 \\ o_2 \\ o_3 \\ o'_3 \\ o_4 \\ o_5 \\ o'_5 \end{pmatrix} \quad (11.5)$$

be the vectors containing all *inner* amplitudes. Then in the inner-outer decomposition all scattering processes are implicitly described by

$$\begin{pmatrix} \hat{O} \\ \overset{\circ}{O} \end{pmatrix} = \begin{pmatrix} S_{11} & S_{12} \\ S_{21} & S_{22} \end{pmatrix} = \begin{pmatrix} \hat{I} \\ \overset{\circ}{I} \end{pmatrix}, \quad (11.6)$$

where the 2×2 matrix $S_{11} = 0$, the 8×8 matrix S_{22} represents the coupling of all inner amplitudes and the matrices S_{12} and S_{21} describe the mixing of inner and outer amplitudes. Further, corresponding to the chosen numbering the arrangement of the building blocks is encoded in the 8×8 connectivity matrix C . It defines which pairs of (inner) incoming and outgoing amplitudes of neighboured scatterers have to be identified:

$$\overset{\circ}{I} = C \overset{\circ}{O}. \quad (11.7)$$

With this setup we now obtain the scattering matrix S corresponding to the composed scatterer to be given as

$$S = S_{11} + S_{12}C(1 - S_{22}C)^{-1}S_{21}. \quad (11.8)$$

This matrix equation can be solved by computer algebra. The expression for the transmission coefficient t in terms of the building block elements turns out to be

$$t = \frac{t_5(t_4 - t_3 e^{i\varphi_4})(t_1 - t_2 e^{i\varphi_1})}{\alpha\beta + \alpha(r_3 r_4 r'_5) + \beta(r_5 r'_1 r'_2) - r_3 r_4 r'_1 r'_2 e^{i\varphi_5}}, \quad (11.9)$$

where $\alpha = t_2 t'_1 - 1$ and $\beta = t_3 t'_4 - 1$ and $\varphi_k \equiv \varphi_{t_k} + \varphi_{t'_k}$.

11.3 Real-Space RG Algorithm and Results

Having derived the analytical expression for one RG step in the last section we now turn to the question how to obtain the flow of the transmission probability $T = |t|^2$ under real-space renormalization. Before explaining the algorithm note that from Eq. (11.9) we conclude $|t_k| = 0 \Rightarrow |t| = 0$ and $|t_k| = 1 \Rightarrow |t| = 1$. Thus, $T = 0$ and $T = 1$ are fixed points. This validates the composed scatterer to be suited for an RG analysis. The RG algorithm consists of the following steps:

1. Consider a system of (linear) size b represented by a composed scatterer. Take the strengths $|t_k|$ of its building block matrix elements from an initial distribution $P_0(T)$ and the phases homogeneously from the interval $[0, 2\pi]$ respecting the constraints Eqs. (11.2). Calculate $T(b) = |t|^2$ by means of Eq. (11.9).
2. Repeat this procedure many times ($\sim 10^3$) to get a new distribution function $P_b(T)$.
3. Repeat steps 1. and 2. n times ($n \sim 10^1$) but now drawing the scattering strength $|t_k|$ from the distribution $P_{b^m}(T)$ which yields the new distribution $P_{b^{m+1}}(T)$ ($m = 1, \dots, n$).
4. Repeat steps 1.-3. for several initial conditions $P_0(T)$ in order to explore the phase space.

Note that for $n = 10$ we end up with a system size of $3^{11} \simeq 1.7 \cdot 10^5$! The algorithm described above takes only some seconds on computers of the current generation. Thus, we are able to investigate large systems with small computational effort. This makes the real-space renormalization method quite powerful.

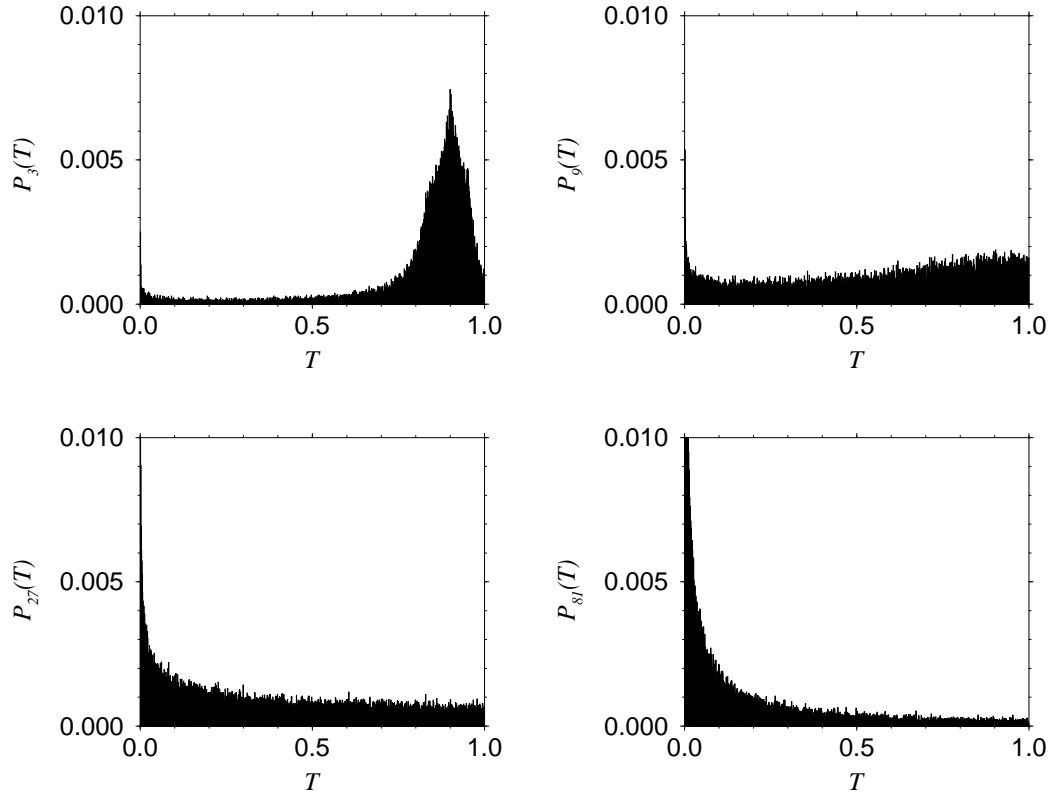


Figure 11.4: Flow of the transmission probability under real-space renormalization for the MM[3/5]. The shown distributions correspond to (linear) system sizes of 3, 9, 27 and 81 sites. The initial distribution was $P_0(T) = 0.9$. The system flows to strong localization.

We have applied this algorithm to the MM[3/5]. The result is shown in Fig. 11.4. We started with the constant initial distribution $P_0(T) = 0.9$, i.e. nearby the delocalization fixed point, and performed only $n = 4$ RG steps. Hence, the (linear) system sizes are 3, 9, 27, and 81 sites. The transmission probability definitely flows towards the localization fixed point $T = 0$. The same behaviour was observed for other initial distributions. Thus, we conclude that the Manhattan model shows always strong localization, which verifies the primary statement.

Chapter 12

Summary and Outlook

In this thesis we have considered non-standard behaviour of the density of states and the problem of delocalization in low-dimensional disordered electron systems. In both cases the unusual physical behaviour is due to the special symmetry of the system under consideration.

In the first part we have investigated the density of states in quasi-1D system of the non-standard $AIII$ symmetry (chGUE). This was motivated by the observation in previous works of an unusual behaviour of spectral and transport quantities at the middle of the tight-binding band. In particular, the singularity of the DoS in the middle of the band is a feature which is in contrast to the uniformity of the spectrum in the standard symmetry classes. Furthermore, at least in 1D, it is known that a divergence of the DoS is related to the divergence of the localization length [106]. Thus, there are indications of delocalized states in two dimensions or less, a feature unexpected from scaling theory [9]. While in 1D a lot of insight could be gained by means of the available rigorous analytical methods, in higher dimensions no consensus has been reached. Recently, a supersymmetric non-linear σ -model for the generalized random magnetic flux model has been derived [22], which allows for the investigation of spectral and transport quantities in both, the perturbative and non-perturbative regime of $AIII$ systems.

We have performed our investigations within this field theoretical approach. Starting from an expression in terms of the quasi-1D non-linear σ -model we have calculated the DoS in the ergodic, diffusive, and quantum regimes. In the ergodic regime we found oscillations on the scale of the mean level spacing. Such a structure is usually known from *two*-point Green functions, as e.g. the level-level correlation function. Indeed, using the sublattice representation we could show that in the expression for the DoS of chiral systems several coupled Green functions are involved. With our findings for the DoS in the ergodic regime we recovered results known from chiral random matrix theory [16,17,67,85]. This shows that the zero-dimensional limit of the random flux model is adequately described

by an ensemble of block-off-diagonal Hermitean random matrices. Moreover, it turned out that the topological term in the action causes a dependence on the parity of the number of sites.

For the investigation of the perturbative regime we have expressed the NL σ M action in terms of EFETOV's Q -matrices. We found no contributions up to three loop order. It is still an open question whether there exist perturbative corrections in quasi-1D at all. For consistency, we have compared the high energy limit of the ergodic result with the zero-mode approximation of the perturbative calculation and found agreement.

The main part of the analysis was dedicated to the quantum regime, where perturbation theory breaks down. Based on the transfer matrix method we have derived a generalized Laplacian on the underlying supergroup. The corresponding partial differential equation is a kind of diffusion equation (heat equation) and its solution (heat kernel) describes the propagation along the wire. Each contribution to the generalized Laplacian corresponds to one of the terms in the NL σ M action. The topological term basically influences the boundary conditions the heat kernel is subject to. We have solved the heat equation and calculated the DoS in the limit of large system size, $L \gg \xi$, and small energies, $\omega = \epsilon/\Delta_\xi \ll 1$. It turned out that the behaviour of the DoS strongly depends on the parity of the number of channels (even-odd effect). Neglecting the Gade term we got for N_c even $\langle \rho(\omega) \rangle \propto \rho_0 |\omega| \ln|\omega|$, whereas for N_c odd the result is given by $\langle \rho(\omega) \rangle - \rho_0 \propto \rho_0 / |\omega \ln^3|\omega||$. The latter formula coincides with result found earlier for strictly 1D, i.e. $N_c = 1$ [11,12]. The result for even N_c agrees with a very recent quasi-1D calculation obtained by a Fokker-Planck equation approach [20]. Taking the Gade term into account has only a very slight impact on the result for an even number of channels, whereas for an odd number of channels the result remains completely unaffected.

Let us finally have a look at the very recent development in that field. In Ref. [24] the first and second moment of the conductance have been calculated. They authors find localization away from the band center and an even-odd effect at $\epsilon = 0$. For an even number of channels the average conductance decays exponentially, whereas they find an algebraic decay for an odd channel number. The divergence of the DoS in the middle of the band has been found by numerical calculations in [28]. In [29] the localization-delocalization transition was studied within a transfer matrix approach, similar to the one used in the second part of this work. Again at the band center delocalization was found in quasi-1D for an odd number of channels.

In the second part of this work we addressed the localization behaviour of a two-dimensional time-reversal invariant disordered electron system with spin-orbit coupling, thus of a system of AII (GSE) symmetry. In this case the effect of weak anti-localization causes *positive* perturbative corrections to the conductance turning the otherwise repulsive delocalization fixed point into an attractive one. Thus, there are arguments for the existence of delocalized states.

We performed our investigations within the framework of a recently developed scattering theoretical network model [46]. First, we constructed the scattering and transfer matrices. By means of the numerical transfer matrix method we calculated quasi-1D renormalized localization lengths, dependent on the system width and the three parameters reflection, transmission, and spin scattering strength. We were able to obtain a detailed localization-delocalization phase diagram by means of the finite-size scaling method. In particular, we could confirm the assumption that extended states exist in 2D systems, provided that the spin-rotational invariance is broken. More precisely, if the disorder is weak enough the system exhibits a localization-delocalization transition when the spin scattering strength is increased. But also for maximal spin scattering about half of the parameter space, viz the region corresponding to sufficiently strong scattering, remains in the localized phase.

In order to explore the universal, i.e. critical properties of the localization-delocalization transition, we first determined a scaling function for the renormalized localization length. Using a numerical fit procedure in combination with a χ^2 -test we got a highly reliable confirmation of the one-parameter scaling assumption. Based on this assumption we were able to calculate the critical exponent of the correlation length. As we have shown, its value depends sensitively on the critical value of the scaling variable. To this end, we again used a numerical fit procedure and tested the confidence of this fit. The result is $\nu = 2.51 \pm 0.18$ which within the errors agrees with the values given in the most recent literature [101–103]. By an argument based on a conformal mapping the critical value of the renormalized localization length is related to the scaling exponent α_0 of the typical local density of states [48], which plays the role of the order parameter for the transition. By means of the fit procedure we could determine the scaling exponent up to a high accuracy, $\alpha_0 = 2.174 \pm 0.003$, which agrees with the only reference value, which is known to us, [104].

At the end of the second part we addressed the question whether the quantum Hall critical point is realized within the Manhattan model. In contrast to the large scale numerics we have done before we used the numerical real-space renormalization group method [49]. It allows for a qualitative overview of the localization behaviour of a system with only little computational effort. We defined a composite scatterer compatible with the channel arrangement of its building blocks and found an analytical expression for its parameters. Starting with a sharply peaked initial distribution of the transmission coefficients we found the distribution to flow into the localized regime after only a few numerical iterations. This scenario holds for initial values arbitrary close to unity. Thus, we conclude that the Manhattan model always shows localized behaviour and not the behaviour of a critical quantum Hall system, a result which agrees with the theoretical prediction made in Ref. [105].

To conclude, we take a look at the still open questions. As for the density of states in quasi-1D systems of *AIII* symmetry we do not know whether there exist perturbative contributions in four-loop order or higher. It is possible that there are no contributions at all. But then one should be able to conclude this by general arguments. Furthermore, solving the heat equation analytically in the quantum regime turns out to be very hard if one is interested in arbitrary (not only very large) system sizes. Therefore, one could try a numerical solution of this partial differential equation in order to get a more exhausting picture of this quantity. In dimensions higher than strictly 1D a rigorous analytical relation between the divergence of the density of states and delocalization is still missing.

Turning to the second subject it is not yet clear whether the delocalization due to spin-orbit scattering is related to the metal-insulator transition observed in experiments on 2D systems. It is argued, that electron-electron interaction plays an important role. Therefore, it is desirable to implement electron-electron interaction in the scattering theoretical network model. Finally, a promising approach, which is in a certain sense a symbiosis of both parts of this thesis, is the investigation of systems with chiral symmetry within the network model. One could use the transfer matrix method as well as the real-space renormalization method in order to gain more insight about the behaviour of 2D chiral systems. In any case, further investigations of these model are worth while.

Appendix A

Power Series of the Adjoint Action

Consider $H = \begin{pmatrix} x & 0 \\ 0 & y \end{pmatrix} \in \mathcal{T}$, where \mathcal{T} is the Cartan subalgebra of $\mathcal{G} = \text{Lie}(G)$. Let $\mathcal{B} = \{\mathbf{e}_1, \mathbf{e}_2\}$ be the basis of the vector space $\mathcal{V} = \text{span}(\mathbf{e}_1, \mathbf{e}_2)$ with $\mathbf{e}_1 = \begin{pmatrix} 0 & \eta_1 \\ 0 & 0 \end{pmatrix}$ and $\mathbf{e}_2 = \begin{pmatrix} 0 & 0 \\ \eta_2 & 0 \end{pmatrix}$.

Sometimes expressions of the form $e^H K e^{-H}$ appear (K some matrix), which equals $e^{[H, \cdot]} K$. This expression is just $e^{\text{ad} H} K$ by definition of the adjoint action. Hence, our objective is to calculate this expression.

Let us start with the adjoint action of H itself. We have

$$\begin{aligned} \text{ad}(H)\mathbf{e}_1 &= [H, \mathbf{e}_1] = (x - y)\mathbf{e}_1, \\ \text{ad}(H)\mathbf{e}_2 &= [H, \mathbf{e}_2] = -(x - y)\mathbf{e}_2. \end{aligned} \tag{A.1}$$

Thus, the representation matrix of the adjoint action with respect to \mathcal{B} is given by

$$\mathbf{M}_{\mathcal{B}}(\text{ad } H) = \begin{pmatrix} x - y & 0 \\ 0 & -(x - y) \end{pmatrix} = (x - y)\sigma_3. \tag{A.2}$$

Obviously, \mathcal{B} is just the eigenbasis and $\pm(x - y)$ are the roots of \mathcal{G} .

We now proceed with calculating the expression $\exp(\text{ad } H)(\mathbf{e}_1 + \mathbf{e}_2)$. Expanding the exponential and separating even and odd powers we obtain

$$\begin{aligned} e^{\text{ad } H} \begin{pmatrix} 0 & \eta_1 \\ \eta_2 & 0 \end{pmatrix} &= [\cosh(x - y)\mathbb{1}_2 + \sinh(x - y)\sigma_3] \begin{pmatrix} 0 & \eta_1 \\ \eta_2 & 0 \end{pmatrix} \\ &= \cosh(x - y) \begin{pmatrix} 0 & \eta_1 \\ \eta_2 & 0 \end{pmatrix} + \sinh(x - y) \begin{pmatrix} 0 & \eta_1 \\ -\eta_2 & 0 \end{pmatrix}. \end{aligned} \tag{A.3}$$

For the square of this expression we obtain

$$\left[e^{\text{ad } H} \begin{pmatrix} 0 & \eta_1 \\ \eta_2 & 0 \end{pmatrix} \right]^2 = \begin{pmatrix} \eta_1 \eta_2 & 0 \\ 0 & -\eta_1 \eta_2 \end{pmatrix}. \quad (\text{A.4})$$

Appendix B

Similarity Transformation of the Laplacian

The radial part of a general Laplace-Beltrami operator on a superspace contains first order derivatives, which appear due to the non-Euclidean geometry of the even sector. Introducing $j := \mathcal{J}^{1/2}$ for convenience, the radial part of the Laplacian is given by

$$\begin{aligned}
 \mathfrak{L}^a &= j^{-2} \partial_i j^2 \partial_i = j^{-1} [j^{-1} \partial_i j] \cdot [j \partial_i j^{-1}] j \\
 &= j^{-1} [\partial_i + (\partial_i \ln j)] \cdot [\partial_i - (\partial_i \ln j)] j \\
 &= j^{-1} [\partial_i^2 - \partial_i (\partial_i \ln j) + (\partial_i \ln j) \partial_i - (\partial_i \ln j)^2] j \\
 &= j^{-1} [\partial_i^2 - (\partial_i^2 \ln j) - (\partial_i \ln j)^2] j,
 \end{aligned} \tag{B.1}$$

where in all expression implicate summation over i . With $\partial_i^2 \ln j = -j^{-2} (\partial_i j)^2 + j^{-1} (\partial_i^2 j)$ and $(\partial_i \ln j)^2 = j^{-2} (\partial_i j)^2$ we obtain the similarity transformed Laplacian,

$$j \mathfrak{L}^a j^{-1} = \partial_i^2 - j^{-1} (\partial_i^2 j) = \partial_i^2 + V_{\text{eff}}(j). \tag{B.2}$$

By a theorem of BEREZIN (cf. [82]) the effective potential is constant for all supergroups, $V_{\text{eff}}(j) = V_{\text{eff}}$, i.e. j is an eigenvector of the operator ∂_i^2 with eigenvalue $-V_{\text{eff}}$:

$$\partial_i^2 j = -V_{\text{eff}} j. \tag{B.3}$$

In particular, if the dimensions of the bosonic and fermionic sector are equal, which is the case for $\text{GL}(1|1)$, or different at most by one, the effective potential vanishes.

Appendix C

Zero-Mode Regime

In order to calculate the zero-mode integral, Eq. (6.3), for an even number of sites we first note that the integrand of Eq. (6.3) is an even function of y , and hence the integration density can be rewritten in the following way

$$\begin{aligned} \sinh^{-2}\left(\frac{x-iy}{2}\right) &= \frac{1}{2} \left[\sinh^{-2}\left(\frac{x-iy}{2}\right) + \sinh^{-2}\left(\frac{x+iy}{2}\right) \right] \\ &= \text{Re} \sinh^{-2}\left(\frac{x-iy}{2}\right) = 2 \frac{\cosh x \cos y - 1}{(\cosh x - \cos y)^2}. \end{aligned} \quad (\text{C.1})$$

Taking the derivative of the DoS w.r.t. ω^+ we obtain

$$\frac{\partial \langle \rho_{0D}(\omega^+) \rangle}{\partial \omega^+} = \frac{\rho_0}{4} \text{Re} i \int_{-\infty}^{\infty} dx \int_0^{2\pi} dy [\cosh x \cos y - 1] e^{i\pi\omega^+(\cosh x - \cos y)}. \quad (\text{C.2})$$

Introducing $\kappa \equiv -i\pi\omega^+$ and $\mu \equiv -\pi\omega^+$ the different integrals are given by

$$\int_{-\infty}^{\infty} dx e^{i\pi\omega^+ \cosh x} = 2 \int_0^{\infty} dx e^{-\kappa \cosh x} = 2K_0(\kappa) \quad (\text{C.3a})$$

$$\int_{-\infty}^{\infty} dx \cosh x e^{i\pi\omega^+ \cosh x} = 2 \int_0^{\infty} dx \cosh x e^{-\kappa \cosh x} = 2K_1(\kappa) \quad (\text{C.3b})$$

$$\int_0^{2\pi} dy e^{-i\pi\omega^+ \cos y} = 2 \int_0^{\pi} dy e^{i\mu \cos y} = 2\pi J_0(\mu) \quad (\text{C.3c})$$

$$\int_0^{2\pi} dy \cos y e^{-i\pi\omega^+ \cos y} = 2 \int_0^{\pi} dy \cos y e^{i\mu \cos y} = 2\pi i J_1(\mu), \quad (\text{C.3d})$$

where $J_\mu(z)$ and $K_\mu(z)$ are Bessel functions. The validity of the first two lines is restricted to $\text{Re } \kappa > 0$, which is satisfied. Using the relations

$$K_0(\kappa) = \frac{\pi}{2} (iJ_0(\mu) - N_0(-\mu)), \quad (\text{C.4a})$$

$$K_1(\kappa) = \frac{\pi}{2} (J_1(\mu) - iN_1(-\mu)) \quad (\text{C.4b})$$

we obtain

$$\begin{aligned} \frac{\partial \langle \rho_{0D}(\omega^+) \rangle}{\partial \omega^+} &= \frac{\pi^2}{2} \rho_0 \text{Re} \left[- (J_1(\mu) - iN_1(-\mu)) J_1(\mu) + i (J_0(\mu) + iN_0(-\mu)) J_0(\mu) \right] \\ &= \frac{\pi^2}{2} \rho_0 [J_0^2(\mu) - J_1^2(\mu)] \\ &= \frac{\pi^2}{2} \rho_0 \frac{\partial}{\partial \omega^+} \omega^+ [J_0^2(-\pi\omega^+) + J_1^2(-\pi\omega^+)]. \end{aligned} \quad (\text{C.5})$$

With $J_0(-z) = J_0(z)$, $J_1(-z) = -J_1(z)$ and performing the limit $i\gamma \rightarrow 0$ the zero-mode DoS for an even number of lattice sites is given by

$$\langle \rho_{0D}(\omega) \rangle = \frac{\pi^2}{2} \rho_0 \omega [J_0^2(\pi\omega) + J_1^2(\pi\omega)], \quad (\text{C.6})$$

where the integration constant is zero due to the requirement $\lim_{\omega \rightarrow 0} \langle \rho_{0D}(\omega) \rangle = 0$. Using

$$J_0^2(z) + J_1^2(z) \simeq \frac{2}{\pi z}, \quad \text{for } z \gg 1, \quad (\text{C.7})$$

we have

$$\lim_{\omega \rightarrow \infty} \rho(\omega) = \rho_0. \quad (\text{C.8})$$

Thus, the result is normalized correctly.

For the case of an odd number of sites we first consider the difference in the pre-exponential factor w.r.t. the even case and obtain

$$\begin{aligned} \frac{e^{-(x-iy)} - 1}{\sinh^2\left(\frac{x-iy}{2}\right)} &= -4 \frac{1}{e^{\frac{x-iy}{2}} \left(e^{\frac{x-iy}{2}} - e^{-\frac{x-iy}{2}} \right)} = -4 \frac{e^{x+iy} - 1}{e^{2x} - e^{x-iy} - e^{x+iy} + 1} \\ &= 2 \frac{e^{-x} - e^{iy}}{\cosh x - \cos y} \end{aligned} \quad (\text{C.9})$$

for positive $x > 0$ and, analogously,

$$\frac{e^{x-iy} - 1}{\sinh^2\left(\frac{x-iy}{2}\right)} = 2 \frac{e^x - e^{-iy}}{\cosh x - \cos y}. \quad (\text{C.10})$$

for $x < 0$. The sum of both terms is given by

$$\frac{1}{2} \left(2 \frac{e^{-x} - e^{iy}}{\cosh x - \cos y} + 2 \frac{e^x - e^{-iy}}{\cosh x - \cos y} \right) = 2. \quad (\text{C.11})$$

Thus, for N_s odd, the DoS is given by that for an even number of sites plus an additional term

$$\frac{\rho_0}{2} \operatorname{Re} \int_0^\infty dx \int_0^{2\pi} dy (\cosh x - \cos y) e^{i\pi\omega^+(\cosh x - \cos y)} \quad (\text{C.12})$$

$$= \frac{\rho_0}{2} \operatorname{Re} (2\pi K_1(\kappa) J_0(\mu) - 2\pi i K_0(\kappa) J_1(\mu)) \quad (\text{C.13})$$

$$= -\pi^2 \rho_0 J_0(\pi\omega) J_1(\pi\omega). \quad (\text{C.14})$$

Using the identity $J_1(z) = \frac{z}{2}(J_2(z) + J_0(z))$ we end up with Eq. (6.5).

For the large energy limit of this expression we use the asymptotic formulae for the Bessel functions and obtain

$$\begin{aligned} J_0(z) &= \sqrt{\frac{2}{\pi z}} \left\{ C \left[1 - \frac{1}{8} \frac{\Gamma(\frac{5}{2})}{\Gamma(-\frac{3}{2})} z^{-2} + \frac{1}{384} \frac{\Gamma(\frac{9}{2})}{\Gamma(-\frac{7}{2})} z^{-4} + \mathcal{O}(z^{-6}) \right] \right. \\ &\quad \left. - S \left[\frac{1}{2} \frac{\Gamma(\frac{3}{2})}{\Gamma(-\frac{1}{2})} z^{-1} - \frac{1}{48} \frac{\Gamma(\frac{7}{2})}{\Gamma(-\frac{5}{2})} z^{-3} + \mathcal{O}(z^{-5}) \right] \right\} \quad (\text{C.15}) \\ &\simeq \sqrt{\frac{2}{\pi z}} \left\{ C \left[1 - \frac{9}{128} z^{-2} + \frac{3675}{32768} z^{-4} \right] + S \left[\frac{1}{8} z^{-1} - \frac{75}{1024} z^{-3} \right] \right\} \end{aligned}$$

with $C \equiv \cos(z - \frac{\pi}{4})$ and $S \equiv \sin(z - \frac{\pi}{4})$. In the next step we calculate J_0^2 . Since the trigonometric functions are strongly fluctuating (as functions of ω), we average over one period. This removes all term containing the product CS . Up to forth order we obtain

$$J_0^2(z) \simeq \frac{2}{\pi z} \left[C^2 \left(1 - \frac{9}{64} z^{-2} + \frac{3675 + 81}{16384} z^{-4} \right) + S^2 \left(\frac{1}{64} z^{-2} - \frac{75}{4096} z^{-4} \right) \right]. \quad (\text{C.16})$$

Analogous calculations for $J_1(z)$ yield

$$\begin{aligned} J_1(z) &= \sqrt{\frac{2}{\pi z}} \left\{ \tilde{C} \left[1 - \frac{1}{8} \frac{\Gamma(\frac{7}{2})}{\Gamma(-\frac{1}{2})} z^{-2} + \frac{1}{384} \frac{\Gamma(\frac{11}{2})}{\Gamma(-\frac{5}{2})} z^{-4} + \mathcal{O}(z^{-6}) \right] \right. \\ &\quad \left. - \tilde{S} \left[\frac{1}{2} \frac{\Gamma(\frac{5}{2})}{\Gamma(\frac{1}{2})} z^{-1} - \frac{1}{48} \frac{\Gamma(\frac{9}{2})}{\Gamma(-\frac{3}{2})} z^{-3} + \mathcal{O}(z^{-5}) \right] \right\} \quad (\text{C.17}) \\ &\simeq \sqrt{\frac{2}{\pi z}} \left\{ \tilde{C} \left[1 + \frac{15}{128} z^{-2} - \frac{4725}{32768} z^{-4} \right] - \tilde{S} \left[\frac{3}{8} z^{-1} - \frac{105}{1024} z^{-3} \right] \right\} \end{aligned}$$

with $\tilde{C} \equiv \cos(z - \frac{\pi}{4} - \frac{\pi}{2}) = S$ and $\tilde{S} \equiv \sin(z - \frac{\pi}{4} - \frac{\pi}{2}) = -C$, and

$$J_1^2(z) \simeq \frac{2}{\pi z} \left[S^2 \left(1 + \frac{15}{64} z^{-2} - \frac{4725 - 225}{16384} z^{-4} \right) + C^2 \left(\frac{9}{64} z^{-2} - \frac{315}{4096} z^{-4} \right) \right]. \quad (\text{C.18})$$

Combining both results we end up with Eq. (6.6).

Appendix D

Efetov's Q -Matrices

In supersymmetric non-linear σ -models for the orthogonal and unitary symmetry class derived by EFETOV [59] the elements of the saddle point manifold are identified as supermatrices Q given by $Q = \tilde{g}\Lambda\tilde{g}^{-1}$, where $\Lambda = \sigma_3^{AB}$ is the saddle point and $\tilde{g} \in \tilde{G}/\mathbb{K}$ are elements of the coset space G/\mathbb{K} . Here, \tilde{G} is the group of transformations on Λ which let the saddle point equations invariant and the index "AB" denotes grading in the sublattice space. The coset structure is obtained by dividing off all these transforms \mathbb{K} which commute with Λ , $\mathbb{K} = \{\exp K | [K, \Lambda] = 0\} \subset \tilde{G}$. This decomposition automatically satisfies the non-linear constraint $Q^2 = 1$.

Let $\tilde{W} \in \text{GL}(1|1)$ be two-dimensional supermatrices "generating" the coset in the following way, $\tilde{g} = \exp(\tilde{W} \otimes \sigma_2^{AB})$. This structure is enforced by the chiral symmetry which requires $[\tilde{W} \otimes \sigma_2^{AB}, \sigma_2^{AB}] = 0$. Obviously, there exists a bijective mapping

$$\begin{aligned} \tilde{G}/\mathbb{K} &\rightarrow G \\ \tilde{g} &\mapsto g := \exp(W), \end{aligned} \tag{D.1}$$

where $G = \text{GL}(1|1)$ and $W = 2\tilde{W}$. However, a further constraint given by the symmetry of the system is $g^{\text{ff}} \in \text{U}(1)$ and $g^{\text{bb}} \in \text{GL}(1)/\text{U}(1) = \mathbb{R}$, where the superscripts ff and bb denotes the Fermi-Fermi block and Bose-Bose block of the supermatrix, respectively.

In terms of the generators we have

$$Q = e^{\tilde{W} \otimes \sigma_2} \Lambda e^{-\tilde{W} \otimes \sigma_2}. \tag{D.2}$$

Using

$$\begin{aligned}
\sigma_3 e^{-\tilde{W} \otimes \sigma_2} &= \sigma_3 \sum_{n=0}^{\infty} \frac{(-\tilde{W} \otimes \sigma_2)^n}{n!} = \sigma_3 \sum_{n=0}^{\infty} \left(\frac{(\tilde{W} \otimes \sigma_2)^{2n}}{(2n)!} - \frac{(\tilde{W} \otimes \sigma_2)^{2n+1}}{(2n+1)!} \right) \\
&= \left[\sum_{n=0}^{\infty} \left(\frac{(\tilde{W} \otimes \sigma_2)^{2n}}{(2n)!} + \frac{(\tilde{W} \otimes \sigma_2)^{2n+1}}{(2n+1)!} \right) \right] \sigma_3 \\
&= e^{\tilde{W} \otimes \sigma_2} \sigma_3
\end{aligned} \tag{D.3}$$

we get

$$\begin{aligned}
Q &= e^{2\tilde{W} \otimes \sigma_2} \sigma_3 = e^{W \otimes \sigma_2} \sigma_3 = \cosh(W) \otimes \sigma_3 + \sinh(W) \otimes \sigma_2 \sigma_3 \\
&= \cosh(W) \otimes \sigma_3 + \sinh(W) \otimes (i\sigma_1)
\end{aligned} \tag{D.4}$$

from Eq. (D.2). In the following we calculate the four parts of the Lagrangian in Eq. (4.22) in terms of Q . (We start with the result and show that it yields the corresponding term in (4.22).)

fluctuation term

$$\begin{aligned}
\frac{1}{2} \text{str}[\partial Q \partial Q] &= \frac{1}{2} \text{str} \left[(\partial \cosh W)(\partial \cosh W) \otimes \mathbb{1} - (\partial \sinh W)(\partial \sinh W) \otimes \mathbb{1} \right. \\
&\quad \left. + (\partial \cosh W)(\partial \sinh W) \otimes \underbrace{(\sigma_3(i\sigma_1) + (i\sigma_1)\sigma_3)}_{=0} \right] \\
&= \text{str} \left[(\partial \cosh W)(\partial \cosh W) - (\partial \sinh W)(\partial \sinh W) \right. \\
&\quad \left. - (\partial \sinh W)(\partial \cosh W) + (\partial \sinh W)(\partial \sinh W) \right] \\
&= \text{str} \left[(\partial \cosh W + \partial \sinh W)(\partial \cosh W - \partial \sinh W) \right] \\
&= \text{str} [\partial e^W \partial e^{-W}] \\
&= \text{str}[\partial g \partial g^{-1}].
\end{aligned} \tag{D.5}$$

energy term

$$\begin{aligned}
\text{str}[Q\sigma_3] &= \text{str}[e^{W \otimes \sigma_2}] = \text{str}[\cosh(W) \otimes \mathbb{1}] + \underbrace{\text{str}[\sinh(W) \otimes \sigma_2]}_{=0} \\
&= \text{str}[\cosh W + \sinh W + \cosh W - \sinh W] \\
&= \text{str}[g + g^{-1}].
\end{aligned} \tag{D.6}$$

topological term

$$\begin{aligned}
\frac{1}{2} \text{str}[Q\partial Q\sigma_2] &= \frac{1}{2} \text{str} \left[(\cosh(W) \otimes \sigma_3 + \sinh(W) \otimes \sigma_2\sigma_3) \right. \\
&\quad \left. \times (\partial \cosh(W) \otimes \sigma_3\sigma_2 + \partial \sinh(W) \otimes \sigma_2\sigma_3\sigma_2) \right] \\
\frac{1}{2} &= \text{str} \left[(\sinh(W)\partial \cosh(W) - \cosh(W)\partial \sinh(W)) \otimes \mathbb{1} \right] \\
&\quad + \underbrace{\text{str} \left[(\cosh(W)\partial \cosh(W) - \sinh(W)\partial \sinh(W)) \otimes \sigma_2 \right]}_{=0} \\
&= \text{str} \left[\sinh(W)\partial \cosh(W) - \cosh(W)\partial \sinh(W) \right. \\
&\quad \left. + \frac{1}{2} \partial (\cosh^2(W) - \sinh^2(W)) \right] \\
&= \text{str} \left[\sinh(W)\partial \cosh W - \cosh(W)\partial \sinh W \right. \\
&\quad \left. + \cosh(W)\partial \cosh W - \sinh(W)\partial \sinh W \right] \\
&= \text{str} \left[(\cosh W + \sinh W) (\partial \cosh W - \partial \sinh W) \right] \\
&= \text{str} [e^W \partial e^{-W}] \\
&= \text{str}[g\partial g^{-1}] = -\text{str}[g^{-1}\partial g],
\end{aligned} \tag{D.7}$$

where in the last step we have used $\text{str}[g\partial g^{-1}] = \text{str}[-gg^{-1}\partial gg^{-1}] = -\text{str}[g^{-1}\partial g]$.

Gade term

From Eq. (D.7) we immediately conclude

$$\frac{1}{4} \text{str}^2[Q\partial Q\sigma_2] = \text{str}^2[g^{-1}\partial g]. \tag{D.8}$$

Consequently, the σ -model action in terms of Q is given by

$$\begin{aligned}
S[Q] &= - \int d\lambda \left\{ \tilde{c}_1 \text{str}(\partial Q\partial Q) + \tilde{c}_2 i \text{str}(\epsilon Q \sigma_3^{\text{AB}}) + \tilde{c}_3 \text{str}^2(Q\partial Q\sigma_2^{\text{AB}}) \right. \\
&\quad \left. + \tilde{c}_4 \text{str}(Q\partial Q\sigma_2^{\text{AB}}) \right\}
\end{aligned} \tag{D.9}$$

with $\tilde{c}_1 = c_1/2$, $\tilde{c}_2 = c_1$, $\tilde{c}_3 = c_3/4$ and $\tilde{c}_4 = c_4/2$.

Appendix E

Contraction Rules

In the context of perturbation theory one often has to evaluate gaussian integrals. This is in the presence of higher powers of the pre-exponential factors a quite awkward task, which can be considerably simplified by the use of *Wick's theorem*. This notion comprises some algorithms also called *contraction rules*, which allow to reduce n -point correlations to products of pair correlations. In this chapter we will elaborate the contraction rules for gaussian integrals over $\text{GL}(1|1)$. In the first section we concretely calculate the pair correlations for the group $\text{GL}(1|1)$, in the second and third sections we elaborate the contraction rules for the integrals over the supergroup $\text{GL}(n|n)$ and hermitian $n \times n$ -matrices, respectively. In the last section we calculate the perturbative corrections to the DoS in Eq. (6.13).

E.1 Pair Correlations for $\text{GL}(1|1)$

Let W be the generators of $\text{GL}(1|1)$ parameterized in cartesian coordinates. Hence,

$$W = \begin{pmatrix} W_{11} & W_{12} \\ W_{21} & W_{22} \end{pmatrix} = \begin{pmatrix} v & \xi \\ \chi & iw \end{pmatrix} \quad (\text{E.1})$$

with $v \in \mathbb{R}$, $w \in [0, 2\pi]$ and ξ and χ are arbitrary Grassmann variables. Denoting the corresponding manifold as $\text{gl}^*(1|1)$ let us consider the Gaussian integral

$$\begin{aligned} \int_{\text{gl}^*(1|1)} dW e^{-c \text{str} W^2} &\equiv \frac{1}{2\pi} \int_{-\infty}^{\infty} dv \int_0^{2\pi} dw \int d\xi d\chi e^{-c(v^2+w^2+\xi\chi-\chi\xi)} \\ &= \frac{1}{2\pi} \left(\frac{\pi}{c} 2c \right) = 1, \end{aligned} \quad (\text{E.2})$$

where we have chosen the constant in the integration density to be $\frac{1}{2}$. Then we get for the second moments

$$\langle v^2 \rangle = \frac{1}{2\pi} \int_{-\infty}^{\infty} dv \int_0^{2\pi} dw \int d\xi d\chi v^2 e^{-c(v^2+w^2+\xi\chi-\chi\xi)} = \frac{1}{2c} = \langle w^2 \rangle \quad (\text{E.3})$$

and

$$\langle \xi\chi \rangle \equiv \frac{1}{2\pi} \int_{-\infty}^{\infty} dv \int_0^{2\pi} dw \int d\xi d\chi \xi\chi e^{-c(v^2+w^2+2\xi\chi)} = -\frac{1}{2c} = -\langle \chi\xi \rangle. \quad (\text{E.4})$$

Consequently, we have $\langle \text{str}(W^2) \rangle = 0$.

E.2 Wick's Theorem for Correlations in $\text{GL}(n|n)$

First, we will calculate a general moment of second order. Let W , A and B be $2n$ -dimensional supermatrices, which in boson-fermion decomposition are given by

$$W = \begin{pmatrix} W^{\text{bb}} & W^{\text{bf}} \\ W^{\text{fb}} & W^{\text{ff}} \end{pmatrix}, \quad (\text{E.5})$$

and analogous for A and B . The $n \times N$ -matrices $(W_{\alpha\beta}^{\text{bb}})_{\alpha,\beta}$, $(W_{\alpha\beta}^{\text{ff}})_{\alpha,\beta}$ and $(W_{\alpha\beta}^{\text{bf}})_{\alpha,\beta}$, $(W_{\alpha\beta}^{\text{fb}})_{\alpha,\beta}$ consist of even and odd elements of a Grassmann algebra, respectively. We introduce a *parity* function for a matrix index α and a pair of matrix indices (α, β) in the following way

$$|\alpha| \equiv \begin{cases} 0, & \text{if } 1 \leq \alpha \leq n, \\ 1, & \text{if } n+1 \leq \alpha \leq 2n \end{cases} \quad (\text{E.6})$$

and

$$|(\alpha, \beta)| \equiv \begin{cases} 0, & \text{if } (\alpha, \beta) \text{ belongs to the bb- or the ff-block,} \\ 1, & \text{if } (\alpha, \beta) \text{ belongs to the bf- or the fb-block.} \end{cases} \quad (\text{E.7})$$

Thus, $|(\alpha, \beta)| = 0$ for $W_{\alpha\beta}$ being even and 1 for $W_{\alpha\beta}$ being odd. Note that

$$|(\alpha, \beta)| = |(\beta, \alpha)|, \quad (\text{E.8a})$$

$$(-1)^{|(\alpha, \beta)|} = (-1)^{|\alpha|+|\beta|}, \quad (\text{E.8b})$$

$$(-1)^{|(\alpha, \beta)| \cdot |(\alpha, \beta)|} = (-1)^{|(\alpha, \beta)|}. \quad (\text{E.8c})$$

The supertrace can be expressed in terms of the usual trace

$$\begin{aligned}\text{str } A &= \text{tr } A^{\text{bb}} - \text{tr } A^{\text{ff}} = \text{tr}(\sigma_3^{\text{bf}} A) = (\sigma_3^{\text{bf}})_{\alpha\beta} A_{\beta\alpha} \\ &= (\sigma_3^{\text{bf}})_{\alpha\alpha} A_{\alpha\alpha} = (-1)^{|\alpha|} A_{\alpha\alpha},\end{aligned}\tag{E.9}$$

where here and in the following we use the summation convention.

Now consider the Gaussian superintegral

$$\int d[W] e^{-c \text{str } W^2} = 1,\tag{E.10}$$

where $d[W] \equiv \prod_{i=1}^{2n} dW_{ii} \times \prod_{i < j} dW_{ij} dW_{ji}$. A general moment of second order is then given by

$$\begin{aligned}\langle W_{\alpha\beta} W_{\gamma\delta} \rangle &\equiv \int d[W] W_{\alpha\beta} W_{\gamma\delta} e^{-c \text{str } W^2} = \int d[W] W_{\alpha\beta} W_{\gamma\delta} e^{-c(-1)^{|\lambda|} W_{\lambda\mu} W_{\mu\lambda}} \\ &= \delta_{\alpha\delta} \delta_{\beta\gamma} \begin{cases} (2c)^{-1} (-1)^{|\alpha|}, & \text{if } W_{\alpha\beta} \text{ even,} \\ -(2c)^{-1} (-1)^{|\alpha|}, & \text{if } W_{\alpha\beta} \text{ odd} \end{cases} \\ &= (2c)^{-1} \delta_{\alpha\delta} \delta_{\beta\gamma} (-1)^{|\alpha|} (-1)^{|\alpha, \beta|} \\ &= (2c)^{-1} \delta_{\alpha\delta} \delta_{\beta\gamma} (-1)^{|\beta|} \quad (\text{no summation over } \beta!).\end{aligned}\tag{E.11}$$

It is advantageous to calculate the expressions $\langle \text{str}(AWBW) \rangle$ and $\langle \text{str}(AW) \text{str}(BW) \rangle$ which enable us to find arbitrary contractions (of second order). From Eq. (E.11) we conclude

$$\begin{aligned}\text{str}(AWBW) &= (-1)^{|\alpha|} A_{\alpha\beta} W_{\beta\gamma} B_{\gamma\delta} W_{\delta\alpha} \\ &= (-1)^{|\alpha|} (-1)^{|\beta, \gamma| \cdot |(\gamma, \delta)|} A_{\alpha\beta} B_{\gamma\delta} W_{\beta\gamma} W_{\delta\alpha}\end{aligned}\tag{E.12}$$

and hence

$$\begin{aligned}\langle \text{str}(AWBW) \rangle &= (-1)^{|\alpha|} (-1)^{|\beta, \gamma| \cdot |(\gamma, \delta)|} A_{\alpha\beta} B_{\gamma\delta} (2c)^{-1} \delta_{\beta\alpha} \delta_{\gamma\delta} (-1)^{|\gamma|} \\ &= (2c)^{-1} (-1)^{|\alpha|} (-1)^{|\alpha, \gamma| \cdot |(\gamma, \gamma)|} (-1)^{|\gamma|} A_{\alpha\alpha} B_{\gamma\gamma} \\ &= (2c)^{-1} (-1)^{|\alpha|} A_{\alpha\alpha} (-1)^{|\gamma|} B_{\gamma\gamma} \\ &= (2c)^{-1} \text{str } A \text{str } B,\end{aligned}\tag{E.13}$$

where we have used $|(\gamma, \gamma)| = 0$, independent of γ . Similarly, we obtain

$$\begin{aligned}\text{str}(AW) \text{str}(BW) &= (-1)^{|\alpha|} A_{\alpha\beta} W_{\beta\alpha} (-1)^{|\gamma|} B_{\gamma\delta} W_{\delta\gamma} \\ &= (-1)^{|\alpha| + |\gamma|} (-1)^{|\beta, \alpha| \cdot |(\gamma, \delta)|} A_{\alpha\beta} B_{\gamma\delta} W_{\beta\alpha} W_{\delta\gamma}\end{aligned}\tag{E.14}$$

and therefore

$$\begin{aligned}
\langle \text{str}(AW) \text{str}(BW) \rangle &= (-1)^{|\alpha|+|\gamma|} (-1)^{|\beta,\alpha|+|\gamma,\delta|} (-1)^{|\alpha|} A_{\alpha\beta} B_{\delta\gamma} (2c)^{-1} \delta_{\beta\gamma} \delta_{\alpha\delta} \\
&= (2c)^{-1} (-1)^{|\beta|} (-1)^{|\beta,\alpha|+|\beta,\alpha|} A_{\alpha\beta} B_{\beta\alpha} \\
&= (2c)^{-1} (-1)^{|\beta|} (-1)^{|\alpha|+|\beta|} A_{\alpha\beta} B_{\beta\alpha} \\
&= (2c)^{-1} (-1)^{|\alpha|} A_{\alpha\beta} B_{\beta\alpha} \\
&= (2c)^{-1} \text{str}(AB).
\end{aligned} \tag{E.15}$$

E.3 Contraction Rules for Gaussian Integrals over Hermitean Matrices

We now consider the much easier case of integrals over Hermitean matrices H . Noting that

$$\text{tr} H^2 = \sum_{\lambda,\mu} H_{\lambda\mu} H_{\mu\lambda} = \sum_{\lambda,\mu} H_{\lambda\mu} H_{\lambda\mu}^* = \sum_{\lambda,\mu} |H_{\lambda\mu}|^2 = \sum_{\lambda,\mu} (\text{Re}^2 H_{\lambda\mu} + \text{Im}^2 H_{\lambda\mu}), \tag{E.16}$$

we can calculate a general moment of second order,

$$\begin{aligned}
\langle H_{\alpha\beta} H_{\gamma\delta} \rangle &= \int d[H] H_{\alpha\beta} H_{\gamma\delta} e^{-\text{tr} H^2} \\
&= \int d[H] H_{\alpha\beta} H_{\gamma\delta} e^{-c \sum_{\lambda} \text{Re}^2 H_{\lambda\lambda} - 2c \sum_{\lambda < \mu} (\text{Re}^2 H_{\lambda\mu} + \text{Im}^2 H_{\lambda\mu})} \\
&= \frac{1}{2c} \delta_{\alpha\delta} \delta_{\beta\gamma},
\end{aligned} \tag{E.17}$$

where $d[H] \equiv \frac{1}{\mathcal{N}} \prod_i dH_{ii} \prod_{i < j} d \text{Re} H_{ij} d \text{Im} H_{ij}$, and the normalization constant is given by

$$\mathcal{N} = \langle 1 \rangle = \left(\frac{\pi}{c} \right)^{n^2/2} 2^{-n(n-1)/2}. \tag{E.18}$$

Hence, the contraction rules are given by (A, B arbitrary $n \times n$ matrices)

$$\langle \text{tr}(AHBH) \rangle = (2c)^{-1} \text{tr} A \text{tr} B, \tag{E.19}$$

and

$$\langle \text{tr}(AH) \text{tr}(BH) \rangle = (2c)^{-1} \text{tr}(AB). \tag{E.20}$$

E.4 Perturbative Corrections to the DoS

Using the contraction rules Eqs. (E.13) and (E.15) we are able to calculate the different terms contributing to the DoS in Eq. (6.13).

- 1-loop diagram

$$\sum_k \langle \text{str} [W_k W_{-k} \sigma_3^{\text{bf}}] \rangle \propto \text{str}(\sigma_3^{\text{bf}}) \text{str}(1) = 0. \quad (\text{E.21})$$

- 2-loop diagram A

$$\begin{aligned} & \sum_{l_1, l_2, l_3} \langle \text{str} [W_{l_1} W_{l_2} W_{l_3} W_{-l_1-l_2-l_3} \sigma_3^{\text{bf}}] \rangle \\ &= \sum_{l_1, l_2, l_3} \left\{ \langle (2c_{l_1})^{-1} \text{str} [W_{l_3} W_{-l_1-l_2-l_3} \sigma_3^{\text{bf}}] \delta_{l_2, -l_1} \rangle \right. \\ & \quad + \langle (2c_{l_1})^{-1} \text{str} W_{l_2} \text{str} [W_{-l_1-l_2-l_3} \sigma_3^{\text{bf}}] \delta_{l_3, -l_1} \rangle \\ & \quad \left. + \langle (2c_{-l_1-l_2-l_3})^{-1} \text{str} \sigma_3^{\text{bf}} \text{str} [W_{l_2} W_{l_3}] \delta_{-l_1-l_2-l_3, -l_1} \rangle \right\} \\ &= \sum_{l_1, l_2} \left\{ \langle (2c_{l_1})^{-1} \text{str} W_{l_2} \text{str} [W_{-l_2} \sigma_3^{\text{bf}}] \rangle + 2 \langle (2c_{-l_1})^{-1} \text{str} [W_{l_2} W_{-l_2}] \rangle \right\} \\ &= \sum_{l_1, l_2} \left\{ (2c_{l_1})^{-1} (2c_{l_2})^{-1} \text{str}(1 \cdot \sigma_3^{\text{bf}}) + 2(2c_{-l_1})^{-1} \text{str} 1 \text{str} 1 \right\} \\ &= \frac{1}{2} \sum_{l_1, l_2} (c_{l_1})^{-1} (c_{l_2})^{-1} \end{aligned} \quad (\text{E.22})$$

- 2-loop diagram B

$$\begin{aligned} & \sum_{q_1, q_2, q_3} \frac{Dq_1 q_2 + i\epsilon}{\Delta} \langle \text{str}(\frac{1}{2} \sigma_3^{\text{bf}}) \text{str} [W_{q_1} W_{q_2} W_{q_3} W_{-q_1-q_2-q_3}] \rangle \\ &= \sum_{q_1, q_2, q_3} \frac{Dq_1 q_2 + i\epsilon}{\Delta} (2c_{q_1})^{-1} \langle \text{str} W_{q_2} \text{str} W_{-q_2} \rangle \\ &= \sum_{q_1, q_2, q_3} \frac{Dq_1 q_2 + i\epsilon}{\Delta} (2c_{q_1})^{-1} \text{str} 1 \text{str} 1 = 0 \end{aligned} \quad (\text{E.23})$$

- 2-loop diagram C

$$\begin{aligned}
& \sum_{k,q_1,q_2,q_3} \frac{Dq_1q_2 + i\epsilon}{\Delta} \langle \text{str}[W_{-k}\sigma_3^{\text{bf}}W_k] \text{str}[W_{q_1}W_{q_2}W_{q_3}W_{-q_1-q_2-q_3}] \rangle \\
&= \sum_{k,q_1,q_2,q_3} \frac{Dq_1q_2 + i\epsilon}{\Delta} \left\{ (2c_{q_1})^{-1} \langle \text{str}[\sigma_3^{\text{bf}}W_kW_{q_2}W_{q_3}W_{-q_1-q_2-q_3}] \delta_{k,q_1} \rangle \right. \\
&\quad + (2c_{q_2})^{-1} \langle \text{str}[\sigma_3^{\text{bf}}W_kW_{q_3}W_{-q_1-q_2-q_3}W_{q_1}] \delta_{k,q_2} \rangle \\
&\quad + (2c_{q_3})^{-1} \langle \text{str}[\sigma_3^{\text{bf}}W_kW_{-q_1-q_2-q_3}W_{q_1}W_{q_2}] \delta_{k,q_3} \rangle \\
&\quad \left. + (2c_{-q_1-q_2-q_3})^{-1} \langle \text{str}[\sigma_3^{\text{bf}}W_kW_{q_1}W_{q_2}W_{q_3}] \delta_{k,-q_1-q_2-q_3} \rangle \right\} \\
&= \frac{1}{2} \sum_{q_1,q_2,q_3} \frac{Dq_1q_2 + i\epsilon}{\Delta} [(c_{q_1})^{-1} + (c_{q_2})^{-1} + (c_{q_3})^{-1} + (c_{-q_1-q_2-q_3})^{-1}] \\
&\quad \times \langle \text{str}[\sigma_3^{\text{bf}}W_{q_1}W_{q_2}W_{q_3}W_{-q_1-q_2-q_3}] \rangle \\
&= \frac{1}{2} \sum_{q_1,q_2} \frac{Dq_1q_2 + i\epsilon}{\Delta} [(c_{q_1})^{-1} + (c_{q_2})^{-1}] (c_{q_1})^{-1}(c_{q_2})^{-1} \\
&= \frac{i\omega}{2} \sum_{q_1,q_2} [(c_{q_1})^{-2}(c_{q_2})^{-1} + (c_{q_1})^{-1}(c_{q_2})^{-2}]
\end{aligned} \tag{E.24}$$

Appendix F

Solution of the Heat Equation in the Quantum Regime

In order to solve Eq. (6.58) perturbatively in η we first consider the solution for $\eta = 0$, which is given by

$$\phi_{2,\eta=0}^{e,o}(y) = \begin{cases} 1 + d_1^{e,o}y, & C^{e,o} = 0 \\ d_2^{e,o} e^{i\sqrt{C^{e,o}}y} + d_3^{e,o} e^{-i\sqrt{C^{e,o}}y}, & C^{e,o} \neq 0 \end{cases} \quad d_1^{e,o}, d_2^{e,o}, d_3^{e,o} \in \mathbb{R}$$

Comparing with Eq. (6.55) we conclude $C^o = 0$, $d_1^o = 0$ and $C^e = 1/4$. Furthermore, we see $d_2^e = 1$, $d_3^e = 0$ for $x > 0$ and $d_2^e = 0$, $d_3^e = 1$ for $x < 0$. Therefore, we have

$$\phi_{2,\eta=0}^e(y) = e^{i\chi\frac{y}{2}} \quad \text{and} \quad \phi_{2,\eta=0}^o(y) = 1,$$

where $\chi \equiv \text{sgn } x$. For finite η we write the solution of Eq. (6.58) as a power series in the small parameter η ,

$$\phi_{2,\eta}^{e,o}(y) = \phi_{2,\eta=0}^{e,o}(y) + \eta\phi_{2,1}^{e,o}(y) + \mathcal{O}(\eta^2),$$

where $(\partial_y^2 + C^{e,o})\phi_{2,\eta=0}^{e,o}(y) = 0$, and

$$(\partial_y^2 + C^{e,o})\phi_{2,1}^{e,o}(y) = -\eta \cos y \phi_{2,\eta=0}^{e,o}(y) \quad (\text{F.1})$$

is the differential equation for the first order correction. The solutions of Eq. (F.1) for N even and N odd are given by

$$\phi_{2,1}^e(y) = \chi \left[\frac{1}{4} e^{i\chi\frac{3y}{2}} - \frac{1}{2} i\chi y e^{-i\chi\frac{y}{2}} + h^e(y) \right]$$

and

$$\phi_{2,1}^o(y) = \cos y + h^o(y),$$

respectively, where $h^{e,o}(y)$ are solutions of the homogeneous equation. Omitting these terms the solutions of Eq. (6.58) up to first order in η are given by

$$\phi_2^o(y) = 1 + \eta \cos(y) \quad (\text{F.2})$$

and

$$\phi_2^e(y) = \chi \left[e^{ix\frac{y}{2}} + \frac{\eta}{2} e^{ix\frac{y}{2}} \left(\frac{1}{2} e^{ixy} - i\chi y e^{-ixy} \right) \right]. \quad (\text{F.3})$$

Turning to the x equation, Eq. (6.57), we introduce $u \equiv (2\eta)^{1/2} e^{|x|/2}$ and conclude that the only integrable solution of Eq. (6.61) is given by $c^e K_1(u)$ for even N and $c^o K_0(u)$ for odd N . The constants c^e and c^o are determined by the $\eta \rightarrow 0$ asymptotics Eq. (6.55) as follows. Using the expansion of the Bessel functions for small arguments,

$$K_0(u) \simeq -\ln u \quad \text{and} \quad K_1(u) \simeq u^{-1},$$

we find by comparison with Eq. (6.55)

$$\lim_{\eta \rightarrow 0} \phi^o(x, y) = -\lim_{\eta \rightarrow 0} \frac{c^o}{2} (\ln \eta + |x| + \ln 2) (1 + \eta \cos y) \stackrel{!}{=} -1$$

and

$$\begin{aligned} \lim_{\eta \rightarrow 0} \phi^e(x, y) &= -\lim_{\eta \rightarrow 0} \chi \frac{c^e}{(2\eta)^{1/2}} e^{-|x|/2} \left[e^{ix\frac{y}{2}} + \frac{\eta}{2} e^{ix\frac{y}{2}} \left(\frac{1}{2} e^{ixy} - i\chi y e^{-ixy} \right) \right] \\ &\stackrel{!}{=} -2 e^{-\chi(x-iy)/2}. \end{aligned}$$

Consequently, the normalization factors are given by $c^o = 2 \ln^{-1} \eta$ and $c^e = 2\chi(2\eta)^{1/2}$ and we obtain Eq. (6.62). Keeping only the lowest relevant powers in η the square of the heat kernel simplifies to

$$\begin{aligned} \phi^{e2}(x, y) &= 8\eta K_1^2(u) e^{ixy} \left[1 + \frac{\eta}{2} (e^{ixy}/2 - i\chi y e^{-ixy}) \right]^2 \\ &\simeq 8\eta K_1^2(u) [e^{ixy} + \eta (e^{2ixy}/2 - i\chi y)] \end{aligned}$$

and

$$\phi^{o2}(x, y) = \frac{4}{\ln^2 \eta} K_0^2(u) (1 + 2\eta \cos y + \eta^2 \cos^2 y) \simeq \frac{4}{\ln^2 \eta} K_0^2(u).$$

We insert this result into Eq. (4.33) for the DoS. Starting with N even we get

$$\begin{aligned}
\langle \rho_{\text{quant}}(\epsilon^+) \rangle^e &= \rho_0 + \rho_0 \operatorname{Re} \frac{1}{4\pi} \int_{-\infty}^{\infty} dx \int_0^{2\pi} dy \frac{1}{2} (\cosh x - \cos y) \\
&\quad \times \left[\phi^{e^2}(x, y) + (-1 + 1) \sinh^{-2} \left(\frac{x - iy}{2} \right) \right] \\
&= \rho_0 + \rho_0 \operatorname{Re} \frac{1}{4\pi} \int_{-\infty}^{\infty} dx \int_0^{2\pi} dy \left\{ \frac{\sinh \left(\frac{x+iy}{2} \right)}{\sinh \left(\frac{x-iy}{2} \right)} + \frac{1}{2} (\cosh x - \cos y) \right. \\
&\quad \left. \times \left[\phi^{e^2}(x, y) - \sinh^{-2} \left(\frac{x - iy}{2} \right) \right] \right\} \\
&= \rho_0 \operatorname{Re} \frac{1}{8\pi} \int_0^{\infty} dx \int_0^{2\pi} dy (\cosh x - \cos y) \left[\phi^{e^2}(x, y) - 4 e^{-(x-iy)} \right. \\
&\quad \left. + \phi^{e^2}(-x, y) - 4 e^{-(x-iy)} \right] \\
&= -\rho_0 \operatorname{Re} \frac{1}{2\pi} \int_0^{\infty} dx \int_0^{2\pi} dy \left[2\eta K_1^2(u) - e^{-x} + 4\pi i \eta^2 \cosh x K_1^2(u)(y - y) \right],
\end{aligned}$$

where in the third line we have used that the integrand is dominated by its large $|x|$ asymptotics. Recalling that the Bessel functions decay exponentially for large arguments we can introduce $-\ln \eta$ as an upper cut-off. For the remaining integration interval we use the series representation of the Bessel functions which is given by $K_1^2(u) \simeq u^{-2} + \ln \frac{u}{2} + \mathcal{O}(u^2 \ln^2 u)$ and obtain

$$\begin{aligned}
\langle \rho_{\text{quant}}(\epsilon^+) \rangle^e &= -\rho_0 \operatorname{Re} \int_0^{-\ln \eta} dx 2\eta \left[(2\eta)^{-1} e^{-x} + \frac{1}{2} \ln(2\eta e^x) - \ln 2 - e^{-x} \right] \\
&= -\rho_0 \operatorname{Re} \eta \int_0^{-\ln \eta} dx (\ln \eta - \ln 2 + x) \\
&\simeq \rho_0 \operatorname{Re} \eta \ln^2 \eta.
\end{aligned}$$

Performing an analytic continuation, $\eta \rightarrow -i(\omega + i\gamma/\Delta_\xi)$, we end up with Eq. (6.64). Now, we turn to the analogous calculation for N odd. From Eq. (4.33)

we get

$$\begin{aligned} \langle \rho_{\text{quant}}(\epsilon^+) \rangle^{\circ} - \rho_0 &= \rho_0 \operatorname{Re} \frac{1}{2\pi} \int_0^{\infty} dx \int_0^{2\pi} dy \frac{1}{2} (\cosh x - \cos y) \frac{4}{\ln^2 \eta} K_0^2((2\eta)^{1/2} e^{x/2}) \\ &= \rho_0 \operatorname{Re} \frac{2}{\ln^2 \eta} \int_0^{\infty} dx \cosh x K_0^2((2\eta)^{1/2} e^{x/2}). \end{aligned}$$

Using the series representation of the Bessel function, $K_0^2(u) \simeq \ln^2 u$, we obtain

$$\begin{aligned} \langle \rho_{\text{quant}}(\epsilon^+) \rangle^{\circ} - \rho_0 &= \rho_0 \operatorname{Re} \frac{1}{4 \ln^2 \eta} \int_0^{-\ln \eta} dx e^x (x + \ln \eta - \ln 2)^2 \\ &\propto \rho_0 \operatorname{Re} \frac{1}{\eta \ln^2 \eta}. \end{aligned}$$

Performing an analytic continuation again, we get Eq. (6.65).

Bibliography

- [1] S. Datta, *Electronic Transport in Mesoscopic Systems* (Cambridge University Press, Cambridge, 1995).
- [2] M. Janssen, *Physics Reports* **295**, 1 (1998).
- [3] S. Washburne and R. Webb, *Adv. Phys.* **35**, 375 (1986).
- [4] M. Büttiker, Y. Imry, and R. Landauer, *Phys. Lett.* **96 A**, 365 (1983).
- [5] H. Cheung, Y. Gefen, E. Reidel, and W.-H. Shih, *Phys. Rev. B* **37**, 6050 (1988).
- [6] S. Washburne and R. Webb, *Rep. Prog. Phys.* **55**, 1311 (1992).
- [7] G. Bergmann, *Phys. Rep.* **107**, 1 (1984).
- [8] P. Anderson, *Phys. Rev.* **109**, 1492 (1958).
- [9] E. Abrahams, P. Anderson, D. Licciardello, and T. Ramakrishnan, *Phys. Rev. Lett.* **42**, 673 (1979).
- [10] F. Dyson, *Phys. Rev.* **92**, 1331 (1953).
- [11] G. Theodorou and M. Cohen, *Phys. Rev. B* **13**, 4597 (1976).
- [12] T. Eggarter and R. Riedinger, *Phys. Rev. B* **18**, 569 (1978).
- [13] R. Gade, *Nucl. Phys. B* **398**, 499 (1993).
- [14] R. Gade and F. Wegner, *ibid.* **360**, 213 (1991).
- [15] F. Wegner, *Z. Phys. B* **35**, 207 (1979).
- [16] J. Verbaarschot and I. Zahed, *Phys. Rev. Lett.* **70**, 3852 (1993).
- [17] J. Verbaarschot, *Phys. Rev. Lett* **72**, 2531 (1994).
- [18] F. Dyson, *J. Math. Phys.* **3**, 140 (1962).

- [19] P. Brouwer, C. Mudry, B. Simons, and A. Altland, Phys. Rev. Lett. **81**, 862 (1998).
- [20] P. Brouwer, C. Mudry, and A. Furusaki, Phys. Rev. Lett. **84**, 2913 (2000).
- [21] J. Miller and J. Wang, Phys. Rev. Lett. **76**, 1461 (1996).
- [22] A. Altland and B. Simons, Nucl. Phys. B **562**, 445 (1999).
- [23] M. Favrizio and C. Castellani, cond-mat/0002328.
- [24] C. Mudry, P. Brouwer, and A. Furusaki, Phys. Rev. B **59**, 13221 (1999).
- [25] P. Brouwer, C. Mudry, and A. Furusaki, Nucl. Phys. B **565**, 653 (2000).
- [26] C. Mudry, P. Brouwer, and A. Furusaki, cond-mat/0004042.
- [27] T. Fukui, Nucl. Phys. B **562**, 477 (1999).
- [28] A. Furusaki, Phys. Rev. Lett **82**, 604 (1999).
- [29] P. Biswas, P. Cain, R. Römer, and M. Schreiber, cond-mat/0001315.
- [30] S. Kravchenko *et al.*, Phys. Rev. B **50**, 8039 (1994).
- [31] S. Kravchenko *et al.*, Phys. Rev. B **51**, 7038 (1995).
- [32] S. Kravchenko, D. Simonian, M. Sarachik, and W. M. J. Furneaux, Phys. Rev. Lett. **77**, 4938 (1996).
- [33] V. Pudalov, G. Brunthaler, A. Prinz, and G. Bauer, JETP Lett **65**, 932 (1997).
- [34] D. Simonian, S. Kravchenko, and M. Sarachik, Phys. Rev. Lett **79**, 2304 (1997).
- [35] D. Popović, A. Fowler, and S. Washburn, Phys. Rev. Lett. **79**, 1543 (1997).
- [36] M. Simmons *et al.*, Phys. Rev. Lett **80**, 1292 (1998).
- [37] V. Dobrosavljević, E. Abrahams, E. Miranda, and S. Chakravarty, Phys. Rev. Lett. **79**, 455 (1997).
- [38] S. Chakravarty, L. Yin, and E. Abrahams, Phys. Rev. B **58**, R559 (1998).
- [39] V. Pudalov, JETP Lett. **66**, 175 (1997).
- [40] C. Castellani, C. DiCastro, and P. Lee, Phys. Rev. B **57**, R9381 (1998).
- [41] Y. Lyanda-Geller, Phys. Rev. Lett. **80**, 4273 (1998).

- [42] G.-H. Chen, M. Raikh, and Y.-S. Wu, cond-mat/9904451.
- [43] G. Bergmann, Solid State Comm. **42**, 815 (1982).
- [44] S. Hikami, A. Larkin, and Y. Nagaoka, Prog. Theor. Phys. **63**, 707 (1980).
- [45] S. Maekawa and H. Fukuyama, J. Phys. Soc. Japan **50**, 2516 (1981).
- [46] P. Freche, M. Janssen, and R. Merkt, Phys. Rev. Lett **82**, 149 (1999).
- [47] B. Huckestein, Physica A **167**, 175 (1990).
- [48] M. Janssen, Int. Journal of Mod. Phys. B **8**, 943 (1994).
- [49] D. Arovas, M. Janssen, and B. Shapiro, Phys. Rev. B **56**, 4751 (1997).
- [50] A. Galstyan and M. Raikh, Phys. Rev. B **56**, 1422 (1997).
- [51] M. Janssen, R. Merkt, J. Meyer, and A. Weymer, Physica B **258**, 65 (1998).
- [52] M. Janssen, R. Merkt, and A. Weymer, Ann. Phys. (Berlin) **7**, 353 (1998).
- [53] A. Abrikosov, L. Gorkov, and I. Dzyaloshinskii, *Methods of Quantum Field Theory in Statistical Physics* (Prentice Hall, New York, 1963).
- [54] A. Abrikosov, *Fundamentals of the Theory of Metals* (North Holland, Amsterdam, 1988).
- [55] M. Mehta, *Random Matrices* (Academic Press, New York, London, 1991).
- [56] O. Dorokhov, JETP Lett. **36**, 318 (1982).
- [57] P. Mello, P. Pereyra, and N. Kumar, Ann. Phys. (NY) **181**, 290 (1988).
- [58] L. Schäfer and F. Wegner, Z. Phys B **38**, 113 (1980).
- [59] K. Efetov, Adv. Phys. **32**, 53 (1983).
- [60] M. Zirnbauer, cond-mat/9903338.
- [61] E. Wigner, Ann. Math. **53**, 36 (1953).
- [62] T. Guhr, A. Mueller-Groeling, and H. Weidenmüller, Phys. Rep. **299**, 189 (1989).
- [63] F. Dyson, Commun. Math. Phys. **19**, 235 (1970).
- [64] S. Helgason, *Differential geometry, Lie groups and symmetric spaces* (Academic Press, New York, 1978).

- [65] M. Zirnbauer, J. Phys. A **29**, 7113 (1996).
- [66] M. Zirnbauer, J. Math. Phys. **37**, 4986 (1996).
- [67] E. Shuryak and J. Verbaarschot, Nucl. Phys. A **560**, 306 (1993).
- [68] A. Altland and M. Zirnbauer, Phys. Rev. Lett. **76**, 3420 (1996).
- [69] A. Altland and M. Zirnbauer, Phys. Rev B **55**, 1142 (1997).
- [70] T. Ando, Phys. Rev. B **40**, 5325 (1989).
- [71] H. Mathur, Phys. Rev. B **56**, 15794 (1997).
- [72] A. Eilmes, R. Römer, and M. Schreiber, Eur. Phys. J. B **1**, 29 (1998).
- [73] R. Oppermann and F. Wegner, Z. Phys. B **34**, 327 (1979).
- [74] F. Wegner, Z. Phys. B **44**, 9 (1981).
- [75] T. Ziman, Phys. Rev. B **26**, 7066 (1982).
- [76] M. Inui, S. Trugman, and E. Abrahams, Phys. Rev. B **49**, 3190 (1994).
- [77] G. Gavazzi, J. Wheatley, and A. Schofield, Phys. Rev. B **47**, 15170 (1993).
- [78] A. Aronov, A. Mirlin, and P. Wölfle, Phys. Rev. B **49**, 16609 (1994).
- [79] B. Altshuler and B. Shklovskii, JETP **64**, 127 (1986).
- [80] K. Efetov, JETP Lett. **40**, 738 (1984).
- [81] K. Efetov, *Supersymmetry in Disorder and Chaos* (Cambridge University Press, Cambridge, 1997).
- [82] F. Berezin, *Introduction to Superanalysis* (D. Reidel Publishing Company, Dordrecht, Holland, 1987).
- [83] A. Mirlin, A. Müller-Groeling, and M. Zirnbauer, Ann. Phys. **236**, 325 (1994).
- [84] M. Zirnbauer, priv. comm.
- [85] T. Nagao and S. Slevin, J. Math. Phys. **34**, 2075, 2317 (1993).
- [86] P. Damgaard, J. Osborn, D. Toublan, and J. Verbaarschot, Nucl. Phys. B **547**, 305 (1999).
- [87] P. Freche, Ph.D. thesis, Köln, 1997.

- [88] P. Lee and T. Ramakrishnan, *Rev. Mod. Phys.* **57**, 287 (1985).
- [89] R. Merkt, Diploma Thesis, Köln, 1997.
- [90] J. Chalker and P. Coddington, *J. Phys. C* **21**, 2665 (1988).
- [91] A. Crisanti, G. Paladin, and A. Vulpiani, in *Products of Random Matrices in Statistical Physics*, edited by P. Fulde (Springer-Verlag, Berlin, 1992), Vol. 104, 26.
- [92] J. Pichard and G. Sarma, *J. Phys. C* **14**, L127 (1981).
- [93] B. Kramer and A. MacKinnon, *Rep. Prog. Phys.* **56**, 1469 (1993).
- [94] P. Freche, M. Janssen, and R. Merkt, in *Recent Progress in Many Body Theory*, edited by D. Neilson and R. Bishop (World Scientific, Singapore, 1998).
- [95] D.-H. Lee, Z. Wang, and S. Kivelson, *Phys. Rev. Lett* **70**, 4130 (1992).
- [96] G. Benettin, L. Galgani, A. Giorgilli, and J.-M. Strelcyn, *Meccanica* **15**, 9 (1980).
- [97] B. Martin, *Statistics for Physicists* (Academic Press, London, 1971).
- [98] F. Wegner, *Nucl. Phys. B* **316**, 663 (1989).
- [99] M. Zirnbauer, 4. DFG-Rundgespräch über den Quanten-Hall-Effekt, Schleching, 1989.
- [100] A. MacKinnon, in *Localization and Confinement of Electrons in Semiconductors*, edited by F. Kuchar (Springer Series in Solid State Sciences, Berlin, 1990).
- [101] U. Fastenrath *et al.*, *Physica A* **172**, 302 (1991).
- [102] S. Evangelou, *Phys. Rev. Lett.* **75**, 2550 (1995).
- [103] L. Schweitzer and I. Zharakeshev, *J. Phys. Condens. Matter* **9**, L441 (1997).
- [104] L. Schweitzer, *J. Phys. Condens. Matter* **7**, L281 (1995).
- [105] M. Zirnbauer, *J. Math. Phys* **38**, 2007 (1997).
- [106] D. Thouless, *J. Phys. C* **5**, 77 (1972).

Zusammenfassung

Mesoskopische Physik ist seit etwa 20 Jahren eines der wichtigsten und meistbeachteten Forschungsgebiete der modernen theoretischen und experimentellen Festkörperphysik. Sie behandelt Phänomene in makroskopischen Systemen, die von der Interferenz vielfach gestreuter nicht-wechselwirkender phasenkohärenter Elektronen herrühren.

Eines der bedeutendsten dieser Phänomene ist die starke Lokalisierung [8], bei der die elektronische Wellenfunktion in stark ungeordneten Systemen aufgrund von destruktiver Quanteninterferenz exponentiell um ein Zentrum herum abfällt. Damit einher geht der exponentielle Abfall des Leitwerts über einer charakteristischen Längenskala ξ , der Lokalisierungslänge. Verwandt mit dem Effekt der starken Lokalisierung ist die schwache Lokalisierung. In schwach ungeordneten Systemen beobachtet man ein leichtes Absinken des Leitwerts gegenüber seinem klassischen Wert. Dieses Phänomen ist auf eine Erhöhung der Rückstreuungswahrscheinlichkeit infolge Quanteninterferenz zurückzuführen und ergibt sich störungstheoretisch als kleine negative Korrektur zum Leitwert. In einer berühmten Arbeit haben ABRAHAMS ET AL. 1979 mit Hilfe von Skalenargumenten gefolgert, daß in zwei und weniger Dimensionen alle ungeordneten Systeme (im thermodynamischen Limes) starke Lokalisierung zeigen.

Von besonderem Interesse sind daher Systeme, die ein Verhalten zeigen, das mit der Skalentheorie nicht konform ist. Seit einigen Jahrzehnten sind solche Ausnahmen bekannt. So fand man etwa bei eindimensionalen (1D) Gittermodellen mit ausschließlich außerdiagonaler Unordnung eine in der Bandmitte divergierende Zustandsdichte (DoS). Dies geht gemäß einer Arbeit von THOULESS [106] mit der Existenz eines delokalisierten Zustands einher. Auch in 2D fand man eine Singularität in der Zustandsdichte im Rahmen eines nicht-linearen σ -Modells (NL σ M) für ein Untergittermodell [13,14]. Lange Zeit war der Mechanismus, der zur Delokalisierung führt, unverstanden. Man gewann tiefere Einsicht, als man erkannte, daß außerdiagonale Unordnung und die betrachteten Untergittermodelle ihre Gemeinsamkeit in der chiralen Symmetrie des zugrunde liegenden Hamiltonians haben: In geeigneter Darstellung ist der Hamiltonian block-außerdiagonal. Als Konsequenz ergibt sich, daß alle Eigenwerte in Paaren mit entgegengesetztem Vorzeichen auftreten. Bei einer geraden Zahl an Zuständen führt dies aufgrund von Level-Abstoßung zu einer symmetrischen Lücke in der Zustandsdichte. Ist die Zahl der Zustände ungerade, bleibt ein Zustand "ungepaart" und kann in der Bandmitte eine evaneszente Mode ausbilden. Chirale Systeme unterscheiden sich von Gittermodellen mit diagonaler Unordnung bezüglich der Ungleichförmigkeit des Energiespektrums.

Symmetrien haben auf das Verhalten mesoskopischer Systeme einen großen Einfluß. Neben der chiralen Symmetrie, sind Zeitumkehr- und die Spinrotationssymmetrie von großer Bedeutung. Erstere wird durch Anwesenheit eines Magnetfelds, letztere beispielsweise durch Spin-Bahn-Wechselwirkung gebrochen. Störungstheoretische Berechnungen für diesen Fall haben gezeigt, daß die oben erwähnte Korrektur zum Leitwert infolge schwacher Lokalisierung positiv wird. Daher spricht man auch von schwacher anti-Lokalisierung. Mit Hilfe der Skalentheorie ergibt sich in diesem Fall die Möglichkeit für Delokalisierung in zwei Dimensionen. Da im Fall genügend starker Unordnung aber jedes System (auch in mehr als zwei Dimensionen) unter Renormierung in den Lokalisierungsfixpunkt fließt, sollten 2D Systeme in Anwesenheit von Spin-Bahn-Wechselwirkung einen Lokalisierungs-Delokalisierungs- (LD-) Übergang aufweisen, der durch die Stärke der Unordnung gesteuert wird.

In der vorliegenden Arbeit wurden mesoskopische Systeme behandelt, die, obwohl höchstens zweidimensional, Delokalisierung zeigen können. Der erste Teil beschäftigt sich mit der (unordnungsgemittelten) Zustandsdichte für quasi-1D chirale Systeme mit gebrochener Zeitumkehrinvarianz. Die DoS nicht chiraler Systeme besitzt auf Skalen, die kleiner sind als die Fermi-Energie, keine ausgeprägte Struktur. Qualitative Überlegungen zeigen, daß die Zustandsdichte chiraler Systeme eine höhere Komplexität besitzt, da sie eine komplizierte Kopplung von Greenfunktionen, die zu den beiden Spezies eines Untergittersystems gehören, beinhaltet.

Ein Beispiel für ein nicht zeitumkehrinvariantes chirales System ist das *random flux model* (RFM), ein Gittermodell mit ausschließlich außerdiagonaler unitärer Unordnung. Kürzlich wurde von ALTLAND und SIMONS für das RFM ein supersymmetrisches $NL\sigma M$ abgeleitet [22], das die eingehende Untersuchung von Spektral- und Transportgrößen auf allen relevanten Längenskalen und in allen relevanten Energieregimen erlaubt. Als Besonderheit treten bei diesem $NL\sigma M$ ein topologischer Term und der sogenannte Gade-Term auf, der schon von GADE in [13] identifiziert worden war. Ausgehend von der effektiven Wirkung dieses $NL\sigma M$ wurde die DoS im ergodischen, im perturbativen und im Quantenregime berechnet.

Im ergodischen Regime, wo die Felder als räumlich konstant angesehen werden können, zeigt die Zustandsdichte Fluktuationen auf der Skala des mittleren Niveauabstands. Solche Fluktuationen sind sonst nur von Zwei-Punkt-Greenfunktionen, wie der Zwei-Level-Korrelationsfunktion, bekannt. Hier kommt die oben angesprochene charakteristische Komplexität der chiralen Zustandsdichte zum Ausdruck. Interessanterweise zeigte sich eine Abhängigkeit der Ergebnisse von der Parität der Zahl der Gitterplätze, wofür der topologische Term verantwortlich ist. Ferner bildet die DoS eine symmetrische um die Bandmitte zentrierte Lücke aus. Die erhaltenen Resultate reproduzieren Ergebnisse, die schon aus der Theorie chiraler Zufallsmatrizen bekannt sind [16,17,67,85]. Dies liegt

darin begründet, daß das System im ergodischen Limes universell wird, d.h. nur von den Symmetrien und der Raumdimension abhängt, und daher durch ein statistisches Ensemble von geeigneten Matrizen vollständig charakterisiert wird.

Zur Berechnung der DoS im perturbativen Regime wurde das $NL\sigma M$ in einer Formulierung analog zu Ref. [81] verwendet. Dies erlaubte eine übersichtliche Auflistung der einzelnen Beiträge gemäß diagrammatischer Störungstheorie. Bis einschließlich 3-Loop-Ordnung wurden keine perturbativen Korrekturen gefunden. Ob ab einer bestimmten Loop-Ordnung Beiträge auftauchen oder nicht, ist momentan noch offen.

Das Quantenregime ist der interessanteste und gleichzeitig schwierigste Fall. Hier versagen störungstheoretische Methoden. Daher wurde das Problem der Funktionalintegration im Ausdruck für die DoS mittels der in quasi-1D anwendbaren Transfermatrixmethode auf die Lösung einer Wärmeleitungsgleichung (HEQ) zurückgeführt. Jeder Term des dabei auftretenden verallgemeinerten Laplaceoperators entspricht einem der Beiträge in der Wirkung des $NL\sigma M$. Erwähnenswert ist der Einfluß des topologischen Terms auf die Randbedingungen der Differentialgleichung. Die HEQ konnte im Grenzfall kleiner Energien, $\omega \equiv \epsilon/\Delta_\xi \ll 1$ und großer Systemlängen, $L \gg \xi$ gelöst werden. Das Ergebnis hängt sensibel von der Parität der Kanalzahl N_c des quasi-1D Systems ab. Für eine gerade Anzahl an Kanälen ergab sich für die DoS $\langle \rho(\omega) \rangle \propto \rho_0 |\omega| \ln|\omega|$, für eine ungerade Anzahl $\langle \rho(\omega) \rangle - \rho_0 \propto \rho_0/|\omega| \ln^3|\omega|$. Im letzteren Fall zeigt die DoS eine Divergenz, wie sie auch schon bei der Untersuchung von 1D Systeme mit außerdiagonaler Unordnung aufgetreten war [11,12]. Das Ergebnis für den Fall gerader Kanalzahl, stimmt mit einer vor kurzem gefundenen Beziehung überein [20].

Die Motivation für den zweiten Teil dieser Arbeit lag in einer Reihe von kürzlich durchgeführten Experimenten, die in 2D Systemen delokalisiertes Verhalten gezeigt haben [30–36]. Es wird zur Zeit diskutiert, ob der beobachtete LD-Übergang durch Elektron-Elektron-Wechselwirkung oder Spin-Bahn-Kopplung induziert wird [37–42]. Im Rahmen dieser Arbeit sollte der durch Spin-Bahn-Wechselwirkung induzierte Übergang eingehend untersucht und charakterisiert werden. Durchgeführt wurden die Untersuchungen an einem streutheoretischen Netzwerkmodell [46]. Hierzu mußten zunächst die Streumatrizen konstruiert werden, welche durch drei unabhängige Parameter charakterisiert sind, zwei für die Ortsraumstreuung einer für die Stärke der Streuung im Spinraum.

Nach einer Abbildung der Streumatrizen auf Transfermatrizen wurden mittels der (numerischen) Transfermatrixmethode quasi-1D renormierte Lokalisierungslängen Λ in Abhängigkeit von der Systembreite und den drei Parametern berechnet. Da Λ die Rolle einer Skalenvariable spielt, konnte mittels der Breitenabhängigkeit (*finite-size scaling*) das Lokalisierungsverhalten des Modells bestimmt werden. In diesem Zusammenhang wurde ein Phasendiagramm im dreidimensionalen Parameterraum erstellt. Es zeigte sich, daß das System für hinreichend starke Unord-

nung unabhängig von der Spin-Streustärke lokalisiert ist. Ist die Unordnung aber schwach genug, kann eine metallische Phase auftreten, die um so größer ist, je stärker der Spin gestreut wird. Das Modell weist also bei geeigneter Parameterwahl einen Phasenübergang auf.

Um diesen im Sinne der Theorie kritischer Phänomene charakterisieren zu können, ist es von großer Bedeutung, daß Ein-Parameter-Skalieren erfüllt ist. Um dies zu testen, wurde überprüft, ob es für die Skalenvariable Λ eine Skalenfunktion gibt. Die Konstruktion der Skalenfunktion wurde mittels einer Fitprozedur vorgenommen (vgl. Ref. [47]), um ein möglichst optimales Ergebnis zu erzielen. Weiterhin wurde der Fit mittels eines χ^2 -Tests auf seine Glaubwürdigkeit hin überprüft. Das Ergebnis zeigte, daß Ein-Parameter-Skalieren mit hoher Wahrscheinlichkeit erfüllt ist. Dies legitimierte die weitere Auswertung, im Rahmen derer der kritische Exponent ν der Lokalisierungslänge bestimmt wurde. Nachdem gezeigt worden war, daß diese charakteristische Größe stark mit kleinen Variationen des kritischen Wertes der Skalenvariable schwankt, wurde auch für die Bestimmung von ν eine Fitprozedur mit anschließendem Konfidenztest verwendet. Das Ergebnis ist $\nu = 2.51 \pm 0.18$, was im Rahmen der Fehler gut mit den Literaturwerten der letzten Jahre übereinstimmt [101–103]. Darüber hinaus wurde der Skalenexponenten α_0 der typischen lokalen Zustandsdichte mittels einer Konformrelation [48] aus dem kritischen Wert von Λ bestimmt. Das Ergebnis, $\alpha_0 = 2.174 \pm 0.003$ stimmt gut mit dem einzigen uns bekannten Literaturwert [104] überein.

Am Ende des zweiten Teils der Arbeit wurde eine Alternative zur Transfermatrixmethode vorgestellt, die nach bedeutend weniger Rechenleistung verlangt. Die numerische Ortsraumrenormierungs-Methode [49] ermöglicht es, das Lokalisierungsverhalten eines Modells schon nach wenigen Rechenschritten zu kennen. Das Verfahren wurde benutzt, um einen Anhaltspunkt dafür zu bekommen, ob das sogenannte Manhattan-Modell in der Lage ist, den kritischen Punkt eines Quanten-Hall-Systems zu modellieren. Es zeigte sich, daß die Verteilungsfunktion für den Transmissionskoeffizienten schon nach wenigen Iterationsschritten in den Lokalisierungsfixpunkt fließt, selbst wenn man mit einer δ -förmigen Anfangsverteilung nahe am Delokalisierungsfixpunkt startet. Als Resultat ergab sich somit, daß das Manhattanmodell den Quanten-Hall-Fixpunkt nicht enthält, was eine zuvor theoretisch gemachte Aussage [105] bestätigte.

Zusammenfassend wurden in dieser Arbeit ein- und zweidimensionale ungeordnete Elektronensysteme mit besonderer Symmetrie analytisch und numerisch untersucht. Es stellte sich heraus, daß es in quasi-1D Systemen mit chiraler Symmetrie eine Divergenz der Zustandsdichte in der Bandmitte gibt, was zumindest in strikt einer Dimension in direkter Verbindung mit der Existenz delokalisierte Zustände steht. In 2D Systemen mit hinreichend schwacher Unordnung und hinreichend starker Spin-Bahn-Streuung treten ebenfalls delokalisierte Zustände auf. Beide Arten von Systemen stellen somit Ausnahmen bezüglich der Skalentheorie der Lokalisierung dar.

Dank sage ich allen, ...

... die zum Gelingen dieser Arbeit beigetragen haben, und all denjenigen, die mich in der Zeit meiner Promotion als Freunde, Betreuer oder Arbeitskollegen begleitet haben.

Meine besondere Anerkennung gilt jedoch

- meinem Doktorvater, Prof. Dr. János Hajdu, der es mir ermöglicht hat, meine Promotion ganz nach meinen Vorstellungen an seinem Lehrstuhl durchzuführen,
- meinem Freund und Lehrer, Priv.-Doz. Dr. Martin Janßen, der jederzeit bemüht war, mir die "großen Zusammenhänge" nahezubringen, sich aber auch nie zu schade war, die Details ausdiskutieren,
- Prof. Dr. Alexander Altland, der mir Gelegenheit zu und Hilfestellung bei der Bearbeitung des ersten Teils dieser Arbeit gegeben hat,
- Priv.-Doz. Dr. Bodo Huckestein für seine Unterstützung bei den numerischen Methoden im zweiten Teil der Arbeit, die hilfreichen Antworten auf all die Fragen in Sachen Computer und seine große Hilfe beim sprachlichen Feinschliff der Dissertation,
- Prof. Dr. Martin R. Zirnbauer für seine Bereitschaft, die Rolle des Zweitgutachters zu übernehmen, und für einige interessante und aufschlußreiche Gespräche,
- meinen Zimmerkollegen Julia Meyer und Alexander Tschersich in Bochum, sowie Thorsten Knetter, Frank Pfeiffer, Gerd Schröder und Jesko Sirker in Köln für ein angenehmes und freundschaftliches Arbeitsklima,
- Jan Budczies, Corinna Kollath und Rainer Raupach für sorgfältiges Korrekturlesen der Dissertation,
- Dr. Suzanne Krebs, für die zahlreichen interessanten Gespräche über Musik und Kunst, die mir immer ein willkommener Ausgleich waren,
- Dr. Martina Bremser, die mich fast bis zum Ende meiner Promotion auf meinem Lebensweg begleitet hat,
- meinem Bruder für seine Hilfe in Computerangelegenheiten und in musikalischer Hinsicht
- und meinen Eltern, denen ich diese Arbeit in Dankbarkeit über die jahrelange Unterstützung meiner akademischen Ausbildung widme.

Erklärung

Ich versichere, daß ich die von mir vorgelegte Dissertation selbständig angefertigt, die benutzten Quellen und Hilfsmittel vollständig angegeben und die Stellen der Arbeit – einschließlich Tabellen, Karten und Abbildungen –, die anderen Werken im Wortlaut oder dem Sinn nach entnommen sind, in jedem Einzelfall als Entlehnung kenntlich gemacht habe; daß diese Dissertation noch keiner anderen Fakultät oder Universität zur Prüfung vorgelegen hat; daß sie – abgesehen von unten angegebenen Teilpublikationen – noch nicht veröffentlicht worden ist sowie, daß ich eine solche Veröffentlichung vor Abschluß des Promotionsverfahrens nicht vornehmen werde. Die Bestimmungen dieser Promotionsordnung sind mir bekannt. Die von mir vorgelegte Dissertation ist von Herrn Prof. Dr. J. Hajdu betreut worden.

Teilveröffentlichungen:

- R. Merkt, M. Janssen, and B. Huckestein, Phys. Rev. B **58**, 4394 (1998)
- M. Janssen, R. Merkt, and A. Weymer, Ann. Phys. (Berlin) **7**, 353, (1998)
- M. Janssen, R. Merkt, J.S. Meyer, and A. Weymer, Physica B **258**, 65 (1998)
- P. Freche, M. Janssen, and R. Merkt, Phys. Rev. Lett. **82**, 149 (1999)

Lebenslauf

Name: Rainer Merkt

Geburtsdatum: 25.8.1971

Geburtsort: Wesseling

Familienstand: ledig

Staatsangehörigkeit: deutsch

1977 - 1981 Grundschule

1981 - 1990 St.-Ursula-Gymnasium Brühl (Rheinl.)

1990 Abitur

1990 - 1991 Wehrdienst beim Stabsmusikkorps Bw

1991 - 1995 Physik-Studium an der Universität zu Köln

1996 Diplomarbeit unter Anleitung von Prof. Dr. J. Hajdu
am Institut für Theor. Physik der Universität zu Köln

17.2.1997 Diplomkolloquium

1997 - 2000 Promotion unter Anleitung von Prof. Dr. J. Hajdu
am Institut für Theor. Physik der Universität zu Köln

seit 1994 Studium der Schulmusik an der Musikhochschule Köln

2.7.1998 Fachpraktische Prüfung im Hauptfach Klavier

1993 - 1996 Stipendiat der "Studienstiftung des deutschen Volkes"